GCA-TR-67-19-N

FINAL REPORT

for

YAW ATTITUDE SENSOR

(23 June 1965 to 15 February 1968)

Contract No. NAS5-9642

Goddard Space Flight Center

Contract Officer: Max Weiner
Technical Monitor: H. Paul Scherer

Prepared by:

GCA CORPORATION
GCA TECHNOLOGY DIVISION
Bedford, Massachusetts

Project Manager: Wallace S. Kreisman

for

GODDARD SPACE FLIGHT CENTER
Greenbelt, Maryland

TABLE OF CONTENTS

Section	Title	Page
1	INTRODUCTION	1
2	THEORY	5
	A. General Considerations	5
	B. Error Analysis	11
	C. System Analysis	13
	D. Test System	23
3	DESIGN	29
	A. Overall System Design	29
	B. Vacuum Gauge Theory and Characteristics	30
	C. Mechanical Cycling Valve Designs	32
	D. Electronic Systems Design	46
	E. Packaging	58
	F. Test System	67
4	Construction	71
	A. Mechanical Cycling Valves	71
	B. Electronics	78
	C. Packaging	83
	D. Test System	83
5	TESTS AND RESULTS	87
	A. Mechanical Cycling Valves	87
	B. Electronics	105
	C. Magnetic Shielding Measurements	112
	D. Test System Operation	113
	E. Pressure Cycling Experiments with the Rotary Valve	116
	F. Overall Test of the Yaw Attitude Sensor System	121
6	CONCLUSIONS AND RECOMMENDATIONS	131
	A. Overall System	131
	B. Pressure Sensor	131
	C. Mechanical Cycling Valves	132
	D. Electronics	133
	E. Packaging	133
	F. Test System	134
	REFERENCES	135

LIST OF ILLUSTRATIONS

Figure No.	Title	Page
1	Schematic diagram of spacecraft yaw attitude sensor system.	3
2	Ratio of internal (gauge) to external ambient pressure for nitrogen (N_2) and oxygen as a function of angle of attack, θ.	7
3	Graphical solution of the equation $1 + \text{erf } s = \left(\frac{2V}{\sqrt{\pi}\ V_m} \sin\theta \tan\theta\right) \exp(-s^2)$	8
4	Typical error curves for a yaw attitude sensor system.	15
5	Schematic of sensor components.	17
6	Diagram of experimental equipment to determine the valve, gauge and amplifier transfer function.	21
7	Transfer function of the gauge.	22
8	Yaw attitude sensor null-signal noise record.	24
9	Two-chamber simulation method schematic.	25
10	Photograph of the GCA Model R-5 cold cathode ionization gauge and magnet.	33
11	Linear reciprocating valve schematic.	34
12	Detailed layout of linear reciprocating valve.	36
13	Mechanical cam follower drive for the linear reciprocating valve.	37
14	Linear reciprocating valve, gauge and magnet assembly.	38
15	Rotary valve schematic.	40
16	Detailed layout of rotary valve.	41
17	Experimental electromagnetic drive for the rotary valve.	42

LIST OF ILLUSTRATIONS (continued)

Figure No.	Title	Page
18	Rotary valve, gauge and magnet assembly.	44
19	Flexure-pivot oscillating valve schematic.	45
20	Detailed layout of flexure-pivot oscillating valve.	47
21	Electromagnetic drive for the flexure-pivot oscillating valve.	48
22	Flexure-pivot oscillating valve, gauge and magnet assembly.	49
23	Block diagram of the yaw attitude sensor system electronics.	50
24	Typical calibration curve for GCA logarithmic amplifier.	52
25	Electrometer amplifier schematic.	54
26	Synchronizer schematic.	56
27	Detector schematic.	57
28	Differential amplifier schematic.	59
29	Front view of rotary valve and flexure-pivot valve version of yaw attitude sensor package.	60
30	Side view of rotary valve and flexure-pivot valve version of yaw attitude sensor package.	61
31	Top view of rotary valve and flexure-pivot valve version of yaw attitude sensor package.	62
32	Front view of linear reciprocating valve version of yaw attitude sensor package.	63
33	Side view of linear reciprocating valve version of yaw attitude sensor package.	64
34	Schematic of simple mass-spring system.	66
35	Transmissability curve for spring-mass system.	66

LIST OF ILLUSTRATIONS (continued)

Figure No.	Title	Page
36	Vacuum test system for yaw attitude sensor.	68
37	Photograph of comparative sizes of the three mechanical cycling valves.	72
38	Photographic exploded view of the rotary valve.	73
39	Photographic exploded view of the flexure-pivot oscillating valve.	75
40	Photograph of the flexure-pivot valve electromagnetic drive units.	77
41	Photograph of electrometer amplifier, high voltage power supply and synchronous detector-differential amplifier.	79
42	Photograph of the electrometer amplifier.	80
43	Photograph of the synchronous detector-differential amplifier.	81
44	Photograph of the dc to dc converter.	82
45	Photograph of the support frame and split base plate.	84
46	Photograph of the test system.	85
47	Rotary valve drive rotors and external magnet drive.	88
48	Butterfly test valve schematic.	91
49	Flexural-pivot bearing.	94
50	Flexural-pivot center shift vs angular deflection for cantilever and double end supported flexural pivots under no-load conditions.	96
51	Flexural-pivot hysteresis vs angular deflection for cantilever and double end supported flexural pivots under no-load conditions.	97

LIST OF ILLUSTRATIONS (continued)

Figure No.	Title	Page
52	Flexural pivot predicted life for radial tension loading.	98
53	Flexural pivot predicted life for radial compression loading.	99
54	Flexural pivot life test jig.	100
55	High voltage modulation test circuit.	107
56	Block diagram of yaw attitude sensor electronics	109
57	Typical operational waveforms of the yaw attitude sensor electronics.	110
58	Synchronizing pulse.	123
59	Electrometer output, right chamber pressure = 1×10^{-7} torr, left chamber pressure = 8.4×10^{-7} torr.	123
60	Electrometer output, right chamber pressure = 8.2×10^{-7} torr, left chamber pressure = 8.5×10^{-7} torr.	124
61	Left chamber gate, right chamber pressure = 8.2×10^{-7} torr, left chamber pressure = 8.5×10^{-7} torr.	124
62	Right chamber gate, right chamber pressure = 8.2×10^{-7} torr, left chamber pressure = 8.5×10^{-7} torr.	124
63	Differential amplifier output, right chamber pressure = 1.0×10^{-7} torr, left chamber pressure = 8.3×10^{-7} torr.	125
64	Differential amplifier output, right chamber pressure = 8.4×10^{-7} torr, left chamber pressure = 1.0×10^{-7} torr.	125
65	Left chamber gate, right chamber pressure = 4.5×10^{-7} torr, left chamber pressure = 4.5×10^{-7} torr.	126

LIST OF ILLUSTRATIONS (continued)

Figure No.	Title	Page
66	Right chamber gate, right chamber pressure = 4.5×10^{-7} torr, left chamber pressure = 4.5×10^{-7} torr.	126
67	Differential amplifier output, right chamber pressure = 4.5×10^{-7} torr, left chamber pressure = 4.5×10^{-7} torr.	126
68	Left chamber gate, right chamber pressure = 4.5×10^{-8} torr, left chamber pressure = 9.0×10^{-7} torr.	127
69	Right chamber gate, right chamber pressure = 4.5×10^{-8} torr, left chamber pressure = 9.0×10^{-7} torr.	127
70	Differential amplifier output, right chamber pressure = 4.5×10^{-8} torr, left chamber pressure = 9.0×10^{-7} torr.	127
71	Right chamber gate, right chamber pressure = 9.0×10^{-7} torr, left chamber pressure = 5.0×10^{-8} torr.	128
72	Left chamber gate, right chamber pressure = 9.0×10^{-7} torr, left chamber pressure = 5.0×10^{-8} torr.	128
73	Electrometer output, right chamber pressure = 9.2×10^{-7} torr, left chamber pressure = 4.0×10^{-8} torr.	129
74	Differential amplifier output, right chamber pressure = 9.2×10^{-7} torr, left chamber pressure = 4.0×10^{-8} torr.	129

LIST OF TABLES

Table No.	Title	Page
1	Error Analysis Assumptions and Definitions	12
2	Error Analysis for a Typical Sensor System	14
3	Winds in the Upper Atmosphere	16
4	Ball Bearing Tests	92
5	GCA Test Results for Bendix 5016-800 Flexure Pivots	102
6	Bendix Test Results for Bendix 5016-800 Flexure Pivots	103
7	High Voltage Power Supply Output Voltages and the Corresponding Input Modulation	107
8	Data and Results Obtained in a Two-Chamber Cycling Valve Experiment Using a GCA Model R-5 Cold Cathode Gauge Exposed to an 8.5 to 1 Nitrogen Gas Pressure Ratio	117
9	Data and Results Obtained in a Two-Chamber Cycling Valve Experiment Using a GCA Model R-5 Cold Cathode Gauge Exposed to a 25 to 1 Nitrogen Gas Pressure Ratio	118
10	Data and Results Obtained in a Two-Chamber Cycling Valve Experiment Using a GCA Model R-5 Cold Cathode Gauge Exposed to a 1.63 to 1 Nitrogen Gas Pressure Ratio	119
11	Data and Results Obtained in a Two-Chamber Cycling Valve Experiment Using a GCA Model R-5 Cold Cathod Gauge Exposed to a 1.2 to 1 Nitrogen Gas Pressure Ratio	120

YAW ATTITUDE SENSOR

By Wallace S. Kreisman
GCA Corporation
GCA Technology Division
Bedford, Massachusetts

SUMMARY

A yaw attitude sensor system was designed and constructed to measure the angle between a chosen axis of a space vehicle and the relative wind. The system works by periodically connecting a cold cathode ionization gauge, via a mechanical cycling valve, to one of two independent tubulations that extend beyond the vehicle surface and are symmetrically located about the vehicle chosen axis. The ionization gauge measures the low pressures that develop within the tubulations and delivers a modulated output signal to a logarithmic electrometer and synchronous detector. The gauge signal modulation amplitude is converted to a dc voltage which is proportional to the yaw angle.

1. INTRODUCTION

The principle of the yaw attitude sensor had its conception in the techniques employed to measure atmospheric densities and pressures aboard high velocity rockets and satellites. The gas density which develops within a chamber located aboard a fast moving vehicle depends on the angle between the relative movement of the atmospheric gas molecules and atoms and the aperture or opening to the chamber. For example, a pressure gauge located on a spinning rocket or satellite develops an oscillating output signal due to the rotation [1].* The gauge actually scoops up more gas per unit time when facing forward into the relative wind than when facing away from the wind and into the wake.

In addition to the above observations of pressure and density, other measurements aboard a fast moving vehicle also depend on the relative motion of the air stream past the vehicle. Measurements of gas composition, and electron and positive ion densities, for example, normally depend on the direction of motion [2,3]. In general, measurement of the properties of the ambient atmosphere are affected by the velocity of the measuring instruments.

---

*Numbers in [ ] represent reference numbers.

A second important category of phenomena that are affected by the relative motion of a vehicle through the atmosphere involve those of aerodynamic drag and heating. The drag forces that retard the movement of a slender body (and thus help expend the propulsion energy) can be minimized by pointing the long axis of the body in the direction of the relative wind. Similarly, the heating of sensitive areas of the vehicle can be minimized by proper vehicle orientation. In both cases, a yaw attitude sensor may be used to determine the direction of the relative wind.

A further application of a yaw attitude sensor would be its use to determine the relative motion of the atmosphere with respect to the earth. Real neutral particle winds can be measured if one already has a knowledge of the motion and orientation of the vehicle with respect to the earth [4].

Since rockets, satellites, and space vehicles move at relatively high velocities of the order of 1 km/sec to about 8 km/sec, and since this velocity is an appreciable fraction of or exceeds the velocity of ambient atmospheric molecules and atoms, there is a "molecular ram" effect which acts to increase the gas pressure within any chamber that "looks into the wind." Conversely, any chamber which faces away from the wind (i.e., looks in the direction of the wake) will have a pressure created within it that is lower than the ambient pressure. Very roughly, one can say that the pressure within such a chamber varies approximately with the cosine of the angle between the relative wind velocity vector and the normal to the chamber aperture.

The yaw attitude sensor system operates on the principle of the familiar angle-of-attack sensor used in missile and aircraft instrumentation. A measurement of the relative wind direction is made by means of pressure measurements on two ram-air sampling tubes or tubulations which face obliquely in a forward direction. A nulling of the pressure between the tubes indicates a head-on attitude of the vehicle.

As shown in Figure 1, the yaw attitude sensing system consists of several basic elements. The heart of the system is the pressure sensor, in this case a cold cathode ionization gauge. The pressure sensor is periodically connected via a mechanical valve to one or the other of two gauge tubulations that extend beyond the spacecraft surface and are symmetrically located with respect to a chosen axis (for example, the yaw axis) of the vehicle. Any angular misalignment between the chosen vehicle axis (coinciding with the sensor null axis) and the velocity vector of the vehicle will cause the ionization gauge pressure sensor to deliver unequal signals for the two gauge tubulations. The mechanical valve is cycled at a low frequency of a few cycles per second so that the gauge output signal is a low frequency alternating current. The modulation amplitude of the gauge output current, which is proportional to the differential pressure between the gauge tubulations, is a direct analog measurement of the misalignment angle, the angle between the sensor null axis and the relative wind.

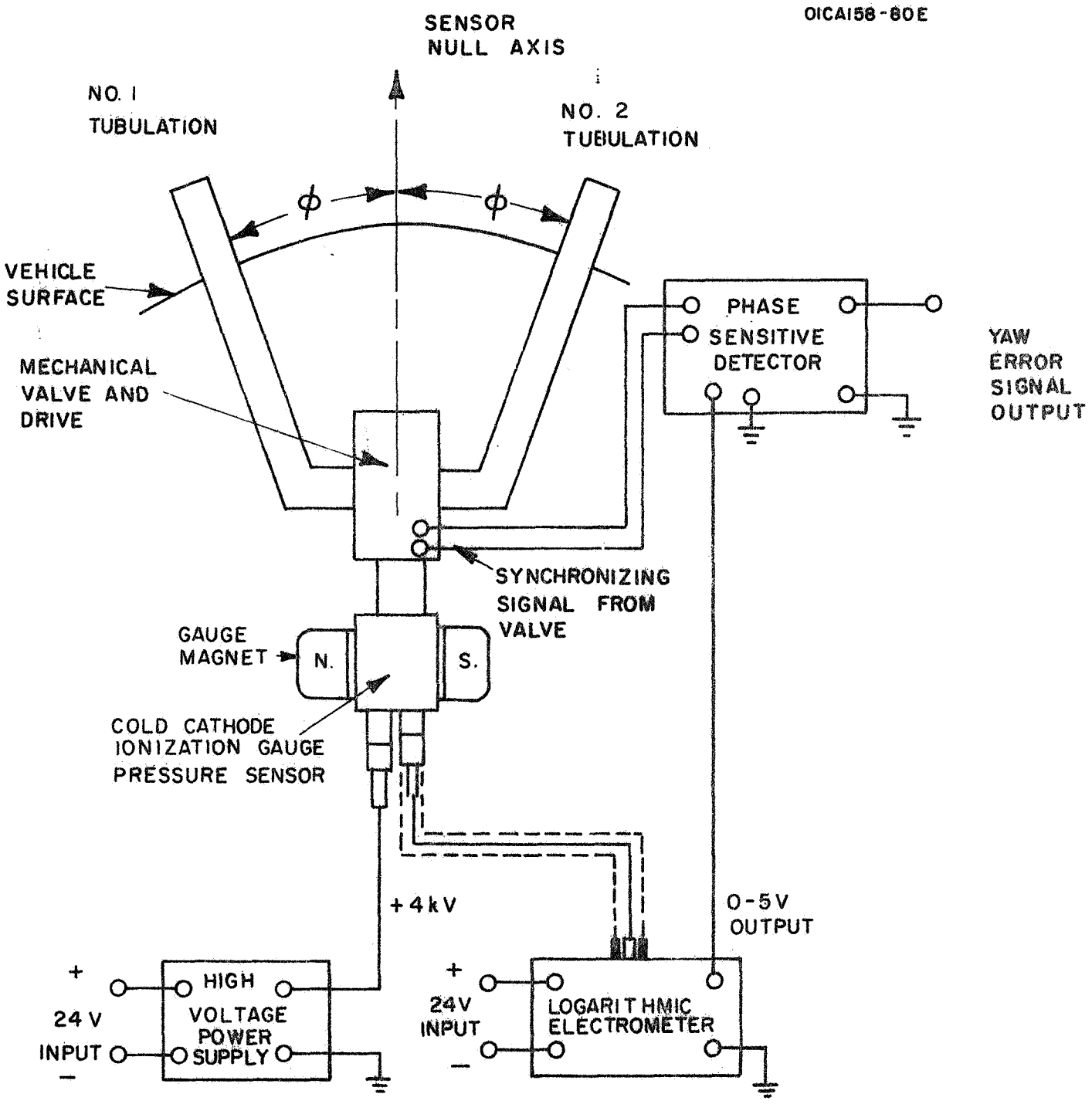

Figure 1. Schematic diagram of spacecraft yaw attitude sensor system.

The cold cathode ionization gauge requires a high voltage of the order of 1 to 4 kV at low current drain. This voltage is provided by a compact power supply in which a high frequency oscillation is stepped up via a transformer and is then rectified, filtered, and regulated. The output current of the ionization gauge is amplified by a logarithmic type amplifier that can cover a wide range of many decades. The wide dynamic range capability of the amplifier and the ionization gauge pressure sensor is a necessity since the pressure can vary over many orders of magnitude in the altitude regime of interest [5]. The logarithmic amplifier output, together with synchronizing signals from the mechanical valve or its driving circuit, is delivered to a phase sensitive detector in which the ac modulation is converted into a dc error signal which is a measure of the angular departure from the equilibrium or null orientation position.

The research program made use of the GCA Corporation Model R5 cold cathode ionization gauge which had been developed under a previous NASA program. This gauge is capable of measuring pressure in the range from 10^{-3} torr to 10^{-12} torr [6].

The logarithmic amplifier and phase sensitive detector were developed especially for the yaw attitude sensor system. Solid state electronics were used throughout the system.

Three different mechanical cycling valves were designed for this system. The linear oscillating valve was only partially constructed due to a lack of funds and time. The other two valves were constructed and tested. One of the two valves constructed, the flexure-pivot oscillating valve, is rather unique, and may have applications beyond the present system. There is no metal-to-metal contact during valve closure in any of the three designs. The valves simply present a high ratio between their open and closed vacuum conductances.

A special two-chamber test system was designed and developed to furnish two independent gas pressures that could be sampled by the ionization gauge via the mechanical cycling valve. The two pressure levels of the test chamber could be conveniently adjusted within the pressure range from 10^{-10} to 10^{-3} torr for nitrogen gas, air or any other desired pure gas or gas mixture.

2. THEORY

A. General Considerations

When a pressure gauge is located on a fast moving vehicle such as a rocket, satellite, or spacecraft, the pressure which develops within the sensitive volume of the gauge depends not only on the external ambient pressure but also on the external temperature, the gauge temperature, the velocity of the vehicle, the mass of the gas molecules and the angle-of-attack, that is, the angle between the relative wind and the normal to the gauge aperture.

The exact expression for the ratio of the internal gauge pressure P_i to the external ambient pressure P_o has been derived by several investigators and is given by the equation [7]

$$\frac{P_i}{P_o} = \sqrt{\frac{T_i}{T_o}} \left[\exp(-s^2) + s\sqrt{\pi}\,(1 + \operatorname{erf} s)\right] = \sqrt{\frac{T_i}{T_o}}\; f(s) \qquad (1)$$

where

$$f(s) = \exp(-s^2) + s\sqrt{\pi}\,(1 + \operatorname{erf} s)$$

$$s = V \cos\theta / V_m$$

$$V_m = \sqrt{\frac{2k\,T_o}{m}}$$

P_i = internal (gauge) pressure

P_o = external ambient pressure

T_i = internal (gauge) absolute temperature

T_o = external ambient absolute temperature

V = spacecraft velocity

V_m = most probable particle velocity

k = Boltzmann gas constant, 1.381×10^{16} erg per deg K

m = particle mass

θ = angle-of-attack

In Figure 2, solutions to Equation (1) are presented for a typical satellite moving through nitrogen and atomic oxygen and illustrate the manner in which the ratio of internal gauge pressure to external ambient pressure varies with the angle of attack. It can be seen that for angles of attack less than 90 degrees, the ratio P_i/P_o is greater than unity, indicating that the actual gauge pressure is amplified by the motion of the vehicle. This amplification is often called "molecular ramming" due to the "scooping-up" of the ambient gas by the fast-moving vehicle. The faster the vehicle moves and the heavier the ambient gas, the greater the pressure amplification or ramming. Atomic oxygen is the most abundant constituent in the Earth's upper atmosphere at altitudes of about 500 miles [8].

It is evident from Equation (1) and Figure 2 that the pressure versus angle-of-attack relationship is not linear. It should be noted that there is very little change of pressure with the angle-of-attack for angles near zero degrees. This circumstance will reduce the contribution of cross coupling from pitch and roll variations, say $\pm$ 5 degrees, to the yaw sensor to a negligible level. At the same time, it can be seen that over a relatively large range of angles of attack, the nonlinear true pressure versus angle relationships can be approximated by straight lines (shown as dashed lines in Figure 2). The linear approximations to the two ram effect curves in the figure intersect the angle-of-attack axis at two points (labelled θ_o) that are only two degrees apart.

The operating point angle ϕ for a yaw attitude sensor is defined as the angle between the normal to the gauge aperture (gauge tubulation direction) and the sensor null axis, as shown in Figure 1. The operating point angle may be selected on the basis of particular requirements. For example, a careful inspection of the curves in Figure 2 reveals that each curve has a point of inflection corresponding to a maximum value of the slope. The angle-of-attack for these positions of maximum rate of change of pressure may be determined analytically. The sensitivity of a pressure sensor for small changes of the angle of attack will be a maximum at these positions.

To find the values of the angles of attack corresponding to the points of inflection of the curves of Figure 2, Equation (1) is differentiated twice with respect to the angle θ, and the second derivative expression is set equal to zero. The result is

$$1 + \text{erf } s = \frac{2V}{\sqrt{\pi}\, V_m} \sin\theta \tan\theta \exp(-s^2) \qquad (2)$$

Equation (2) is best solved graphically. The graphical solutions for atomic oxygen and atomic hydrogen are shown in Figure 3. The angle of attack for maximum incremental sensitivity in an atomic oxygen atmosphere is 80 degrees. For atomic hydrogen, this angle of attack is 62.5 degrees. For gases of intermediate atomic weight, such as helium, the angle would lie between 62.5 degrees and 80 degrees.

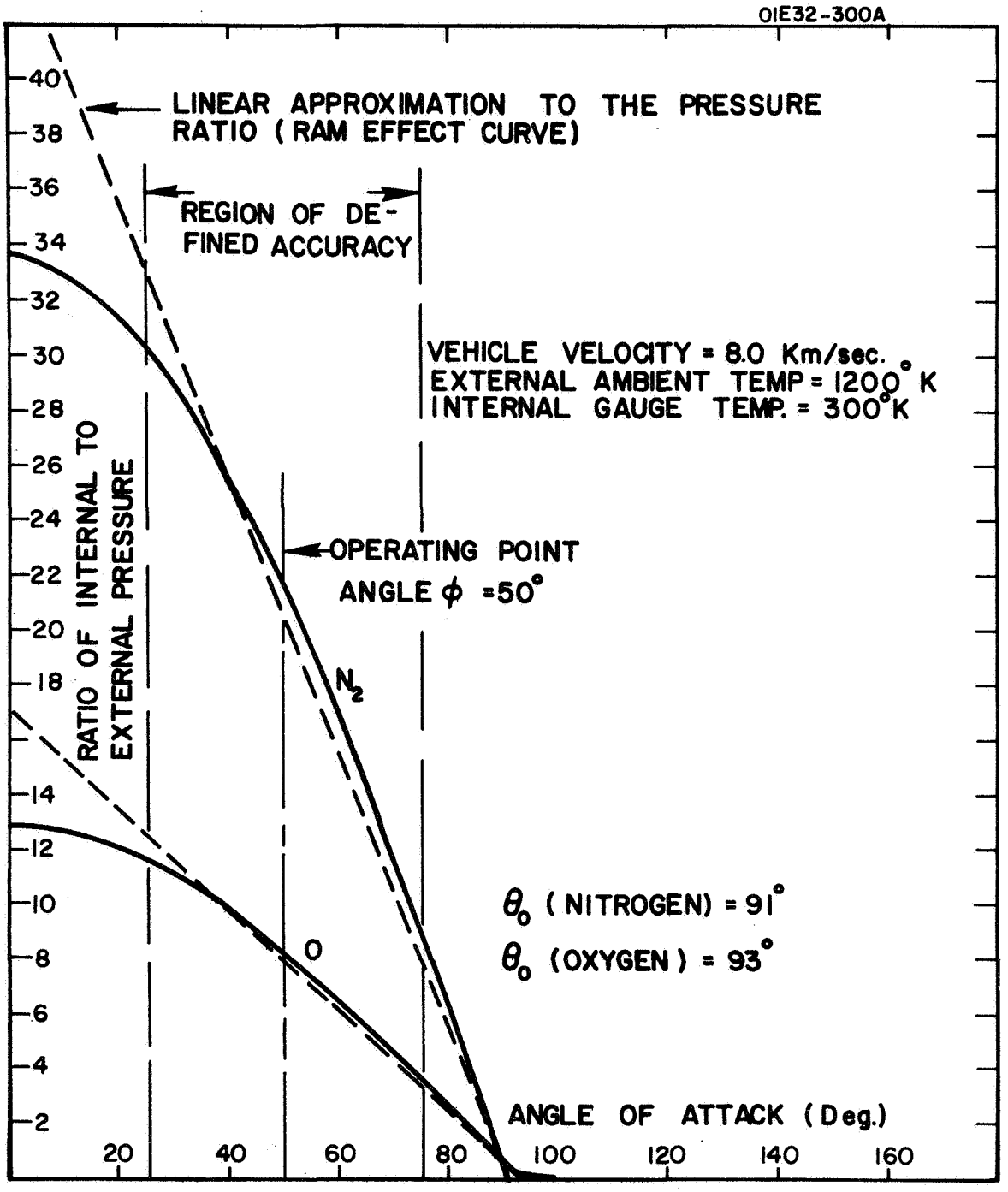

Figure 2. Ratio of internal (gauge) to external ambient pressure for nitrogen (N_2) and oxygen as a function of angle of attack, θ.

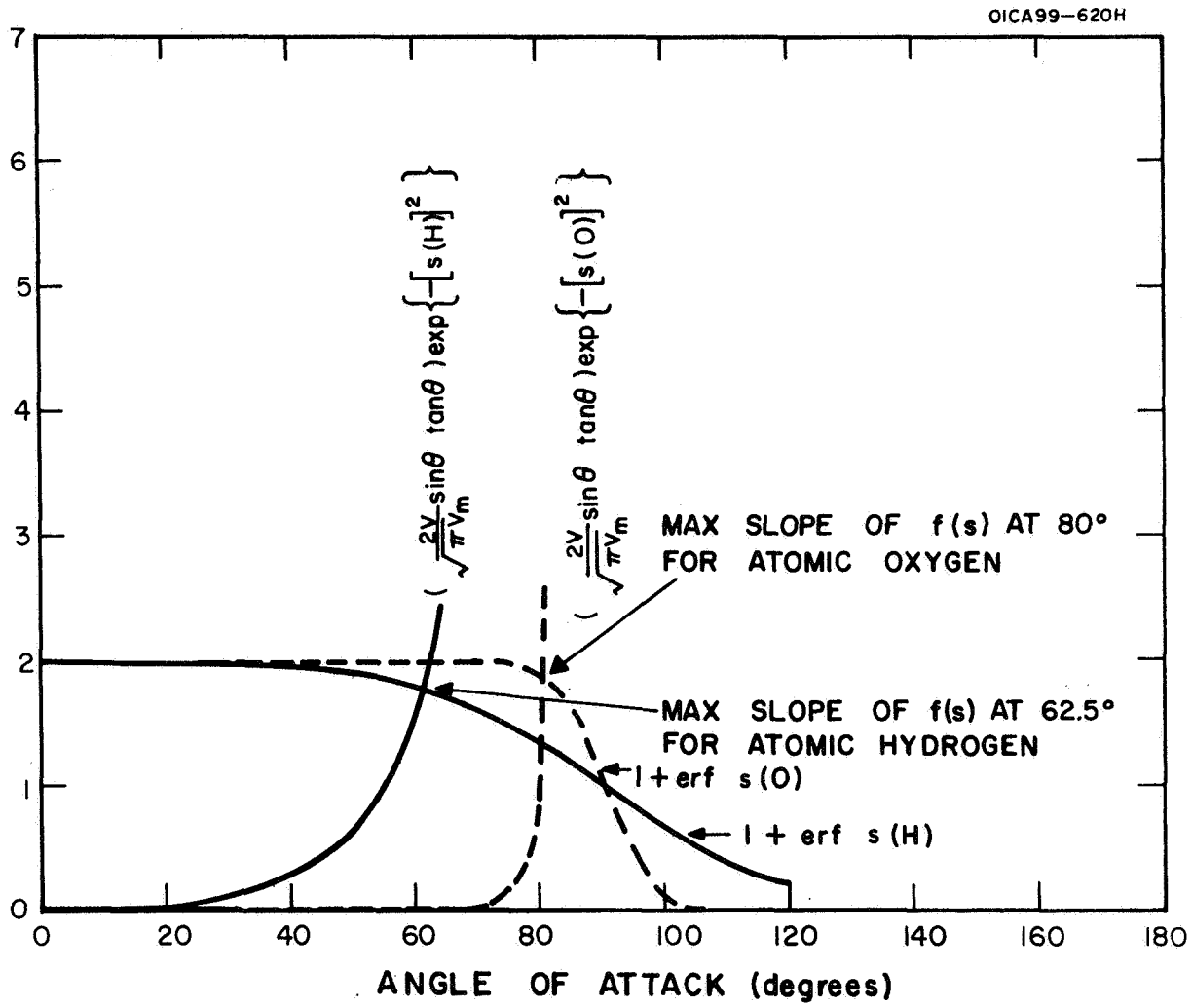

Figure 3. Graphical solution of the equation

$$1 + \text{erf } s = \left(\frac{2V}{\sqrt{\pi}\ V_m} \sin\theta \tan\theta\right) \exp\left(-s^2\right).$$

In addition to a consideration of the inremental sensitivity, one must consider other matters such as the range of control, the overall accuracy of a linear approximation to the ram effect curve of Figure 2, the signal level and the availability of certain locations on the vehicle for positioning the sensor. As can be seen graphically from Figure 2, the range of control can be relatively broad, but the overall accuracy in the so-called "Region of Defined Accuracy" decreases as the range widens. The departure from linearity is most pronounced for angles of attack which are less than about 30 degrees and greater than 90 degrees. An operating point angle located at about $\phi = 50$ degrees yields a range of control of plus or minus 25 degrees (from $\theta = 25$ degrees to $\theta = 75$ degrees) that has a reasonably linear approximation. For this situation, the included angle between the two tubulations of the yaw attitude sensor would be 100 degrees, and at null, with the sensor null axis aligned with the relative wind, each tubulation will subtend an angle of 50 degrees with respect to the relative wind. In this case, the pressure amplification factor or ram factor will be about 22 for molecular nitrogen and 8 for atomic oxygen. It should be noted that at an angle of attack of 25 degrees, the linear approximation to the ram curve is high, while at an angle of attack of 75 degrees, the linear approximation is low. It will be seen later that the effect of these errors will be to balance out another error that results from a simplification of the equation of operation.

Shifting the operating point angle from a value that lies between 60 and 80 degrees to a smaller angle such as 50 degrees, increases the general signal level, since the amplification factor is greater. Such a change can be very important for high altitude applications where the pressure and resulting ionization gauge signals are quite small. At very low altitudes, the pressure and gauge signals may actually be too large for the logarithmic electrometer and so an increase in the operating point angle would be desirable.

An important final consideration in the choice of the operating point angle and the range of control involves the location of such accessory equipment as attitude control jets and other sources of gas. Ideally, the yaw sensor tubulations should "look away" from all portions of the vehicle, so that any emanations of gas from the vehicle cannot directly enter the sensor tubulations. The matter of sensor contamination and interference caused by control jets is discussed in greater detail elsewhere [8].

The basic equation of operation of the yaw attitude sensor, that is, the relationship between the misalignment angle α between the relative wind and the sensor null axis and the output voltage, V, of the sensor system, will be derived in such a way that the errors of approximation can be evaluated.

The relationship between the gauge pressure P_i and the angle of attack θ can be written as:

$$P_i = \ell_\theta \left(nP_o - \frac{nP_o}{\theta_o} \theta \right) \tag{3}$$

where ℓ_θ is a correction factor for the nonlinearity of the P_i versus θ relationship. P_o is the external ambient pressure, θ_o is the θ intercept of the linear approximation and n is the maximum pressure amplification at zero angle of attack for the linear approximation. In Figure 2, for example, the value of n for atomic oxygen is seen to be 17, while the value of ℓ_θ for $\theta = 0$ degree is 13/17. For this same curve, $\ell_\theta = 1$ for $\theta \cong 35$ degrees and $\ell_\theta > 1$ for 35 degrees $< \theta <$ 85 degrees.

The ionization gauge pressure sensor responds to the pressure by producing a gauge current I which is effectively proportional to the pressure P_i as follows:

$$I = m_\theta \, c \, P_i = \ell_\theta \, m_\theta \, c \left(nP_o - \frac{nP_o}{\theta_o} \theta \right) \tag{4}$$

where m_θ is a correction factor for any nonlinearity in the gauge output current, I, as a function of the pressure range covered. Next, the output voltage of the electrometer varies approximately linearly with the log of the input current:

$$V' = A_\theta + B \log I = A_\theta + B \log \left\{ \ell_\theta \, m_\theta \, c \left(nP_o - \frac{nP_o}{\theta_o} \theta \right) \right\} \tag{5}$$

where A_θ is a correction factor for deviations from a true logarithmic characteristic.

The difference between two output voltages, V_1' and V_2', corresponding to two angles of attack, θ_1 and θ_2, can be written as:

$$V_1' - V_2' = \left\{ \left(A_{\theta_1} - A_{\theta_2} \right) + B \log \frac{\ell_{\theta_1} \, m_{\theta_1} \, c \, nP_o \left(1 - \frac{\theta_1}{\theta_o} \right)}{\ell_{\theta_2} \, m_{\theta_2} \, c \, nP_o \left(1 - \frac{\theta_2}{\theta_o} \right)} \right\} \tag{6}$$

If the voltage difference, $V_1' - V_2'$, is multiplied by a gain factor, G, to obtain a desired output voltage per degree of misalignment, the operating equation may be written as:

$$V = G \, (V_1' - V_2') = G \left\{ \left(A_{\theta_1} - A_{\theta_2} \right) + B \log \frac{\ell_{\theta_1} \, m_{\theta_1}}{\ell_{\theta_2} \, m_{\theta_2}} + B \log \frac{\left(1 - \frac{\theta_1}{\theta_o} \right)}{\left(1 - \frac{\theta_2}{\theta_o} \right)} \right\} \tag{7}$$

Next, one can write the angles, θ_1 and θ_2, in terms of the operating point angle, ϕ, and the misalignment angle, α:

$$\frac{\theta_1}{\theta_o} = \frac{\phi + \alpha}{\theta_o} \; ; \; \frac{\theta_2}{\theta_o} = \frac{\phi - \alpha}{\theta_o} \tag{8}$$

Using the above expressions and expanding the log of the angle ratio in series, one obtains

$$V = G \left\{ \left(A_{\theta_1} - A_{\theta_2} \right) + B \log \frac{\ell_{\theta_1} m_{\theta_1}}{\ell_{\theta_2} m_{\theta_2}} + 2B \left[\left(\frac{\alpha}{\theta_o - \phi} \right) + \frac{1}{3} \left(\frac{\alpha}{\theta_o - \phi} \right)^3 + \frac{1}{5} \left(\frac{\alpha}{\theta_o - \phi} \right)^5 + \cdots \right] \right\} \tag{9}$$

This last equation may be simplified as follows:

$$V = G \left\{ E(\alpha) + L(\alpha) + 2B \frac{\alpha}{\theta_o - \phi} \left[1 + \frac{1}{3} \left(\frac{\alpha}{\theta_o - \phi} \right)^2 + \frac{1}{5} \left(\frac{\alpha}{\theta_o - \phi} \right)^4 + \cdots \right] \right\} \tag{10}$$

where the abbreviated letters, $E(\alpha)$ and $L(\alpha)$, represent the first two terms in the right-hand member of Equation (9). Finally, the series in the square brackets of the above equation can be represented by the factor, $f(\theta_o, \alpha)$, and this equation can then be solved to yield the misalignment angle, α:

$$\alpha = \frac{\left[\frac{V(\alpha)}{G} - E(\alpha) - L(\alpha) \right] (\theta_o - \phi)}{2B \, f(\theta_o, \alpha)} \tag{11}$$

The defining equation above is repeated in Table 1 together with an explanation of the various quantities that appear in this equation.

B. Error Analysis

Having developed the above general expression for the relationship between the misalignment angle, α, and the output voltage, V, of the yaw attitude sensor, it is now easy to find the errors in any <u>indicated</u> attitude angle. This error is simply the difference between the two angles

TABLE 1

ERROR ANALYSIS

Assumptions and Definitions

Defining equation for the misalignment angle α:

$$\alpha = \frac{\left[\frac{V(\alpha)}{G} - E(\alpha) - L(\alpha)\right](\theta_o - \phi)}{2B\ f(\theta_o, \alpha)}$$

V is the output voltage of the yaw attitude sensor (YAS)

G is the effective amplification factor of the system beyond the log amplifier

B is the log amplifier sensitivity in volts per decade change in current

ϕ is the operating point angle of the system

θ_o is the angle of attack intercept of the linear approximation to the pressure versus angle of attack relationship

E is a correction term for any deviations from a true logarithmic characteristic in the log electrometer

L is a correction factor for both the nonlinearity of the pressure versus angle of attack relationship and for any nonlinearity in the pressure sensor (gauge) output current as a function of the pressure input

f is the correction factor for the first-order approximation to a logarithmic function involving the misalignment angle

Random errors in the constant terms G and B and the voltage V are assumed to be small compared with the known error terms, E, L, θ_o, and f. Alignment of the YAS null axis and vehicle axis will be within 4 minutes of arc. Roll and pitch cross coupling will be negligible within about $\pm$ 5 degrees. Wind errors are negligible.

as expressed with and without the correction terms. The final expression for the error angle, $\Delta\alpha$, between the true misalignment angle, α, and the uncorrected indicated angle, α_u, is given in Table 2.

A computation of the error angle was made next for a yaw attitude sensor system having the following characteristics:

(1) an ideal log amplifier, which can be approached in practice,

(2) a linear pressure sensor, which is approached in practice,

(3) linearization of the ram effect curves as drawn in Figure 2,

(4) an operating point angle of ϕ equal to 50 degrees,

(5) a log amplifier sensitivity of 1 volt per decade of current,

(6) an average intercept angle of θ'_o equal to 92 degrees, and

(7) a system gain, G, equal to 10.5 to yield an uncorrected sensitivity of 0.5 volts per degree of misalignment.

The results of the error computation are shown in Table 2 and Figure 4. Notice that errors due to the linear approximation of the ram effect curve (factor L) are negative while errors due to the simplification of the logarithmic term in the operating equation (factor Δf) are positive. The errors for the computation above for molecular nitrogen and atomic oxygen are shown as the lower two curves in Figure 4. The upper two curves in this figure refer to errors caused only by the simplification of the logarithmic term in the operating equation when an operating point angle of 65 degrees is used for the yaw attitude sensor.

Although the neutral atmosphere is relatively quiet and smooth, experiments have shown that large-scale high velocity winds are present up to altitudes of 130 km. These winds are caused by gravitational forces rather than pressure forces, and they have typical periods of the order of 12 hours. Table 3 lists five major wind flows. It can be seen from the table that only horizontal wind gradients and the effective wind due to rotation of the Earth can affect a neutral particle sensor. Any real cross wind of sufficient magnitude will change the direction of the relative wind vector and should be detected.

C. System Analysis

1. Transfer function. — The components of the yaw attitude sensor system that enter into the determination of the transfer function are shown schematically in Figure 5. The responses of each of the components of the system to an impulse function are represented on this schematic

TABLE 2

ERROR ANALYSIS FOR A TYPICAL SENSOR SYSTEM

The uncorrected operating equation of the sensor is:

$$\alpha_u = \frac{\frac{V}{G}(\theta'_o - \theta)}{2B},$$

where θ'_o is an assumed constant angle of attack intercept of the linear approximation to the pressure versus angle of attack relationship.

The error angle $\Delta\alpha$ between the true misalignment angle α and the uncorrected angle α_u is:

$$\Delta\alpha = \alpha_u - \alpha = \frac{1}{2B\,f}\left\{\frac{V}{G}(\theta'_o - \theta)\,\Delta f + \left[\frac{V}{G} - (E + L)\right]\Delta\theta_o + (E + L)(\theta'_o - \theta)\right\}$$

B = 1 volt/decade; G = 10.5, θ'_o = 92 degrees, $\Delta\theta_o = \pm 1$ degree, θ = 50 degrees

α DEG.	V VOLTS	V/G VOLTS	E VOLTS	L VOLTS	f	Δf	$\frac{V}{G}(\theta'-\theta)\,\Delta f$ VOLT-DEGREE	$\left[\frac{V}{G} - (E+L)\right]\Delta\theta_o$ VOLT-DEGREE	$(E+L)(\theta'-\theta)$ VOLT-DEGREE	$\Delta\alpha$ DEGREE
				-.0809		+	+	±1.271	-3.398	+
25	12.5	1.190	NEGL	(.0362)	1.1493	0.1493	7.462	(1.226)	(1.520)	2.32
				.0630				1.015	2.646	+(3.12)
20	10.0	0.952		(.0386)	1.0880	3.0880	3.518	(.991)	(1.621)	+ 0.87
				.0462				0.760	2.646	+(1.33)
15	7.5	0.714		(.0292)	1.0466	0.0466	1.397	(.743)	(1.226)	- 0.23
				.0292				0.505	1.226	+(0.44)
10	5.0	0.476		(.0246)	1.0196	0.0196	0.392	(.501)	(1.033)	- 0.16
				.0132				0.251	0.554	-(0.07)
5	2.5	0.238		(.0132)	1.0048	0.0048	0.048	(.251)	(0.554)	- 0.13
				0				0	0	0
0	0	0		(0)	1.0000	0	0			

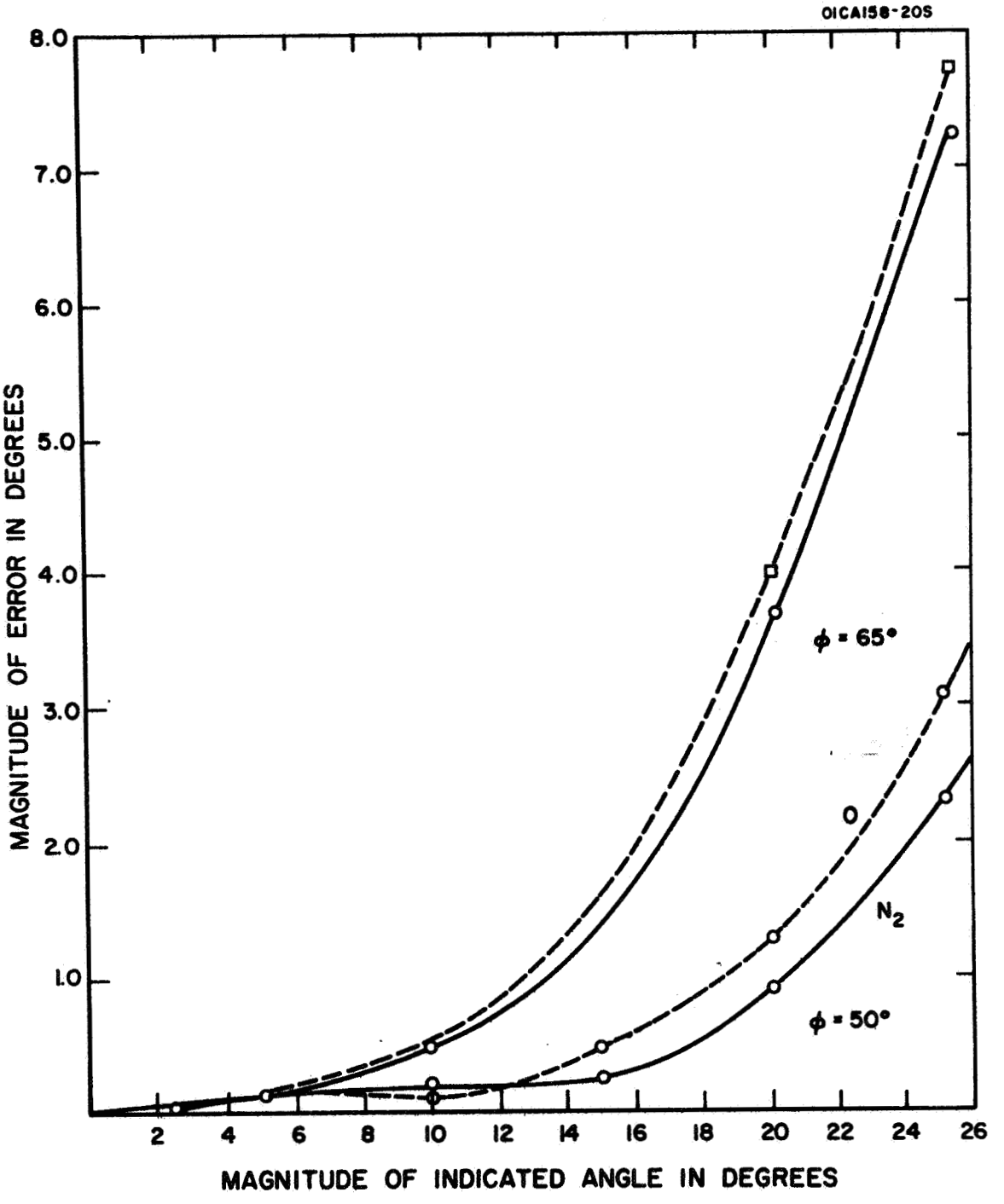

Figure 4. Typical error curves for a yaw attitude sensor.

TABLE 3

WINDS IN THE UPPER ATMOSPHERE

Type of Wind or Wind Gradient	Altitude Region	Wind or Gradient Amplitude	Typical Period
Tidal Flow	Up to 85 km	------	12 hours
Horizontal Shear Winds	100 to 130 km	Up to 200 m/sec	12 hours
Vertical Wind Gradients	100 to 130 km	Up to 100 m/sec per km	------
*Horizontal Wind Gradients	100 to 130 km	Up to 10 m/sec per km	------
**Effective Wind Due to Rotation of the Earth	Over the orbit	488 m/sec at the equator 0 m/sec at the poles	T/4

*The horizontal wind gradient can produce a change in wind velocity of about 80 m/sec near perigee. This is just 1 percent of the satellite velocity. The result of this wind change is to raise or lower the ram pressure for a head or tail wind by 1 percent. For a cross wind, the angle of the relative wind will change by 0.01 radians or 0.59 degrees. The YAS should detect this change and respond to it.

**For a satellite in a polar orbit this wind would be a max at the equator and would fall to zero at the poles a quarter of the orbital period T later. The YAS should detect and respond to this wind. The maximum angle for this relative wind is about 3.5 degrees.

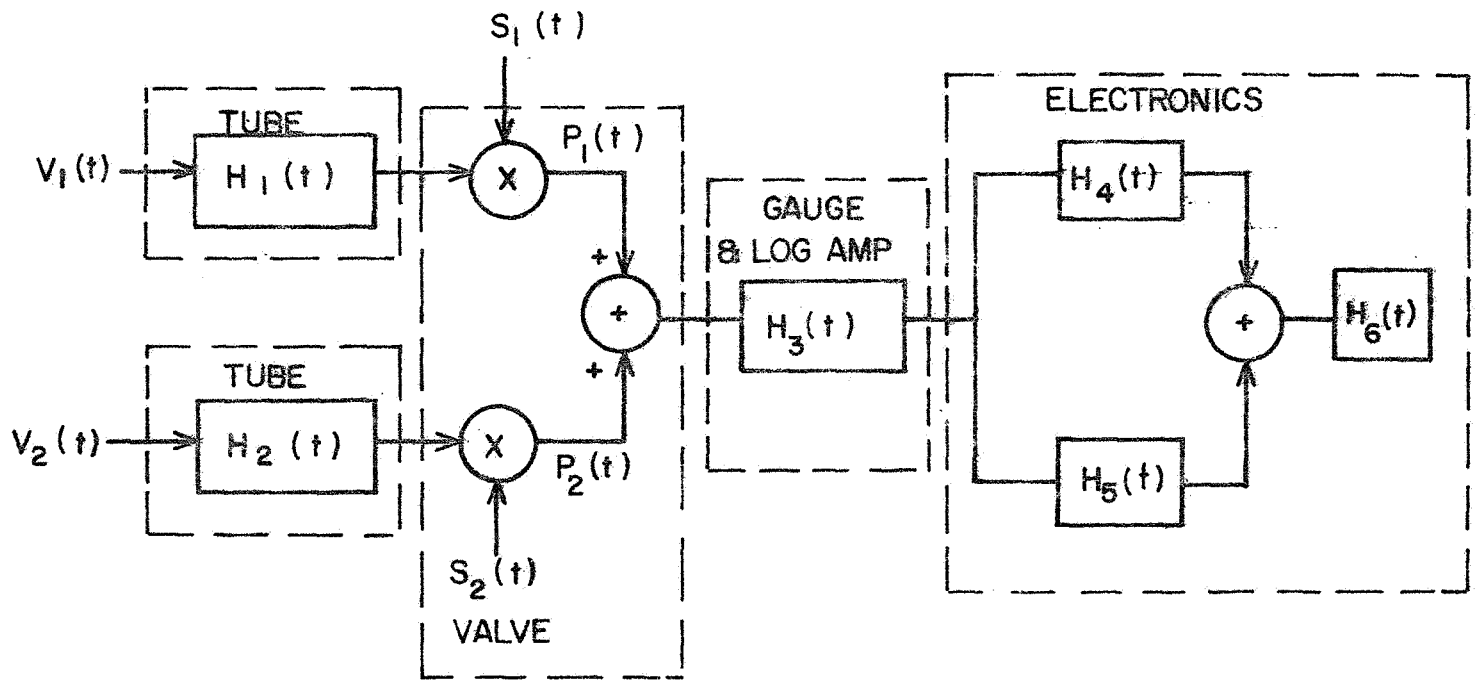

Figure 5. Schematic of sensor components.

as follows:

$H_1(t)$, $H_2(t)$ = response functions of the tube connected to the ports of the valve

$H_3(t)$ = response function of the valve, gauge, and log amplifier

$H_4(t)$, $H_5(t)$, $H_6(t)$ = response of the electronics that process the signal out of the log amplifier

The functions, $v_1(t)$ and $v_2(t)$, are time functions of the attitude angle of each tube which produce a change in the pressure at the input ports of the valve. $S_1(t)$ and $S_2(t)$ are periodic time functions which represent the opening and closing of the ports of the valve. The operation of the valve can be accurately represented as the product of $S_1(t)$ with the signal out of $H_1(t)$ added to the product of $S_2(t)$ with the signal out of $H_2(t)$.

The transfer function of the system is determined in stages starting with $v_1(t)$ and $v_2(t)$ and working progressively through the components of the system to the output. The signal at the first input port of the valve can be specified in the frequency domain as follows:

$$V_3(j\omega) = V_1(j\omega)\ G_1(j\omega) \tag{12}$$

where

$V_1(j\omega)$ = spectrum of $v_1(t)$

$V_3(j\omega)$ = spectrum of the signal at one port of the valve

$G_1(j\omega)$ = Fourier transform of $H_1(t)$

The output of the valve resulting from $V_3(j\omega)$ is

$$V_4(j\omega) = V_3(j\omega)\ S(j\omega) \tag{13}$$

where

$V_4(j\omega)$ = spectrum of the signal out of the valve due to the signal at the input of one port of the valve

$S(j\omega)$ = spectrum of the signal, $S_1(t)$

Since the signal, $S_1(t)$, is defined as a periodic function of time, its spectrum can be represented as follows:

$$S_1(j\omega) = A_n\ \delta\left(\omega - \frac{2\pi n}{T}\right) + \frac{1}{2} A_o \tag{14}$$

where

$\delta\left(\omega - \frac{2\pi n}{T}\right)$ = the delta function

A_n = a coefficient corresponding to the amplitude of the nth harmonic

A_o = the dc component

T = the period of $S_1(t)$;

therefore,

$$V_4(j\omega) = A_n V_3\left(\omega - \frac{2\pi n}{T}\right) \tag{15}$$

The signal at the input of the other port of the valve can be derived in the same manner. It should be noted that a relationship exists between $V_1(j\omega)$ and $V_2(j\omega)$ which can be used to simplify the derivation. For each frequency component of v_1, there is a corresponding frequency component of v_2 having the same amplitude but out of phase by 180 degrees. Therefore, $V_2(j\omega) = - V_1(j\omega)$. Also, the switching function, $S_2(t)$ is the same as $S_1(t)$ but shifted 180 degrees in phase. Therefore, $S_2(j\omega) = - S_1(j\omega)$. The frequency spectrum of the signal applied to the gauge is

$$V_5(j\omega) = \sum_{n=1}^{\infty} \left\{G_1\left[j\left(\omega - \frac{2\pi n}{T}\right)\right] + G_2\left[j\left(\omega - \frac{2\pi n}{T}\right)\right] A_n V_1\left[j\left(\omega - \frac{2\pi n}{T}\right)\right]\right\}$$

$$+ A_o V(o) \tag{16}$$

The signal out of the gauge and the log amplifier is

$$V_6(j\omega) = G_3(j\omega) V_5(j\omega) \tag{17}$$

where $G_3(j\omega)$ is the Fourier transform of $H_3(t)$.

The remainder of the electronics recovers the signal $V_1(j\omega)$ from $V_6(j\omega)$. This consists of translating the frequency spectrum of $V_6(j\omega)$ down by an amount equal to $2\pi/T$ and eliminating the higher harmonics of the valve frequency. The output signal is

$$V_7(j\omega) = \left[G_1(j\omega) - G_2(j\omega)\right] A_n V_1(j\omega) G_3\left[j\left(\omega + \frac{2\pi}{T}\right)\right] \tag{18}$$

The transfer function of the system is therefore

$$\frac{V_7(j\omega)}{V_1(j\omega)} = K A_n \left[G_1(j\omega) + G_2(j\omega)\right] G_3 \left[j\left(\omega + \frac{2\pi}{T}\right)\right] \tag{19}$$

The tubes leading to the valves are sufficiently short and large enough in diameter to indicate that $G_1(j\omega)$ and $G_2(j\omega)$ can be considered as constant up to a frequency that exceeds the frequency spectrum of interest. Therefore, the transfer function of the system is the same as the transfer function of the valve and log amplifier translated down in frequency by an amount equal to the valve frequency and is

$$G(j\omega) = G_3 \left[j\left(\omega + \frac{2\pi}{T}\right)\right] \tag{20}$$

2. Determination of gauge and valve transfer function. — The transfer function, $G_3(j\omega)$, was determined experimentally. A schematic diagram of the experimental system is given in Figure 6. A pressure, P_1, was applied to one input port of the valve and a pressure, P_2, different from P_1, was applied to the other input port. The valve was rotated at a specified frequency causing a periodic pressure variation to be applied to the gauge and log amplifier. The fundamental frequency of this periodic pressure signal was equal to the valve frequency. The voltage out of the log amplifier was applied to a pen recorder, and a strip record of the voltage signal was made. A phase reference signal was also recorded on the strip record by applying to another channel of the recorder a signal that indicated the time when one port of the valve began to open.

An analysis of the strip recording produced points on asymptotic lines of the transfer function giving corner frequencies of 0.154 c/s at the lower corner frequency and 4.45 c/s at the upper corner frequency. Therefore,

$$G_3(j\omega) = \frac{j\omega}{(j\omega - \omega_o)\,(j\omega - \omega_1)} \tag{21}$$

where

ω_o = 0.97 radians per second

ω_1 = 28 radians per second

The transfer function of the yaw sensor system is

$$G(j\omega) = \frac{j\left(\omega + \frac{2\pi}{T}\right)}{\left[j\left(\omega + \frac{2\pi}{T}\right) - \omega_o\right]\left[j\left(\omega + \frac{2\pi}{T}\right) - \omega_1\right]} \tag{22}$$

The transfer function of the gauge is shown in Figure 7.

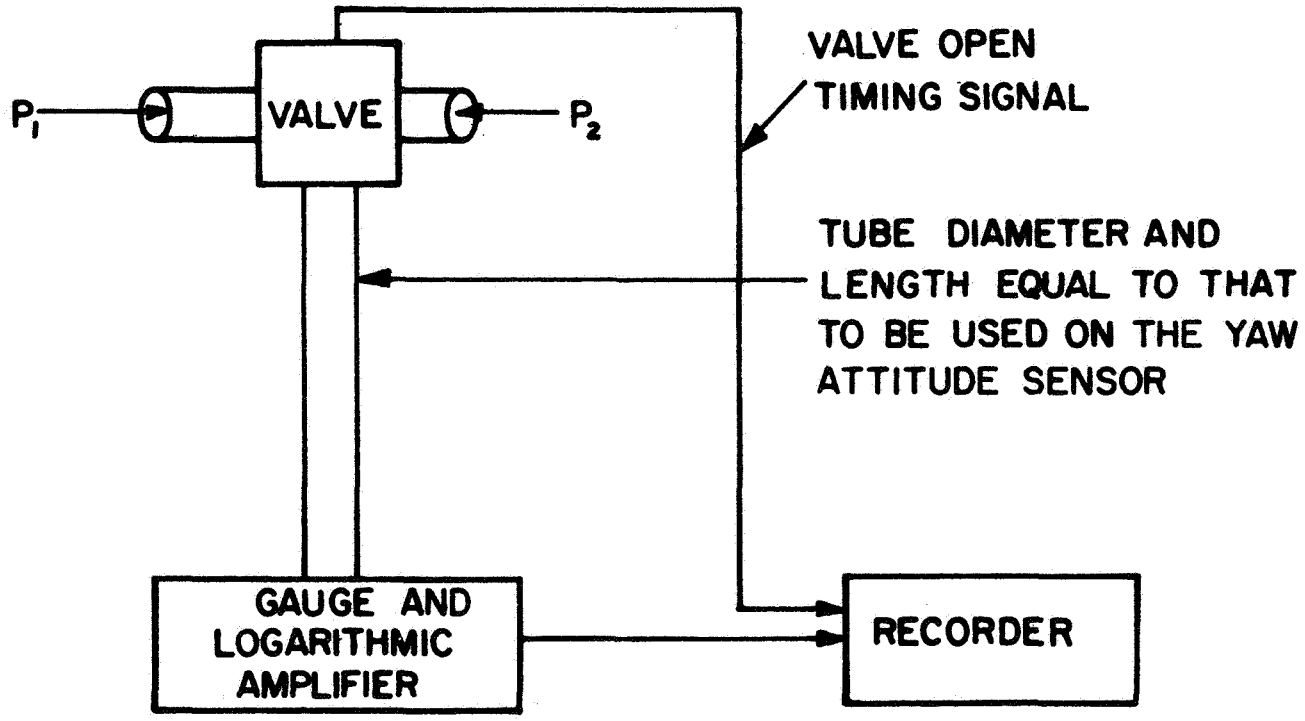

Figure 6. Diagram of experimental equipment to determine the valve, gauge and amplifier transfer function.

01E32-270S

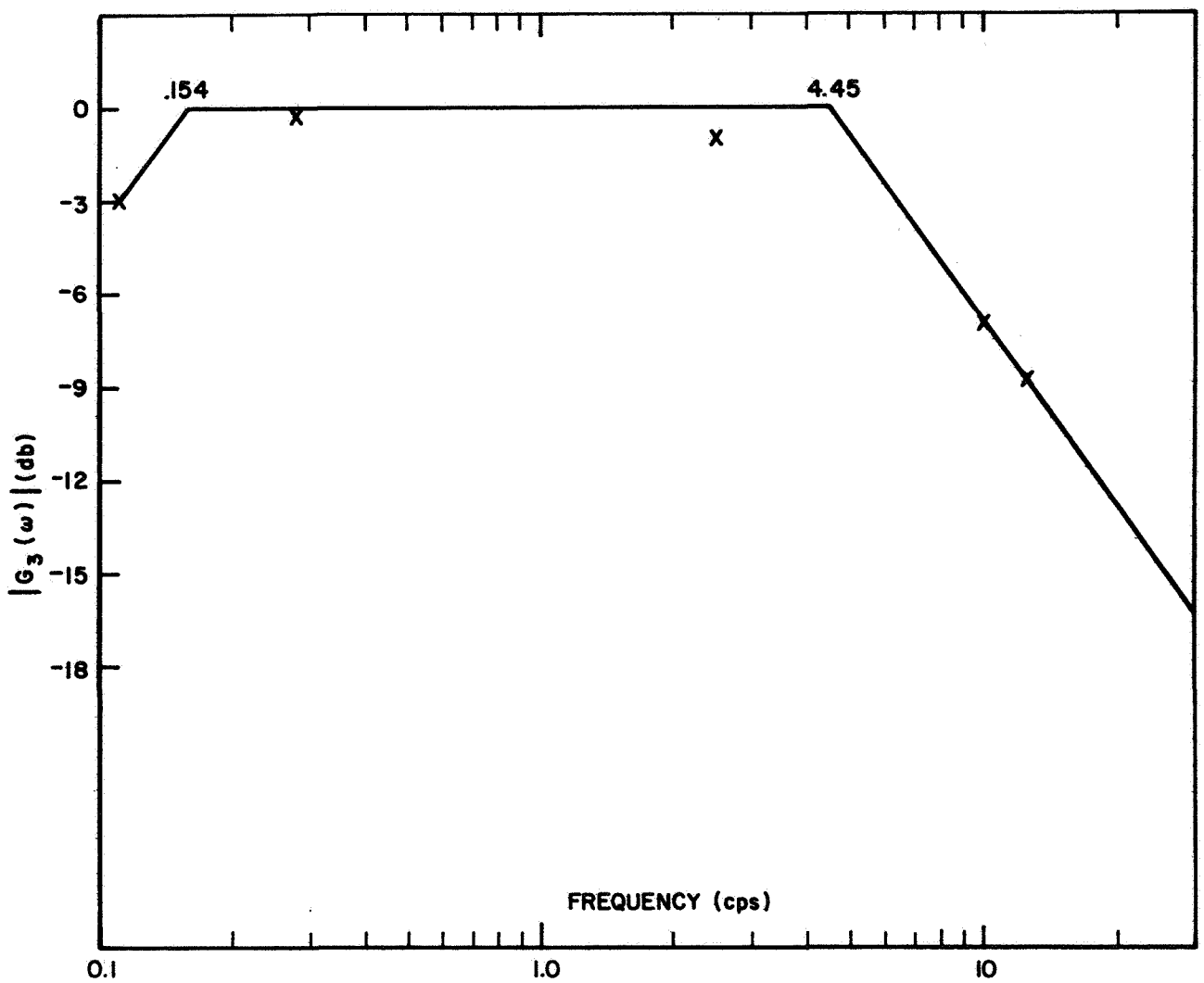

Figure 7. Transfer function of the gauge.

As a result of this analysis, it was discovered that the upper corner frequency was approximately the same as the valve frequency. It is recognized that some adjustment should be made in the design of the system such that the valve frequency is somewhat lower than the upper corner frequency.

3. Yaw attitude sensor noise. — The experimental system shown in Figure 6 was also used to obtain a record of the noise voltage. In this case, the pressure on one input port of the valve was set equal to the pressure on the other input port of the valve. The voltage output of the experimental system was recorded. Figure 8 shows a two-second segment typical of this record with the valve operating at approximately 4 c/s.

No thermal or random noise was observed in the recording. A sinusoidal noise signal at the frequency of the valve is observed to be the dominant undesirable signal with a very small signal component also visible, which appeared to be 60 c/s pickup. The magnitude of the voltage at the valve frequency corresponded to an input angular error signal of about $\pm$ 1/8 degree. It is expected that this signal is caused by the demodulator synchronizing signal that is derived at the valve being coupled into the output circuits.

D. Test System

One method of simulating the pressure input to a yaw attitude sensor system is to connect each gas input tubulation to a source of low pressure gas having the same composition as the gas to be measured in flight. A zero angle of attack condition would be simulated by having the same pressure at each tubulation of the cycling valve. Non-zero angles of attack would be simulated by having one tubulation at a higher pressure than the other. Since each gas input tubulation is connected to a separate source of low pressure gas as developed in separate chambers by separate vacuum pumping systems, the general method of simulation will be called the "two-chamber simulation method."

The two-chamber method of simulation is illustrated graphically in Figure 9. The mechanical cycling valve operates by providing a relatively large vacuum conductance (say 20 or 30 liter/s) in the "open" position and a relatively small vacuum conductance (of the order of 10^{-3} liters/s) in the "closed" position. The "closed" or leakage vacuum conductance of the valve is small enough so that a relatively large pressure difference can be maintained between the high and the low pressure chambers. The amount of gas that the valve transfers from the high pressure to the low pressure chamber per unit time is simply the product of the valve and pressure gauge volume, V, and the valve cycling frequency, f. For example, if the volume, V, is 0.1 liter and the valve rotates at a frequency of 1 cycle per second, it will transfer 0.1 liter/s of "high"

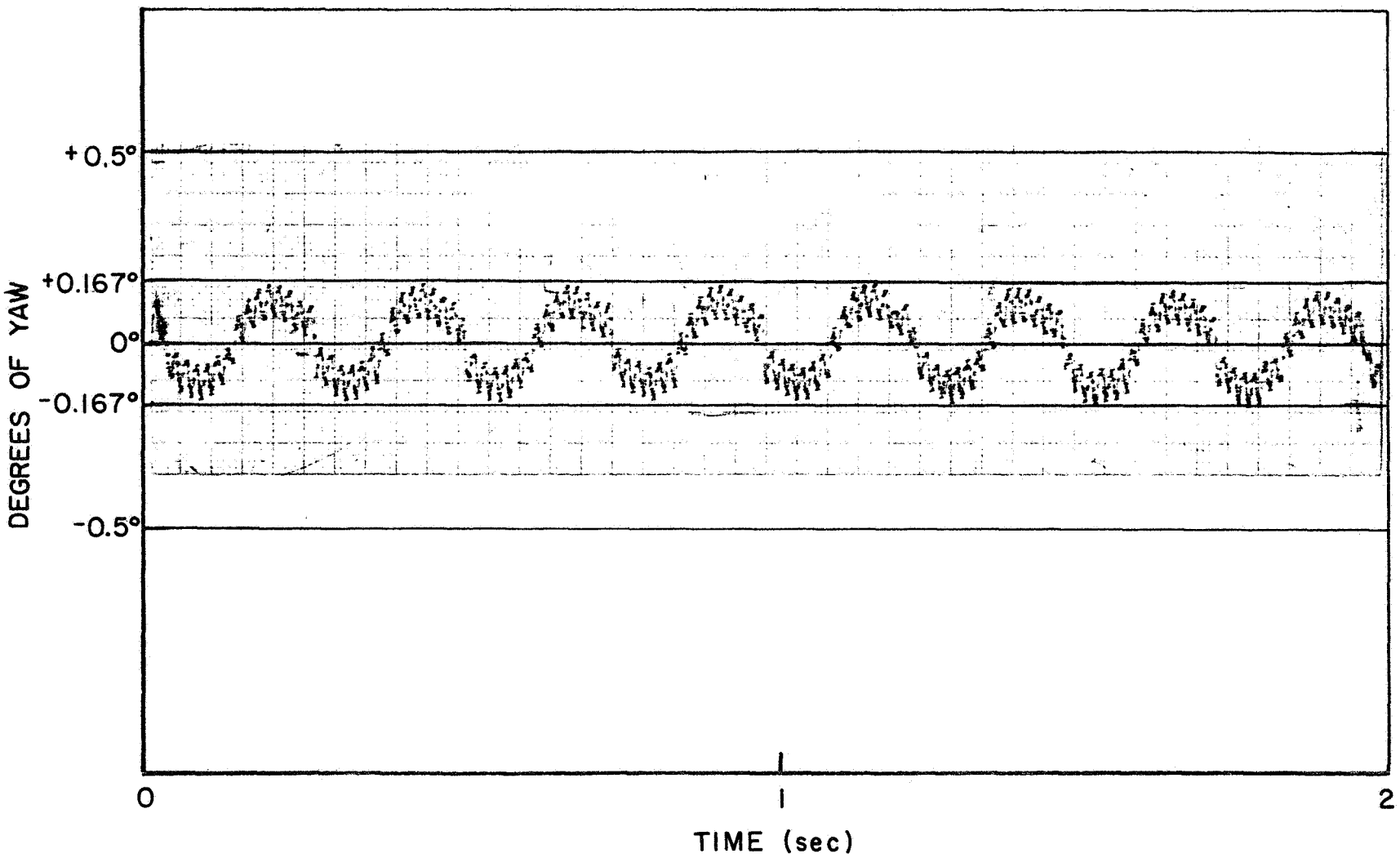

Figure 8. Yaw attitude sensor null-signal noise record.

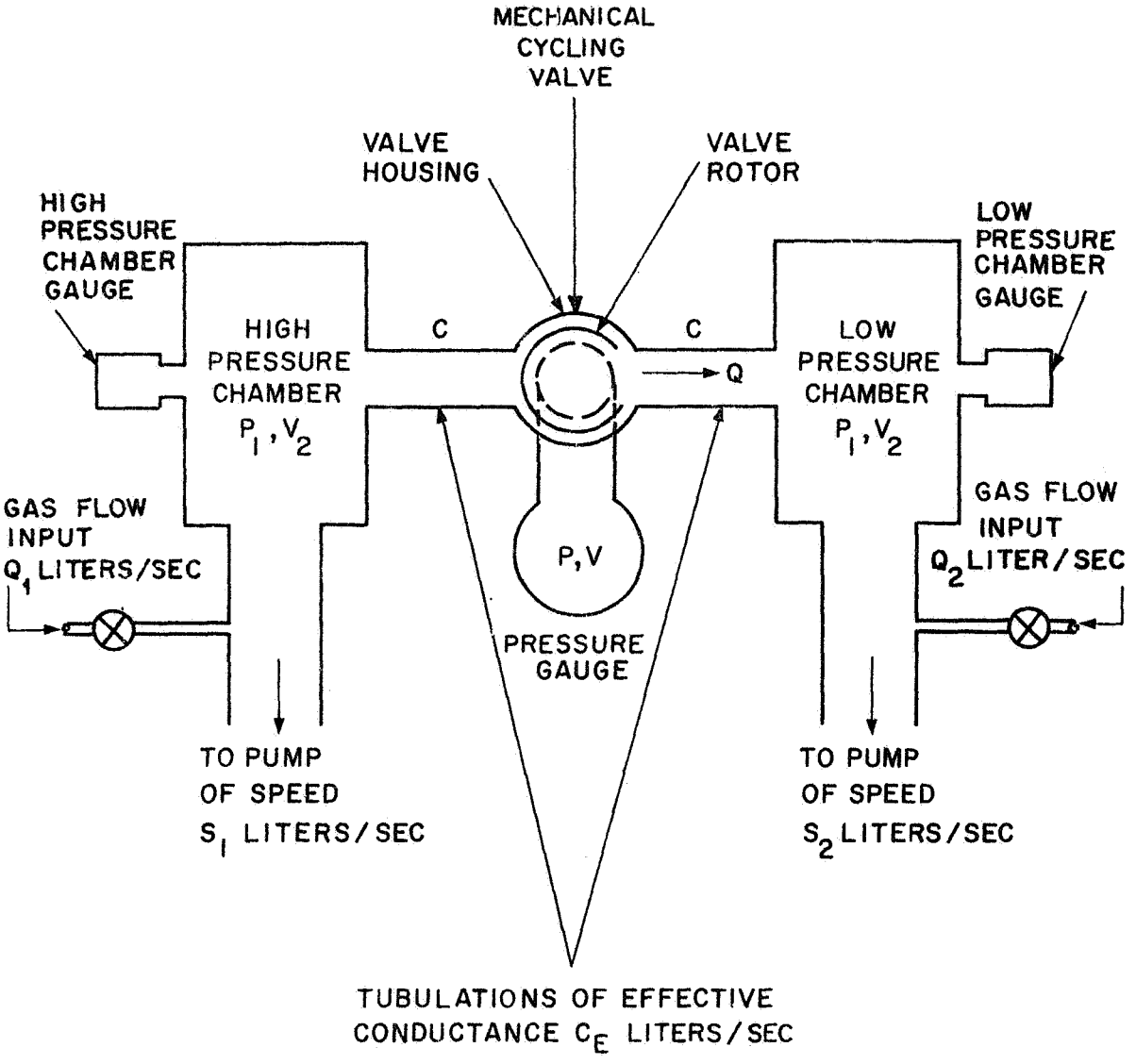

Figure 9. Two-chamber simulation method schematic.

pressure gas to the low pressure chamber. Another way of stating this is to say that the "effective operating vacuum conductance," C_E, of the valve when operating at 1 c/s is 0.1 liter/s. The term "high" pressure as used here simply means a higher pressure than that which exists in the "low" pressure chamber. Actually, the gas pressure in either chamber is many orders of magnitude below atmospheric pressure.

The maximum ratio of high pressure to low pressure that can be maintained in the two chambers depends on the "effective operating vacuum conductance" of the mechanical cycling valve as defined above. Consider, for example, the flow of gas from the high pressure chamber to the cycling valve, to the low pressure chamber and then to the pump of the low pressure chamber. Equating the gas flow through the valve to the gas pumped out of the low pressure chamber (assuming that the external gas flow input Q_2 to the low pressure chamber, as shown in Figure 9, is zero), one obtains

$$\frac{P_1}{P_2} = 1 + \frac{S_2}{C_E} \tag{23}$$

The ratio of the high pressure P_1 to the low pressure P_2 may be 1000 or greater if the pumping speed S_2 of the low pressure chamber is large compared to the effective operating vacuum conductance C_E of the valve. When the valve is in the closed position, the effective conductance, C_E, becomes the valve leakage conductance, which is much less than the effective operating conductance.

The operating time constant of the two-chamber simulation system for gas exchange may be derived in the following manner. Consider the situation that exists when the mechanical cycling valve and the pressure gauge have been filled with a sample of high pressure gas at a pressure P_1 and the valve just begins to discharge this high pressure gas into the the low pressure chamber which is at a pressure P_2. The low pressure chamber then has gas flowing into it from two sources: a flow, Q, from the valve and pressure gauge, and a gas flow input, Q_2, from an external source. The pressure P_2 in the low pressure chamber will then be

$$P_2 = \frac{(Q + Q_2)}{S_2} \tag{24}$$

The gas flow, Q, may be expressed in terms of the total valve tubulation conductance, C (see Figure 9) and the pressure difference $P - P_2$ across this conductance. If the gas flow, Q, is also equated to the change in the quantity of high pressure gas within the valve and pressure gauge, one has

$$Q = C(P - P_2) = - V \frac{dP}{dt} \tag{25}$$

The pressure, P, is the time varying pressure within the valve and pressure gauge and the volume, V, is the volume of the valve and pressure gauge as before. From the two equations above, one derives the differential equation

$$\frac{dP}{dt} + \left[\frac{CS_2}{V\ (C + S_2)} \right] P = \frac{CQ_2}{V\ (S_2 + C)} \tag{26}$$

The conductance, C, is really a function of time since it involves the changing aperture conductance of the valve as well as the fixed conductance of the long tubulations that join the valve to the test chambers. However, as a first approximation, assume that C has a constant average value during the valving cycle. Equation (26) then becomes a first order, linear differential equation with constant coefficients. If one imposes the initial condition that at time $t = 0$, $P = P_1$, the solution becomes:

$$P = \frac{Q_2}{S_2} + \left[P_1 - \frac{Q_2}{S_2} \right] \exp\left(- \frac{CS_2}{V\ (C + S_2)}\ t \right) \tag{27}$$

The time constant for this exponential solution is:

$$\tau = \frac{V\ (C + S_2)}{CS_2} \tag{28}$$

Since ordinarily S_2 is much greater than C, one can write

$$\tau \cong \frac{V}{C} \quad S_2 \gg C \tag{29}$$

By making the valve orifice and valve tubulations sufficiently large and the valve and gauge volume small, the time constant for gas exchange can be made small. For example, if the average conductance, C, is 10 liters/s and the volume, V, is 0.1 liter, then $\tau = 0.01$ second.

The two-chamber simulation method should have great usefulness because the pressure modulation amplitude can be varied over a wide range.

3. DESIGN

A. Overall System Design

As shown in Figure 1, the yaw attitude sensor contains six elements. These basic elements are a pressure sensor, a mechanical cycling valve and drive circuit, gas flow tubulations, a high voltage power supply, a logarithmic electrometer, and a phase sensitive detector. The central element of the system is the pressure sensor, in this case a cold cathode ionization gauge. The ionization gauge is periodically and alternately connected, by means of a cycling valve, to one of two gauge position orifices located a few inches away from the vehicle surface and joined to the valve by gas flow tubulations. The period of one complete cycle is of the order of several hundred milliseconds, so that each gauge position pressure is sampled for a period of about 100 milliseconds. These time periods can be modified as required. The cycling valve is driven via magnetic coupling. In this way, the valve and pressure gauge are sealed off from the interior of the vehicle and cannot be affected by any outgassing within the vehicle. The detailed design and operation of the mechanical cycling valves will be described shortly in a separate section. The use of magnetic coupling provides an additional benefit in that a pickup coil circuit may be used to provide pulse inputs to the phase sensitive detector for phase reference.

The cold cathode ionization type vacuum gauge normally uses a high voltage of approximately 4 kV at low current drain. The current output of the gauge is amplified by a logarithmic electrometer in order to cover a 5 decade range of pressure signals. A wide dynamic range is required to accommodate the molecular ram effect pressure variation and the variation of pressure with altitude.

The output of the logarithmic amplifier is passed on to the phase sensitive detector. In the phase sensitive detector, the dc component of the pressure signal is removed and the ac modulation amplitude is converted into a dc error signal of either polarity, depending on the phase of the modulation. The error signal is, of course, a measure of the departure from the balanced or equilibrium orientation position. The fractional change in the output of the logarithmic amplifier will be less than the fractional change of the current input (corresponding to an equivalent pressure change for a linear pressure gauge). However, for a given fractional change of the current (pressure), the absolute change in the output voltage of the amplifier will not vary over the range of operation. For example, for a logarithmic amplifier that covers the range from 10^{-3} to 10^{-8} amperes and delivers output voltages from 0 to 5 volts over this 5 decade range, a fractional current input change of 7.5 percent (corresponding to a fractional pressure change of 7.5 percent as caused by a 1 degree yaw misalignment) will yield a voltage change of 32.5 millivolts, regardless of the absolute value of the output

voltage. The log electrometer voltage difference of 32.5 millivolts can be amplified to yield an error signal voltage difference of 0.5 volt, or any other desired voltage.

B. Vacuum Gauge Theory and Characteristics

The magnetron type cold cathode ionization type vacuum gauge is basically a crossed electric-magnetic field device. The gauge operates by creating an electrical discharge in a low pressure gas in the presence of a magnetic field. The gauge electrodes are geometrically shaped so as to create an electrical "potential well" within some volume of the gauge when appropriate voltages are applied to these electrodes. Electrons within the region of the electrical potential well (and in the magnetic field) are constrained to move and remain in this region for comparatively long periods of time. In this way, the electrons are more effective in ionizing gas molecules and creating positive ions. The positive ions are collected at the cathode of the gauge. The flow of positive ion current is found to be proportional to the number density or pressure of the gas molecules within the gauge.

Under ordinary conditions, there are always some free electrons within a low pressure gas due to the effects of cosmic rays and naturally occurring radioactive materials. When a high potential of several thousand volts is applied between electrodes that are located within the low pressure gas, the electrons attempt to move in the direction of the electric field. If a strong magnetic field is present, the electrons are forced to move in cycloidal or spiral paths so that they cannot easily reach the anode.

The discharge in a cold cathode gauge is believed to be a self-sustained Townsend discharge. Electrons that are in the gauge initially, and electrons which are emitted from the cathode by cold field emission, have collisions with gas molecules, thereby producing positive ions and additional free electrons. The positive ions are not deflected much by the magnetic field and so they can easily reach the cathode. When the high voltage positive ions bombard the cathode, they cause secondary electrons to be emitted from the cathode, thus further swelling the electron population in the gauge. This multiplication process continues until a self-sustaining discharge occurs. The discharge reaches a stable operating condition when the number of electrons and ions created per unit time just equals the number that are lost per unit time.

The cold cathode ionization gauge pressure sensor will cover a pressure range from the 10^{-12} torr region to the 10^{-3} torr region. The gauge response curve will vary with the details of the gauge construction, the magnetic field, and the applied high voltage. Generally speaking, magnetron type cold cathode ionization gauges are linear in response for pressures from 10^{-3} to 10^{-9} or 10^{-10} torr, with typical sensitivities of 1 to 5 amperes/torr when the magnetic field is 1000 gauss and the high

voltage varies between 1 kV and 4 kV. For pressures below 10^{-9} torr, the gauge is nonlinear, with the output current proportional to approximately the 1.3 power of the pressure. Thus, the sensitivity of the gauge begins to decrease in a known and reproducible manner at these low pressures. At the very lowest pressures, when there are not enough molecules present to support the discharge, the gauge will extinguish. However, due to the presence of a small amount of radioactive material that has been deliberately placed within the gauge, the discharge will start again as soon as the pressure increases above a threshold value.

Some of the advantages of the GCA magnetron type cold cathode ionization gauge as compared with other gauges are as follows:

(1) Only two electrodes are used instead of the three electrodes of Redhead's design.

(2) By placing the metal envelope of the gauge at ground potential, it is impossible to have any electrical surface leakage current from the high voltage anode to the cathode.

(3) There are no glass surfaces present that can become electrically charged and thus distort the electric field.

(4) The aperture in the anode that faces the gauge tubulation gives the gauge a greater speed of response.

(5) The ceramic insulators in the gauge are outside of, and shielded from, the active discharge region.

(6) The metal envelope electrically shields the discharge from external electrical disturbances.

(7) The metal-ceramic structure of the gauge makes it very sturdy mechanically. The gauge has passed the vibration test specified for S-6 satellite prototype components.

The gauge and magnet assembly weighs about 2-1/2 pounds and will fit within a space 3-3/4 x 3 x 2-3/4 inches. Because of its ceramic-metal construction, the gauge will withstand bakeout temperatures up to 500°C, and, in general, will operate over a relatively wide temperature range.

Some of the important gauge specifications are listed below:

(1) Pressure range — 10^{-12} to 10^{-3} torr

(2) Range of linearity — 10^{-9} to 10^{-3} torr

(3) Linear range sensitivity — 4.5 amperes/torr at 4.0 kV

(4) Magnetic field — 1000 gauss

(5) Speed of response — will follow a decade increase in pressure in less than 0.1 second

(6) Starting time — less than 90 seconds at 10^{-12} torr

(7) Environmental — passed S-6 prototype vibration test

(8) Temperature — will operate at least from $-100^{\circ}C$ to $+100^{\circ}C$

A photograph of the GCA cold cathode ionization gauge pressure sensor is shown in Figure 10.

C. Mechanical Cycling Valve Designs

The mechanical valve is a critical part of the complete system since the valve must operate unattended for long periods of time in a hard vacuum. The valve must use only ultra-high vacuum materials since it will be handling gas at very low pressures. Ideally, there should be no metal-to-metal contact within the valve to eliminate the possibility of cold welding and the spurious generation of gas due to surface abrasion.

Because of the stringent requirements enumerated above, three separate paths in the design of the mechanical valve were followed with the expectation that at least one of these designs would prove superior. All of the designs attempt to achieve a high ratio between the open and closed vacuum conductance of the valve from either tubulation to the ionization gauge. Thus, there would be no metal-to-metal contact during valve "closure."

1. The linear reciprocating valve. — The linear reciprocating valve, as shown in the schematic of Figure 11, consists of two metal bellows-sealed poppet assemblies controlling the flow from two inlet ports. An adequate open-to-closed vacuum conductance ratio can be obtained by making the radial clearance between the poppet and inlet port small, about 1 mil, and by selecting the proper insertion depth or overlap of the poppet into the port in the closed position. The valve body containing the two inlet ports, gauge connection and poppet assemblies would be machined from one piece. The poppet assemblies were designed to be welded into the bottom of the valve body. The bottom of the valve body has a flange and O-ring groove to which the drive assembly can be mounted. A magnetic drive assembly would consist of one pair of solenoid coils to drive the poppets and another pair of coils to drive counterbalance assemblies which would have the same mass and spring rate as the poppets. Each counterbalance would operate synchronously with its opposing poppet, resulting in zero reaction within the spacecraft.

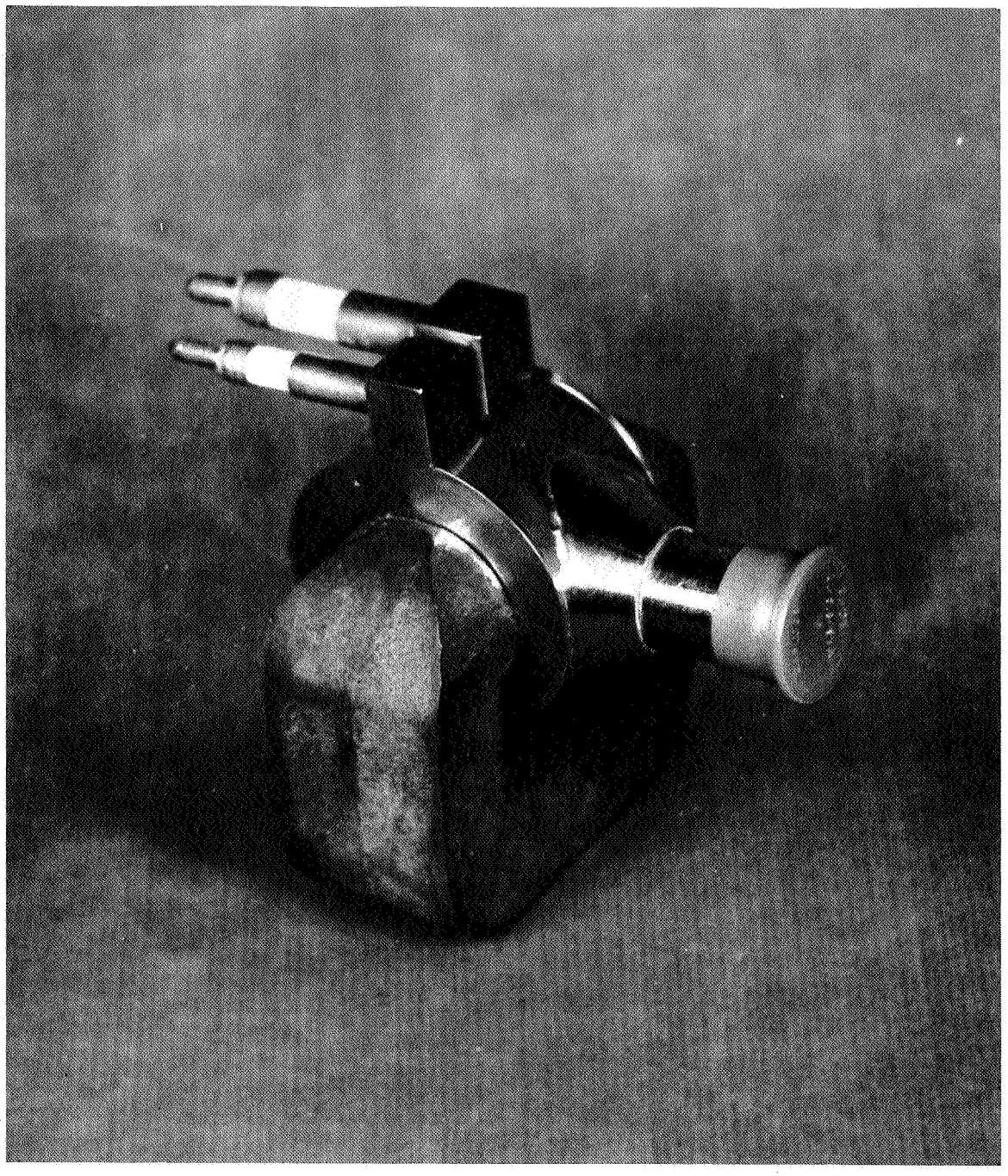

Figure 10. Photograph of the GCA Model R-5 cold cathode ionization gauge and magnet.

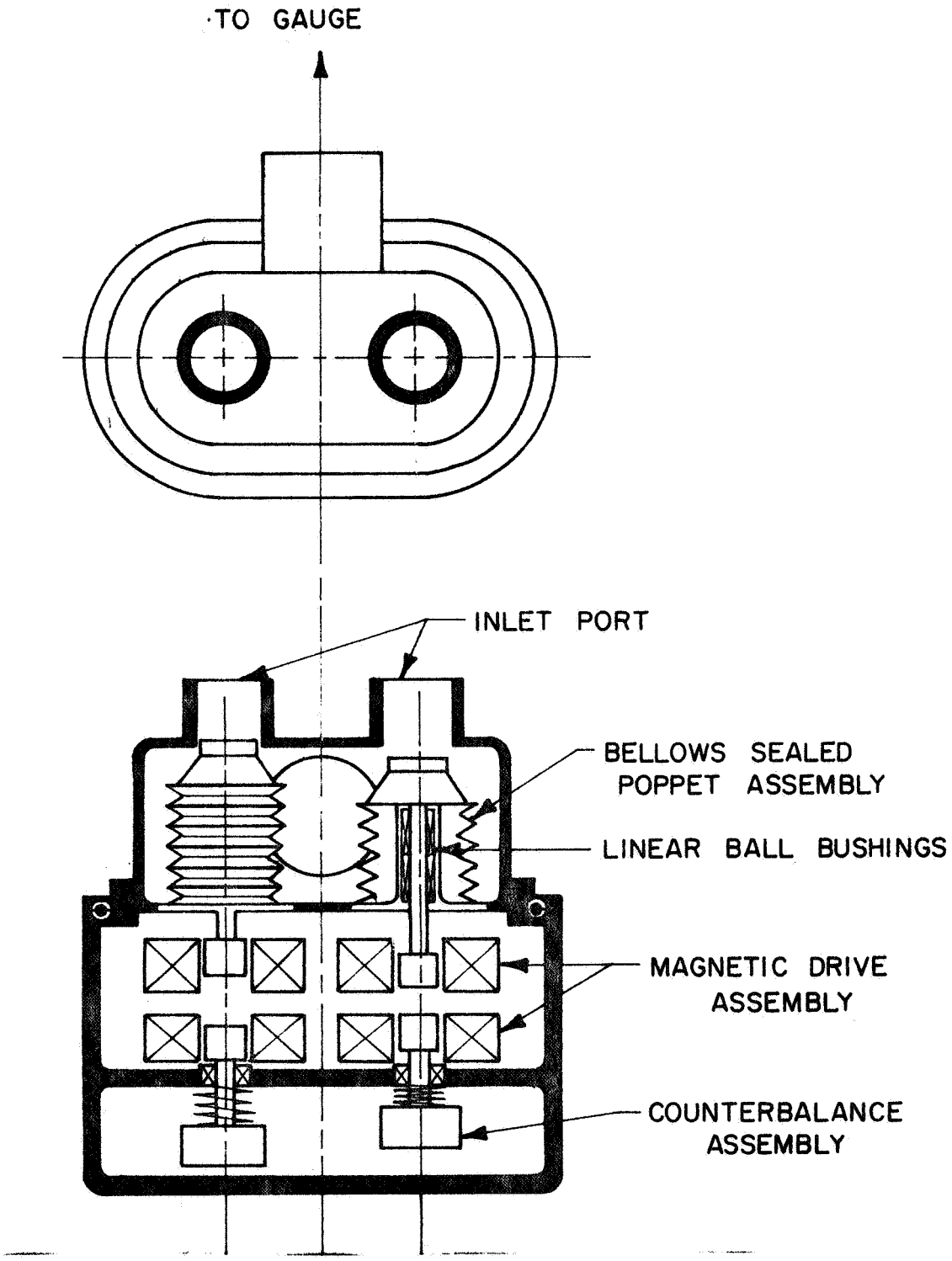

Figure 11. Linear reciprocating valve schematic.

Each poppet would be guided and supported by a pair of Thompson linear ball bushings and factory matched shafts that can be lubricated for a three-year operating life. The matched shafts and ball bushings are concentric within a few tenths of a mil. The bearings and bellows selected can also meet a three-year or 100 million cycle requirement at a 1 c/s rate. The bellows in this valve would be of the welded metal variety. This kind of bellows has a maximum life expectancy and a reasonably low spring rate. They can be made out of any metal that can be welded, but they are quite expensive.

The design of this valve is shown in greater detail in the layout drawing of Figure 12. The design allows the valve body to be removed from the drive assembly to permit high temperature vacuum bakeout of the valve body without breaking the vacuum. If the poppets are counterbalanced, they can be operated non-synchronously to obtain optimum time phasing and on-off time ratios without transmitting undesirable impulses to the vehicle.

As shown in Figure 13, a direct mechanical drive system could consist of a motor-driven drive shaft turning a pair of double eccentrics. Each double eccentric, by means of the cam followers shown, imparts an equal and opposite linear reciprocating motion to one poppet drive shaft and its associated counterbalance drive shaft. The two poppets that open and close the gas inlet ports may be phased independently without unbalancing the system. As the drive shaft is rotated, the poppets operate 180 degrees out of phase, alternately opening the two inlet ports to the gauge. The crossover point, or half-stroke position, of the poppets occurs when both inlet ports are closed, resulting in a "break before make" mode of operation to minimize mixing between the two inlets.

A drawing of the assembly of a linear reciprocating valve, an R-5 gauge and magnet and gas inlet ports is presented in Figure 14. The valve drive mechanism does not appear in this figure. It can be seen that the overall structure is relatively large and rather wasteful of space. The awkward configuration of this valve, together with the high cost of its construction were factors in the decision to stop its construction after about one half of the assembly was completed. Notwithstanding these drawbacks, the linear reciprocating valve has a number of important advantages, some of which are listed below.

(a) The valve can be driven by either magnetic coupling or by a direct mechanical drive.

(b) The design permits the use of lubricated bearings in a sealed drive assembly. These bearings have a proven reliability.

(c) The design uses bellows that have a proven long operating lifetime.

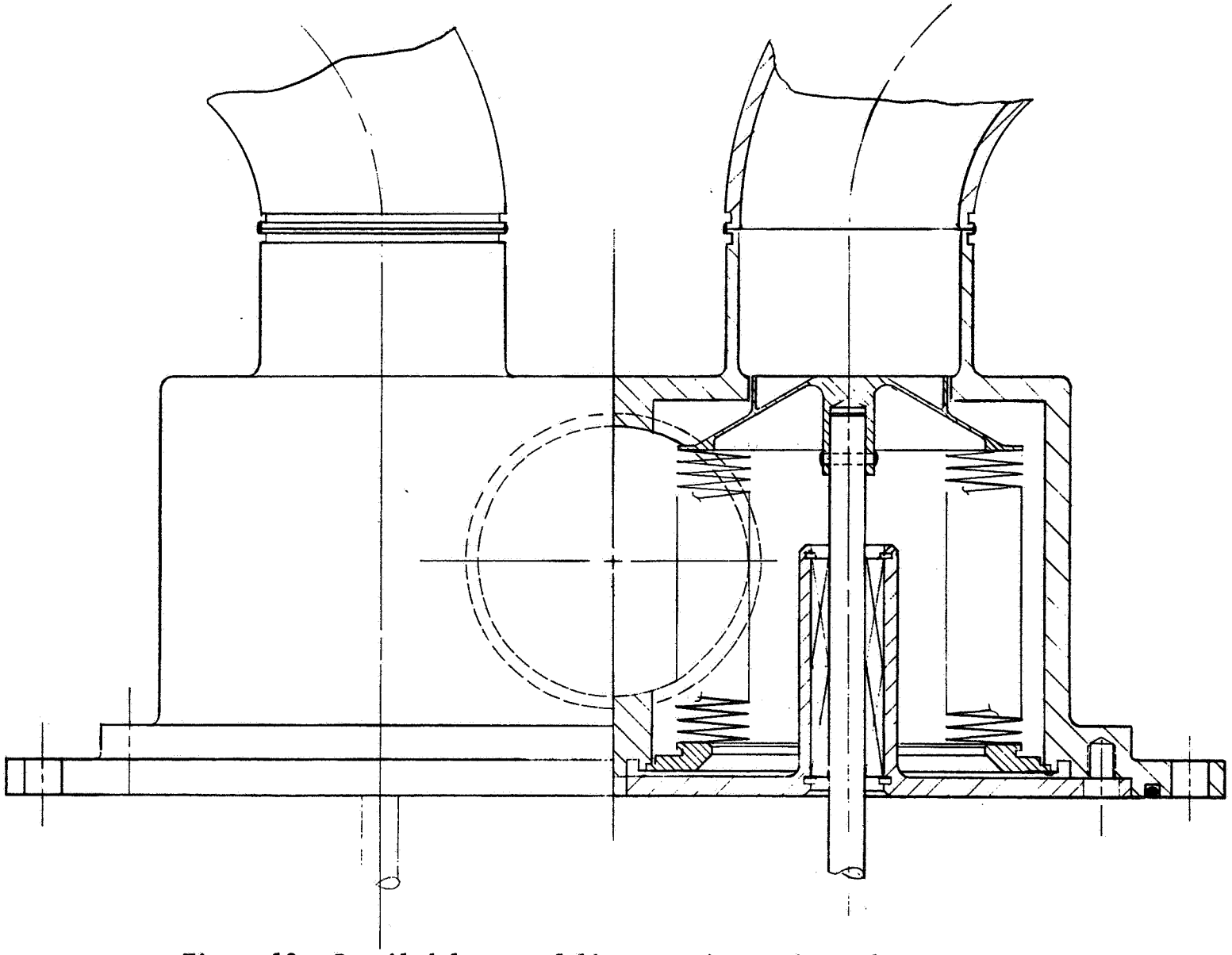

Figure 12. Detailed layout of linear reciprocating valve

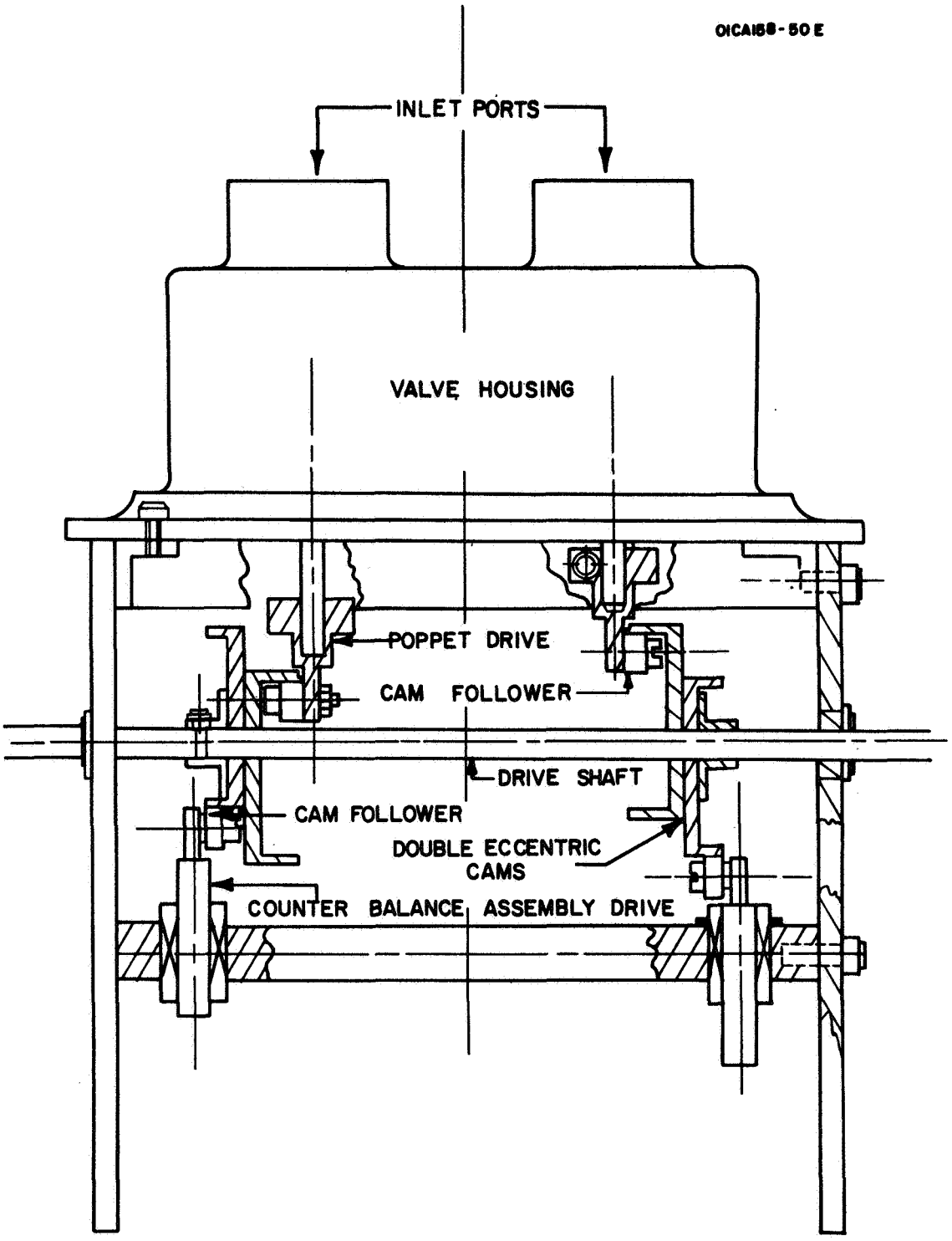

Figure 13. Mechanical cam follower drive for the linear reciprocating valve.

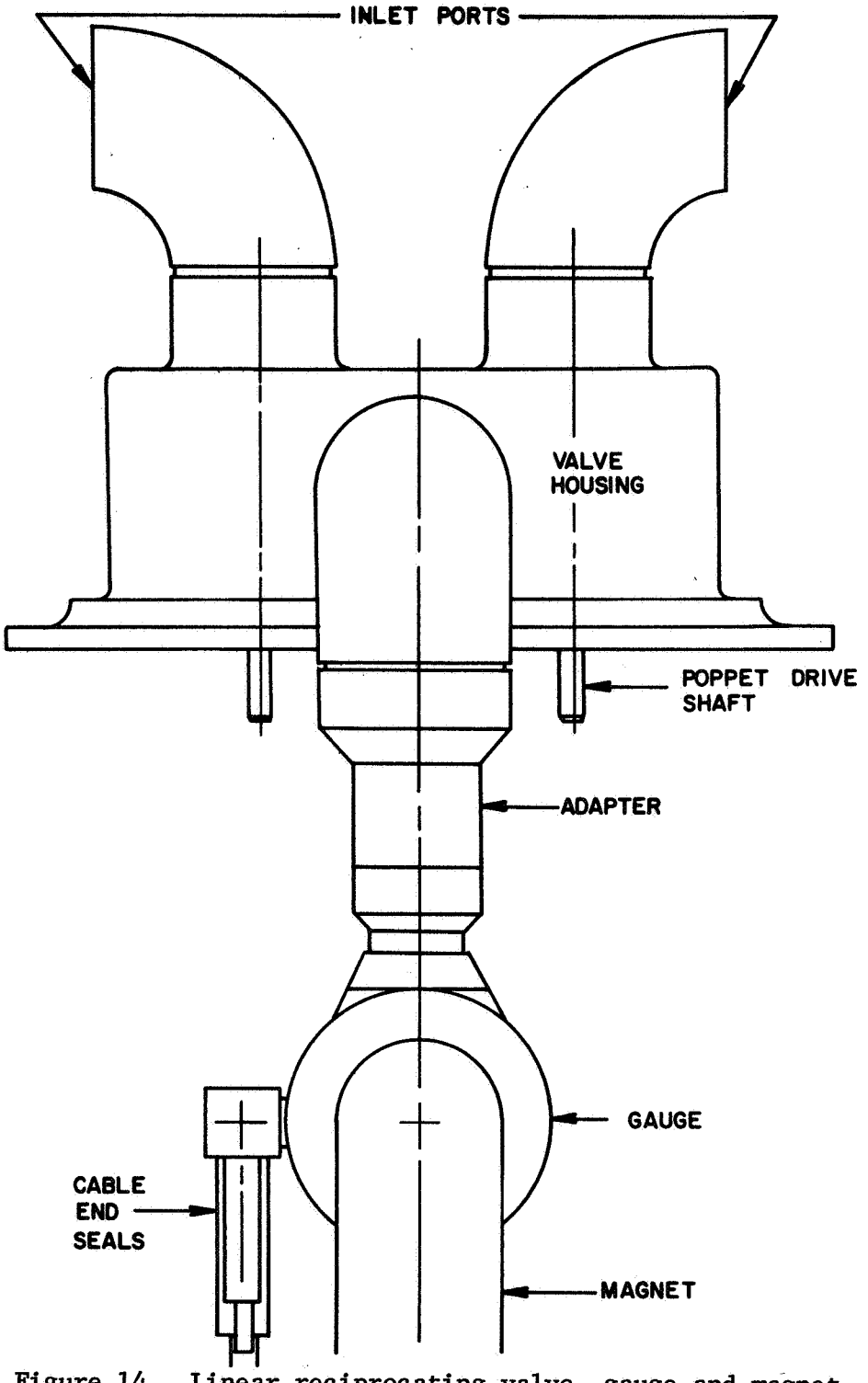

Figure 14. Linear reciprocating valve, gauge and magnet assembly.

(d) The counterbalances of the drive unit can be replaced by poppet assemblies to produce a dual unit with no increase in the drive power required.

(e) With the magnetic coupling solenoid drive, the poppet position indication (phase synchronization) can be derived from the drive pulses.

2. The rotary valve. — The rotary valve shown in Figure 15 consists of a one piece stainless steel cylindrical body with diametrically opposed inlet tubulations. A thin wall cylindrical rotor is mounted between two gold plated miniature precision ball bearings. These bearings have been developed specifically for ultra-high vacuum service where ordinary lubrication methods are unacceptable [9, 10, 11, 12]. The radial clearance between the rotor and valve body is small to obtain a maximum open-to-closed vacuum conductance ratio. The design goal for radial clearance is 1 mil. Mounted to the top of the valve rotor is the drive rotor, which, when acted upon by the electromagnetic drive field assembly will impart the torque necessary to drive the valve rotor at the proper cycling rate. The lower end of the valve rotor and the lower bearing mount are perforated to allow the gas pressure in the valve to reach the ionization gauge. Although Figure 15 shows a flange connection between valve and gauge, in flight configurations, the gauge will be welded to the lower part of the valve housing. A proximity pickup (a small coil not shown in the figure) will indicate rotor position for inlet port identification and synchronization purposes. A small torque will be imparted to the vehicle due to the rotor spin, but since the second moment of the rotor is orders of magnitude smaller than that of the vehicle, this perturbation will be insignificant. In order to balance the rotor, its wall thickness can be made lighter at a position opposite the aperture. The power required to operate the rotary valve at a constant speed will be the value required to overcome the frictional drag of the bearings. Figure 16 gives a more detailed picture of the construction of this valve.

The experimental electromagnetic drive for the rotary valve is illustrated in Figure 17. Basically, the drive is a two-pole electromagnet in which the poles have been "shaded" to promote starting. The pole pieces and yoke of the drive unit are made of Armco soft iron. The pole pieces are made adjustable so that they can be fitted closely to the O.D. of the valve housing at the upper part of the valve. The two drive coils are wound with enamelled magnet wire and are well insulated from the soft iron yoke. The drive rotor located within the valve consists of a stainless steel disk that contains sealed-in permanent magnets. Magnetic materials such as Alnico V have a high outgassing rate and must be isolated by encapsulation or other means from the vacuum.

The electromagnetic drive unit could equally well be a four-pole electromagnet in which the two-pole pairs are energized in quadrature to create a rotating magnetic field. The two-phase power supply would be somewhat more complex than a single phase supply, but it would no

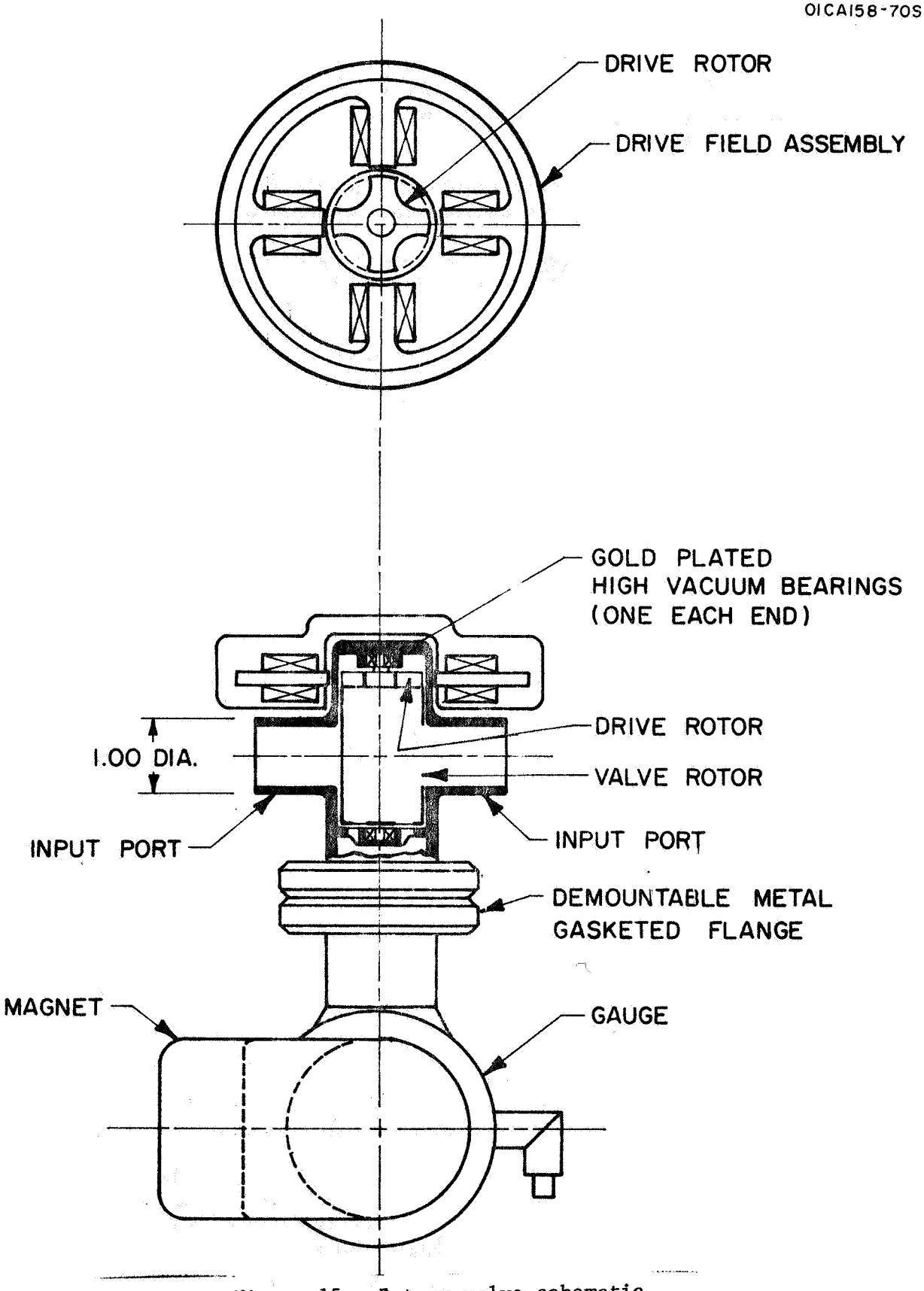

Figure 15. Rotary valve schematic.

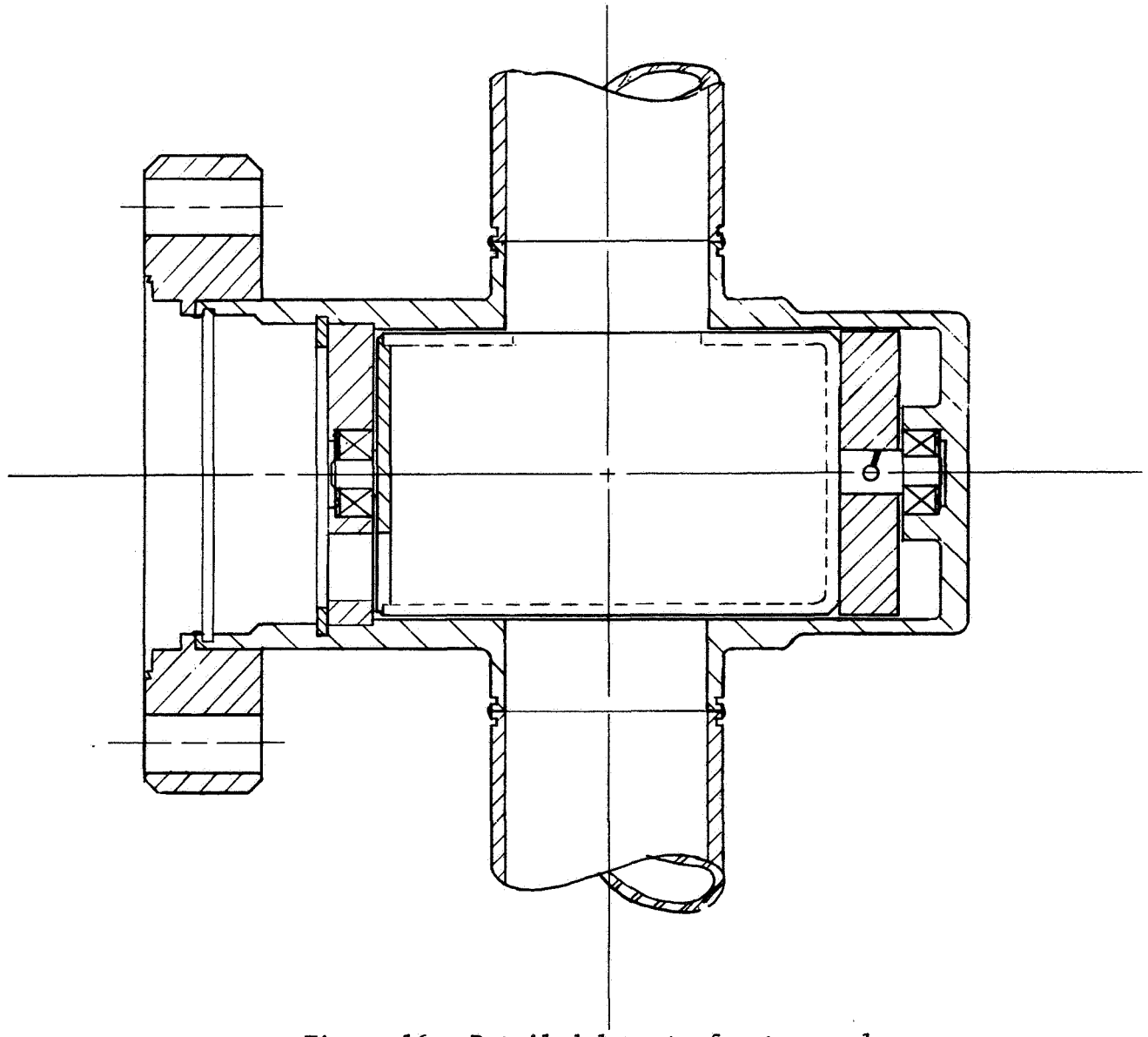

Figure 16. Detailed layout of rotary valve.

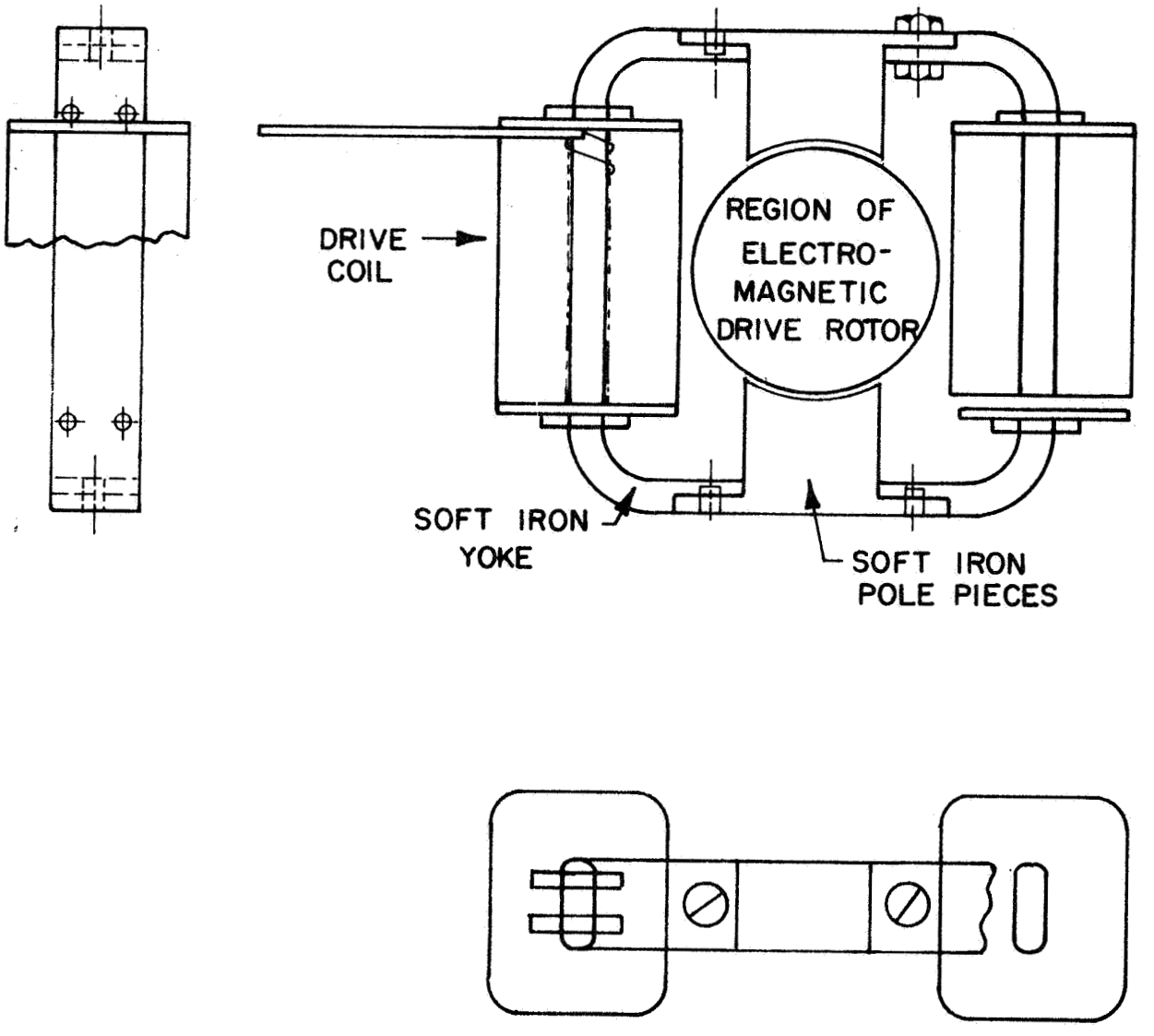

Figure 17. Experimental electromagnetic drive for the rotary valve.

longer be necessary to place sealed permanent magnets within the valve. Synchronizing pulses for the phase sensitive detector can be obtained from either proximity pickup coils or from magnetic reed switches that are activated by magnetic material attached to the valve rotor.

A drawing of the rotary valve, gauge and magnet assembly is shown in Figure 18. The compactness of this assembly is immediately apparent. However, problems can arise both due to the close spacing of the rotor and the housing (differential temperature expansion, for example) and the problems associated with starting the valve in motion and generating rotor phase synchronization.

The principal limiting factor in the rotary valve design is the presence of ball bearings within the valve. At present, it is unlikely that a three-year operating life can be achieved using commercially available bearings. In addition, sliding or rolling surfaces within the valve can generate gas that would limit the lowest pressure at which such a valve would be useful. Work is continuing on improving bearing performance in vacuum environments. This fact, together with certain inherent advantages of a rotary valve, make it desirable to pursue the development of such a device.

Particular advantages of the rotary valve design are: (a) simplicity and economy, (b) small physical size, and (c) high conductance, made possible by optimized tolerance control, port geometry and rotor diameter.

3. Flexure pivot valve. — The flexure pivot oscillating valve, which is illustrated in Figure 19, makes use of a unique frictionless, limited angular travel bearing. The bearing is made of flat, crossed springs supporting rotating sleeves. The unit functions as a precision bearing, requiring no lubrication and is suitable for high vacuum applications. The bearings are commercially available in a wide selection of sizes from Bendix-Utica. Fatigue life of stock units has been tested to more than 1.5×10^9 cycles by the manufacturer. Rotation is accomplished by deflecting the flat springs. This action causes the bearing to act as a torsion spring and can be used advantageously to obtain restoring forces and to minimize power requirements by properly relating valve cycle to the rotor assembly natural frequency.

The flexure-pivot oscillating valve makes use of two closely spaced cylinders in a counter-rotating action through a total angle of about 30 degrees. Each of these cylinders, or rotors, is supported at one end by a flexure pivot, a proprietary bearing made by Bendix-Utica. Gas valving action is obtained by providing two narrow rectangular slots 150 degrees apart in each of the two cylinders. At the limit of travel in one direction, one pair of cylinder slots will be aligned with one another and with one inlet port. The other inlet port will be closed by the overlapping of the cylinders. One-half cycle later, the cylinders will have rotated back to close the first port while the other pair of slots will

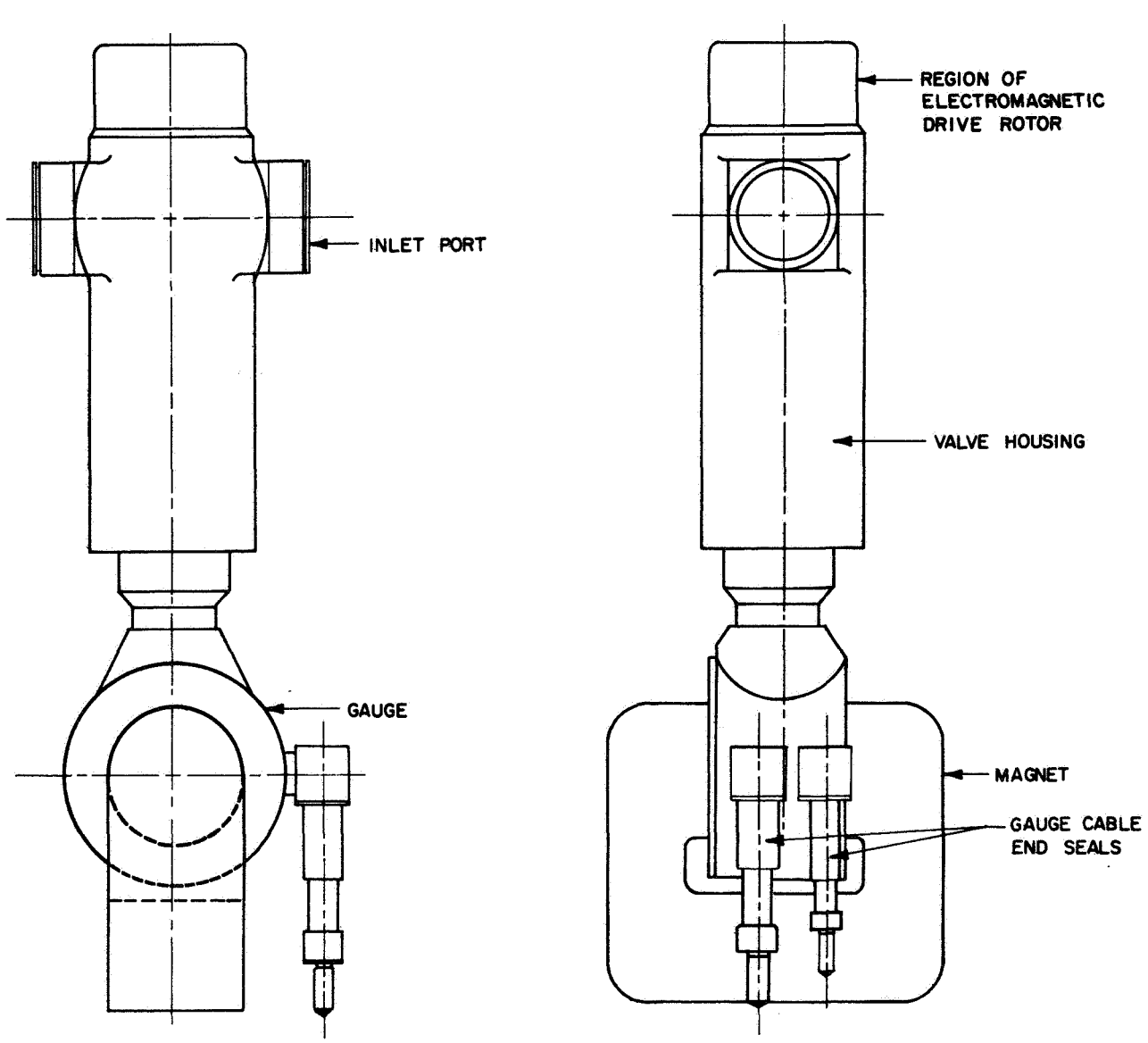

Figure 18. Rotary valve, gauge and magnet assembly.

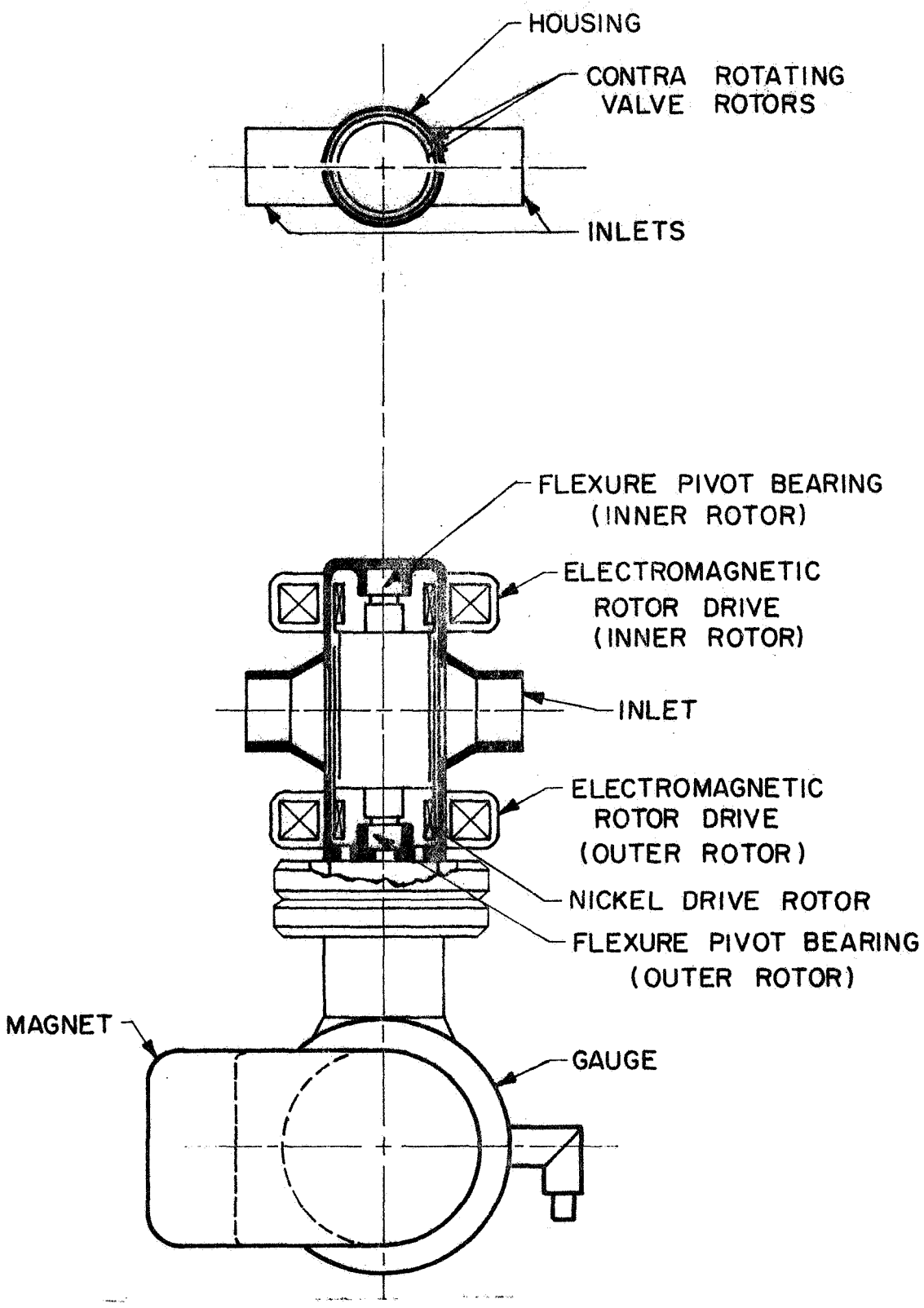

Figure 19. Flexure-pivot oscillating valve schematic.

be aligned with each other and with the second inlet port. The equal and opposite motions of the cylinders will result in a zero net torque reaction. The valve is designed so that in the relaxed position (such as would occur if the driving mechanism were to fail) both inlet ports would be "closed" equally. In addition, this valve is designed so that the normally closed end of the housing will be sealed with a weld which can be easily machined off for disassembly. The detailed arrangement of the two flex-pivots and the two valve rotors is illustrated in Figure 20.

The electromagnetic drive for the flexure-pivot oscillating valve consists of two separate electromagnets of the kind shown in Figure 21. These electromagnets are located outside the valve housing at positions which are adjacent to magnetic material drive rotors attached to each of the valve inner cylinders. The four-pole pieces and yoke of each magnet are made of soft iron. The four-drive coils are wound with enamelled magnet wire and are well insulated from the pole pieces and the yoke. The iron yoke is designed in a two-piece configuration so that it can be easily installed and removed from the valve body. The two-piece construction also makes it easy to adjust the position of the pole pieces so that they fit closely to the O.D. of the valve housing.

The electromagnetic drive unit operates as described below. Diametrically opposite pole pieces are energized alternately. The drive rotors within the valve tend to line up alternately with the two energized pairs of pole pieces. Since the valve cylinders or rotors constitute an oscillatory spring-mass system, the driving frequency will be adjusted to the natural oscillatory frequency of the rotors. The electromagnetic drive would be excited to obtain a displacement of each rotor of $\theta = \theta_o \sin \omega t$ with θ_o equal to 90 degrees. The drive frequency would be set so that $\omega = \sqrt{K/I}$, where K is the torque coefficient of each flexure pivot and I is the second moment of each rotor assembly.

The outline drawing of the flexure-pivot valve and the R-5 gauge and magnet is presented in Figure 22. The space occupied by this assembly will be slightly larger than that occupied by the corresponding rotary valve assembly. The flexure-pivot valve offers the possibility of a long lifetime valve with no internal rolling or sliding friction. The power required to drive the valve will depend on the closeness of coupling between the external pole pieces and the internal magnetic rotors. The phase synchronization of the rotors' positions can be obtained from the driving impulses supplied to the electromagnets. The counter-rotating cylinders within the valve decrease the total required angular travel of each cylinder and provide a net zero torque.

D. Electronic Systems Design

1. General. — Figure 23 is a block diagram of the electronic system. The system consists of an electrometer, synchronous detector, a differential amplifier, and a valve driver. The valve driver produces the

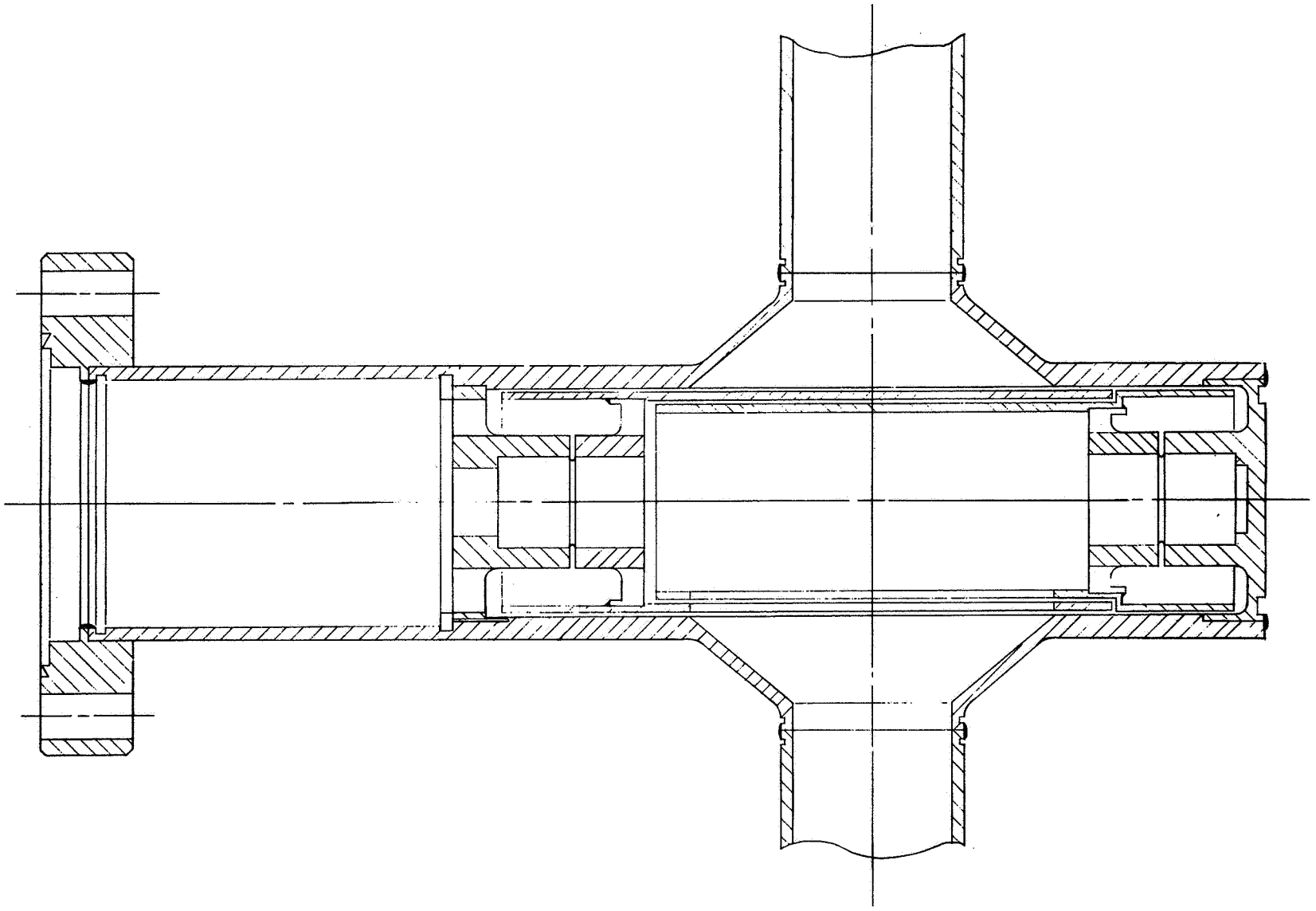

Figure 20. Detailed layout of flexure-pivot oscillating valve.

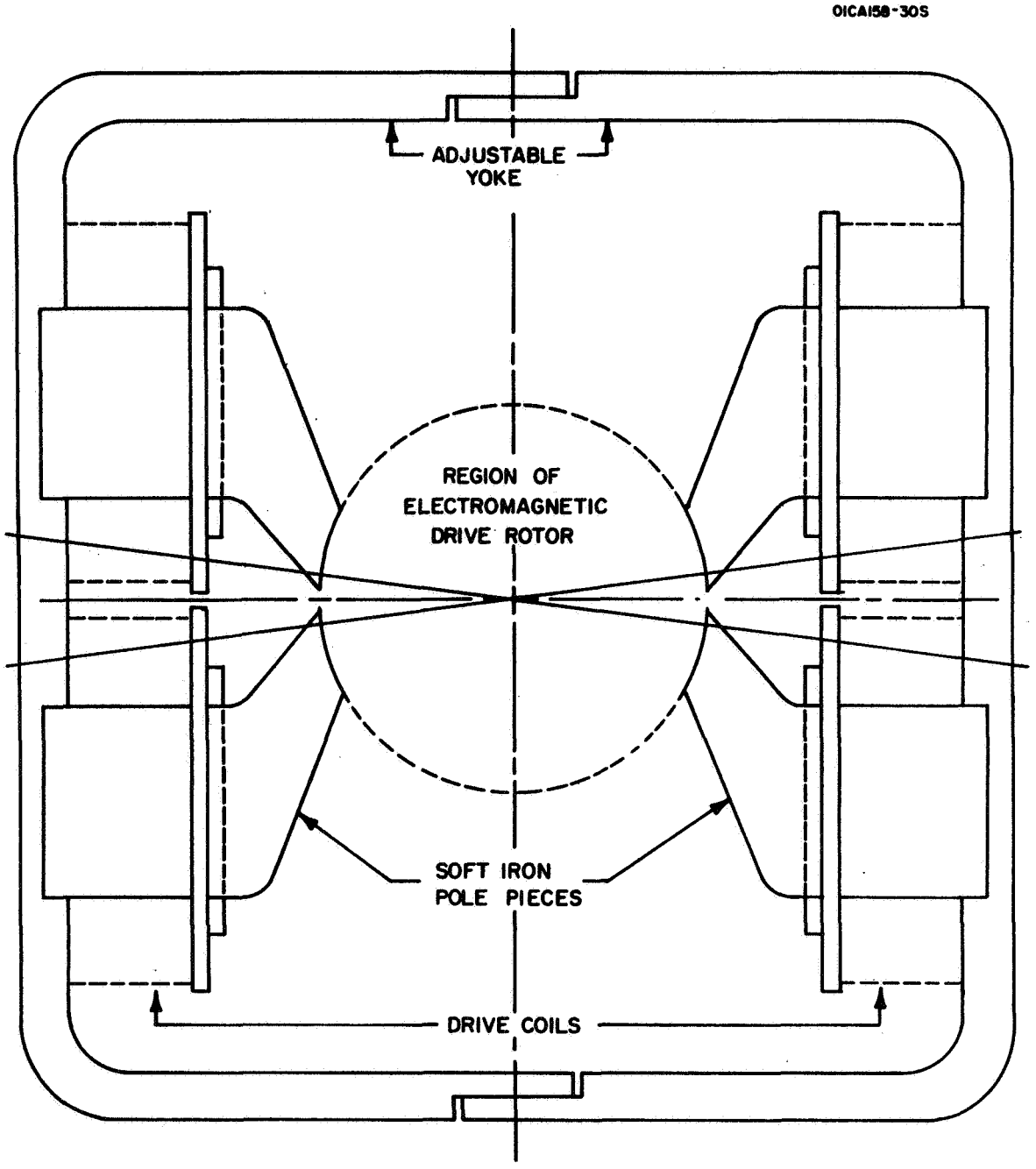

Figure 21. Electromagnetic drive for the flexure-pivot oscillating valve.

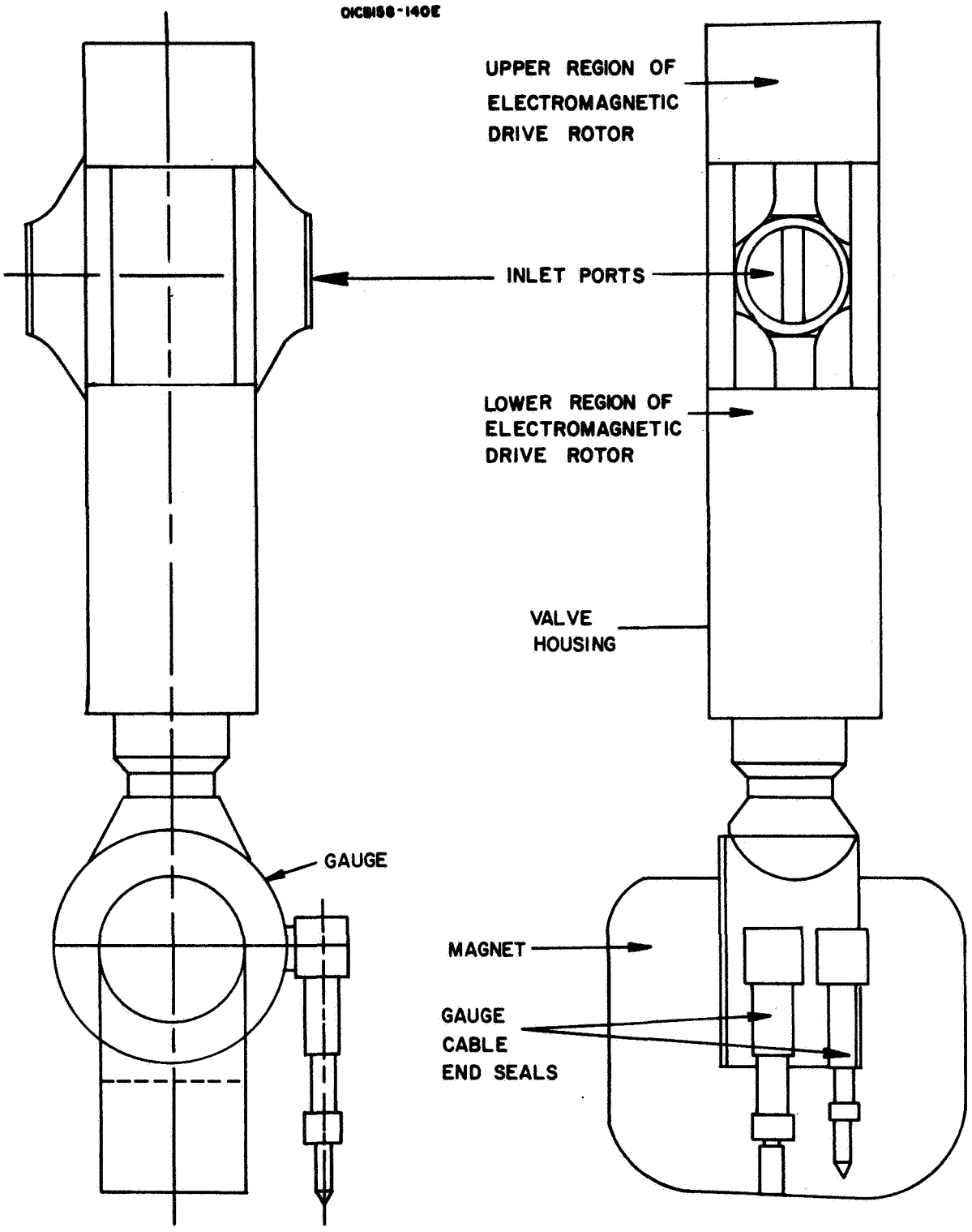

Figure 22. Flexure-pivot oscillating valve, gauge and magnet assembly.

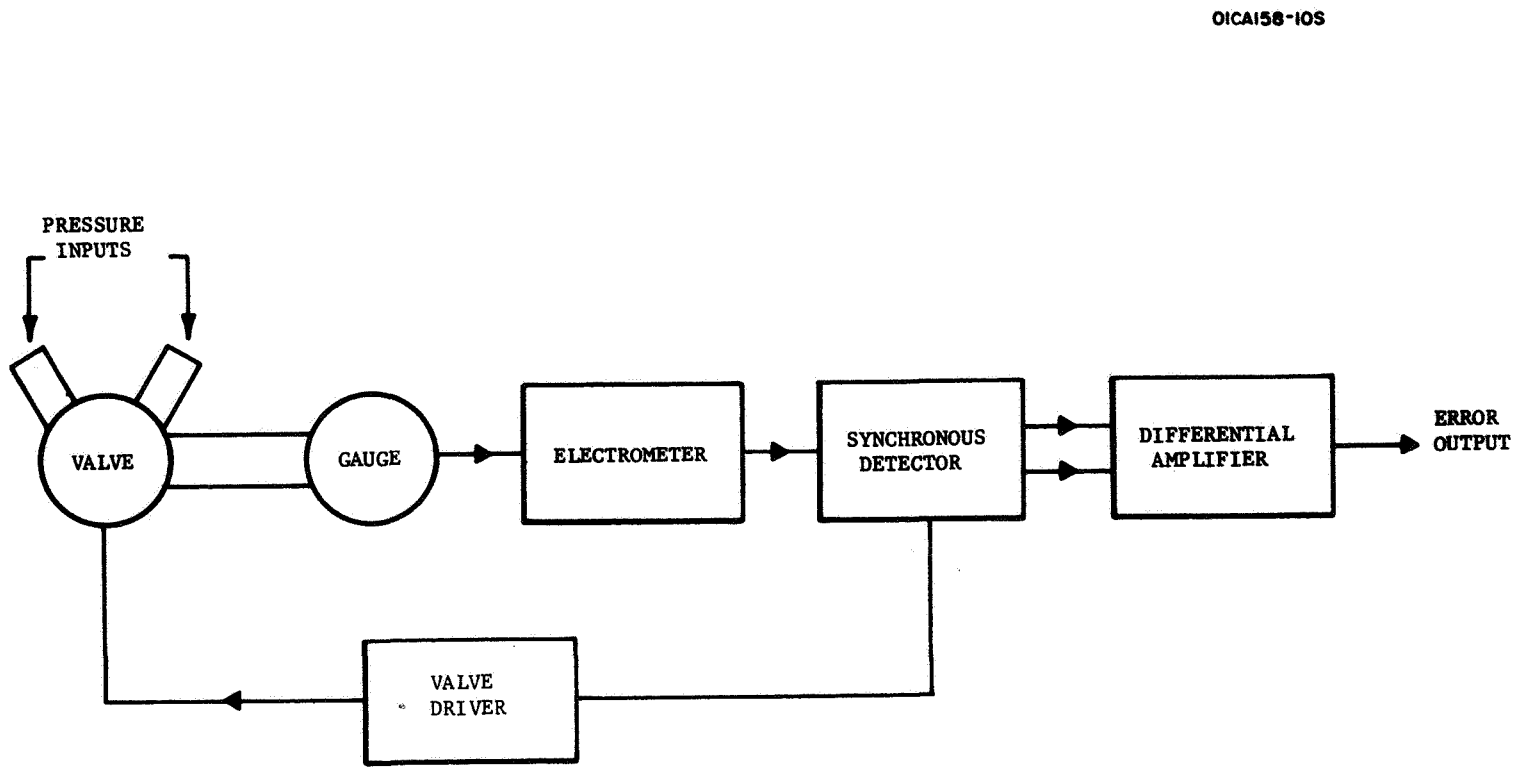

Figure 23. Block diagram of the yaw attitude sensor system electronics.

necessary drive energy to activate the mechanical cycling valve unit. As the valve is cycled, the gauge (sampling the alternate input ports) produces an alternating current signal which is fed into the electrometer amplifier. The electrometer converts these currents into a voltage which is fed into the synchronous detector unit. The synchronous detector receives its synchronizing signal from the valve drive unit and samples the electrometer output in phase with the alternating valve openings. Two outputs are produced by the synchronous detector, each one corresponding to the pressure at one sensor port. These two outputs are fed into a differential amplifier which produces a single output proportional to the angle of attack.

2. Electrometer amplifier. — The electrometer amplifier is designed to provide a logarithmic output over the current range from 10^{-8} to 10^{-3} amperes. It will measure the signal at the sampling rate of 5 to 10 c/s. It will be a modification of an available type that has been successfully flown on sounding rockets, reentry vehicles, and gun launch payloads.

The logarithmic amplifier developed for gun launch use is capable of surviving peak accelerations of 50,000 g and will measure current over a 5-decade range from 10^{-9} to 10^{-4} amperes. Its configuration is a cylinder 1.5 inches in diameter by 0.7 inches high. It is completely encapsulated, weighs 26 grams, and consumes 400 mW of power.

The standard gun probe electrometer amplifier normally operates over the current range from 10^{-9} to 10^{-4} amperes. However, this electrometer amplifier can be adjusted to operate over other ranges with only minor modifications in the feedback loop. A typical calibration curve of a logarithmic electrometer amplifer is shown in Figure 24.

3. The valve drive unit. — The valve driver unit contains a stabilized oscillator which is used to determine the valve operating frequency. The oscillator output is processed through a power amplifier and applied to the coils of the valve drive mechanism. The output of an intermediate stage is used to synchronize the synchronous detector circuitry.

In the event that the flexure-pivot valve is used to perform the mechanical valving, the oscillator will be synchronized or "locked-in" to the oscillating valve motion by means of the rotor pickup coil. This will insure resonance operation of the valve independent of frequency drift.

4. Synchronous detector. — The synchronous detector accepts the signal from the electrometer amplifier and a synchronizing signal from the valve driving unit. A separate detector is employed for each half cycle of the valve operation. Each detector is connected through a gate network that is triggered by the synchronizing signal. The detector outputs are then processed through filters whose outputs are used to drive the differential amplifier.

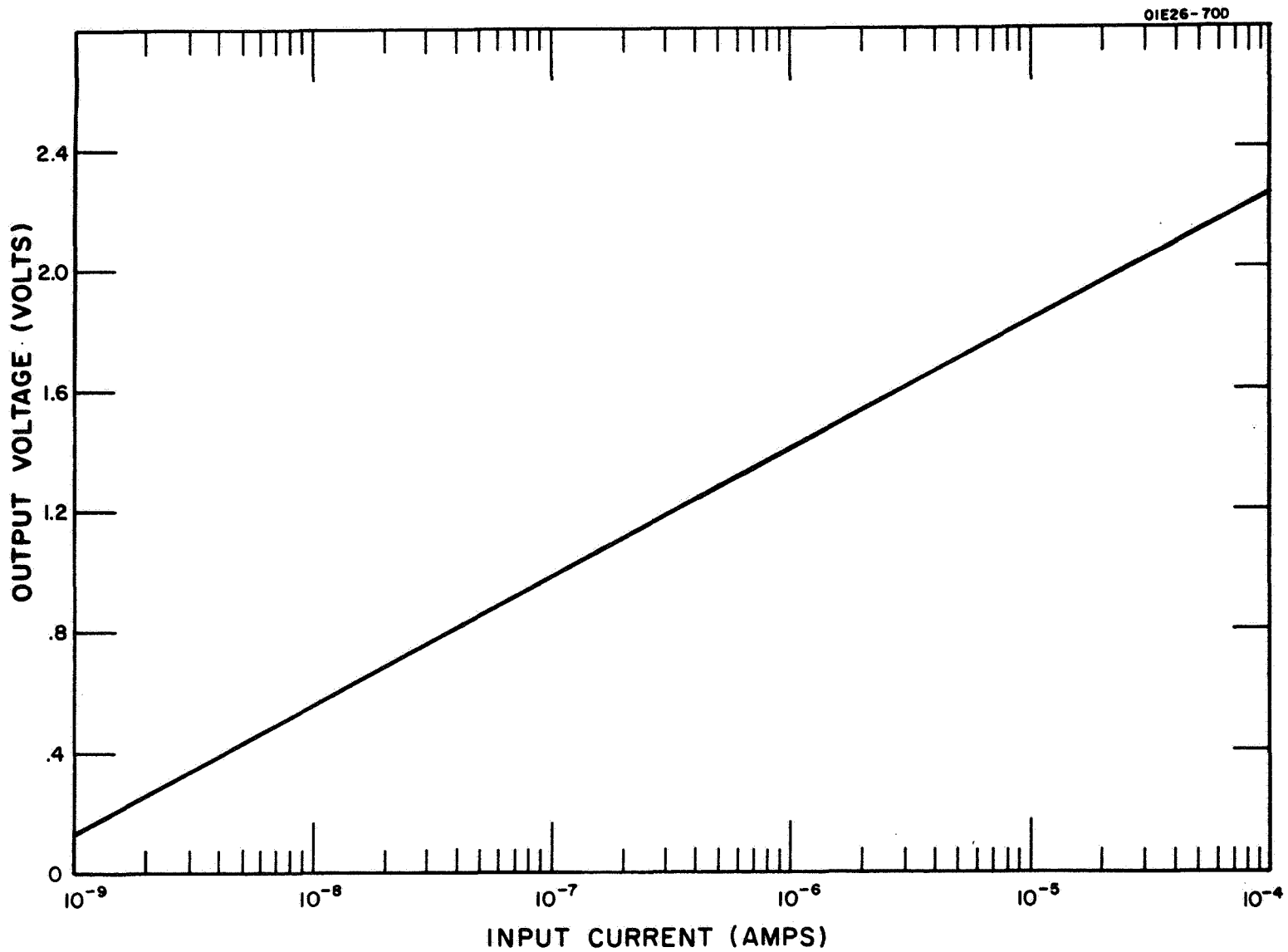

Figure 24. Typical calibration curve for GCA logarithmic amplifier.

5. Differential amplifier. — The differential amplifier accepts the two signals generated in the synchronous detector circuitry and generates the output error signal. The amplifier consists of a high gain integrated circuit operational amplifier with the necessary feedback networks to provide the required stability over the environmental range required. An output power amplifier stage is also provided within the feedback loop to provide the required low impedance interface with the spacecraft system. The overall forward gain of the combined system will be adjusted to provide the required system transfer characteristic.

6. Detailed circuit descriptions. —

a. Electrometer amplifier. — A typical electrometer amplifier schematic is shown in Figure 25. It employs an operational amplifier technique with a separate logarithmic feedback loop. The amplifier is a differential type with a darlington emitter follower input circuit and an integrated circuit for the main amplifier stage. Input transistors Q11 and Q14 are each composed of two separate matched transistors enclosed in a single case to insure low drift with temperature. Transistors Q17 and Q18 are used to amplify the signal at the outputs of Q14 and Q14B. The output is fed into an operational amplifier integrated circuit. An integrated circuit is used as the main gain stage of the amplifier to reduce size, lower the number of components required, and increase the reliability of the system.

The logarithmic feedback loop is composed of resistors R14, R15, R16, R20, R25, and ten accompanying 2N3247 transistors. The emitter-base diode characteristic is employed for the log characteristic. The transistors are used with the diodes in the forward and reverse direction to provide a bipolar logarithmic output characteristic. When used in the above differential mode, the NS7070 has an input leakage current of 10^{-12} amperes. The major portion of input current, therefore, will be developed across the feedback loop. The 2N3247 has a typical reverse leakage of 10^{-10} amperes. An input current of 10^{-9} amperes causes a voltage to be generated across the resistance network. Since R14 (the 100 megohm resistor) is at least ten times the value of any other resistor in the series string, the majority of the voltage will be developed across it. An input current of 10^{-9} amperes will generate an output voltage of 0.1 volt. As the current increases, diode action takes place across Q9, clamping the voltage across R14 at approximately 1/2 volt. As the current increases further, the additional voltage drop occurs across R15 (10 megohm), which requires ten times the current for a similar change in voltage. When the voltage across Q12 exceeds 1/2 volt, that transistor will also conduct. Any additional voltage drop will occur across R16 requiring an additional ten-fold increase in current. In like manner, R20 and R24 will come into play requiring higher currents for a constant increase in voltage.

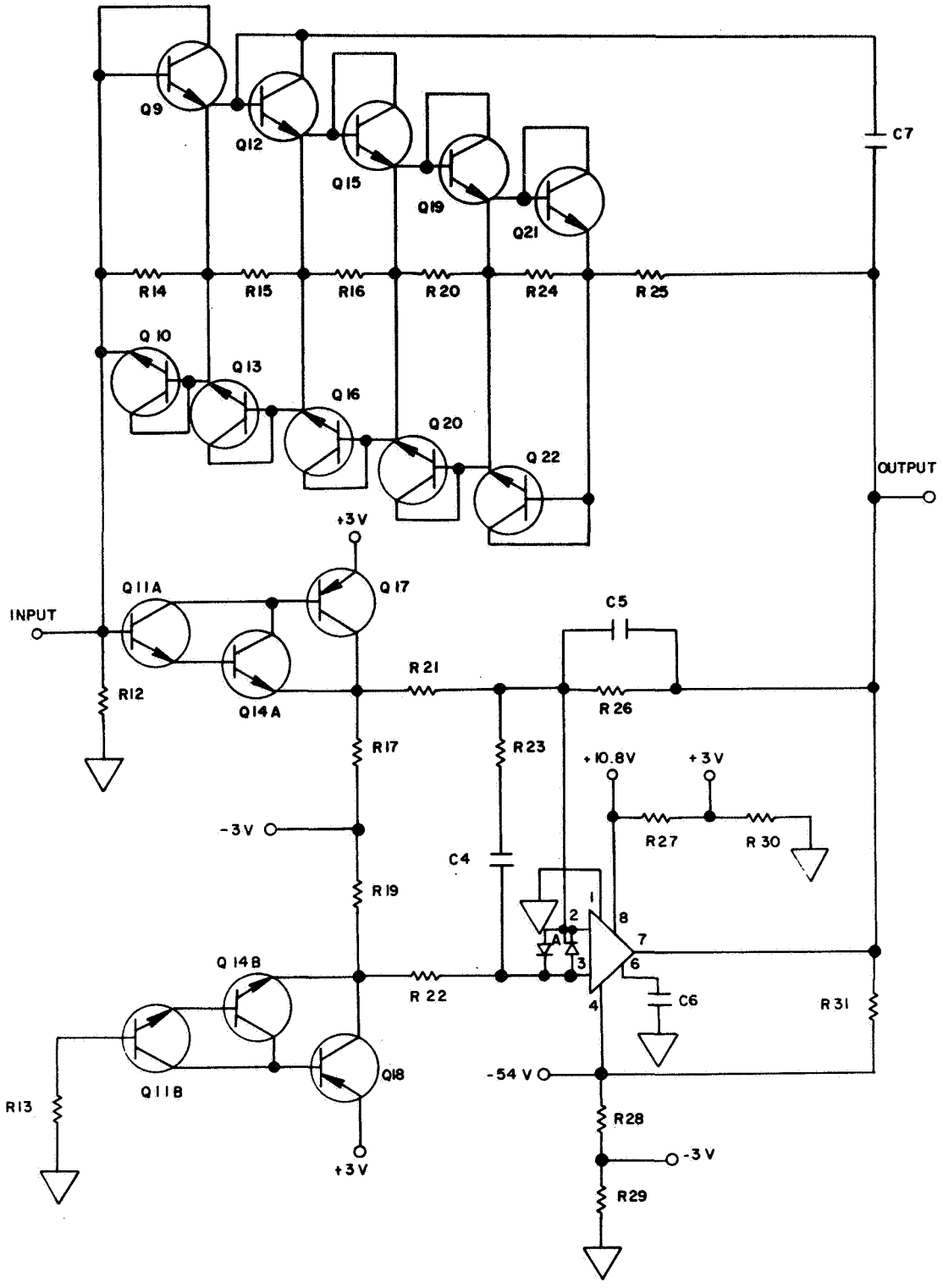

Figure 25. Electrometer amplifier schematic.

The characteristic curve for the amplifier used in the gun launch payload is shown in Figure 24. It operates over a current range of 10^{-9} to 10^{-4} amperes. As can be seen, the gain characteristic may be modified readily to operate over the range from 10^{-8} to 10^{-3} amperes with only changes in the feedback resistors. The frequency response of this amplifier exceeds 100 c/s at an input current of 10^{-8} amperes. The output impedance is typically less than 100 ohms.

b. Synchronizer circuitry. — The synchronous detector circuit is divided into two parts, the synchronizer circuit, as shown in Figure 26, and the detector circuit, as shown in Figure 27. A synchronizing pulse is generated by the valve drive mechanism circuitry. This signal is used to synchronize the detector circuitry which produces a signal proportional to the yaw angle from the composite signal out of the electrometer. Each synchronizer channel consists of three monostable multivibrators and an inverter amplifier. The first multivibrator consists of Q1 and Q2 and the associated circuitry. This circuit is triggered directly by the incoming signal. The delay generator is controlled by variable resistor R5. This delay is set to trigger the following multivibrators in phase with the opening of valve port No. 1. The output of the first multivibrator is amplified and inverted by Q3 which drives the second multivibrator consisting of Q4 and Q5. This circuit provides a reset signal to the detector circuitry. The other output of this multivibrator triggers the third unit which is made up of Q6 and Q7. This third multivibrator period is set by adjusting R18. The width of the pulse generated by this circuit is adjusted to correspond to the open period of port No. 1.

c. Detector circuitry. — The detector circuit as shown in Figure 27 receives three input signals: the electrometer output, a gate pulse from the synchronizing circuit, and a reset pulse also from the synchronizer. When the gate pulse goes positive, the input gate consisting of CR5, CR6, and CR7 is opened, allowing that portion of the electrometer output signal corresponding to the pressure at port No. 1 to pass through. The output of the gate is applied to the base of emitter follower Q8. The emitter follower output charges capacitor C7 through diode CR9. The voltage on the capacitor is now charged to a voltage proportional to the pressure at port No. 1. At the start of the next cycle, the pulse generated by Monostable Multivibrator Q4 and Q5 turns on Q9 for a period of a few microseconds. This discharges capacitor C7 and prepares it for the next charge period. The voltage on the capacitor is monitored by field effect transistor Q10. R27 is of the order of 10^7 ohms so that no measurable leakage error occurs. The output of the field effect transistor is amplified by the emitter follower Q12. The output of Q12 is fed into the filter network where it is conditioned prior to the differential amplifier stage.

Identical synchronizing and detecting circuitry is provided for channel 2. The only difference is that the time delays in channel 2 are adjusted to correspond to the opening of port No. 2.

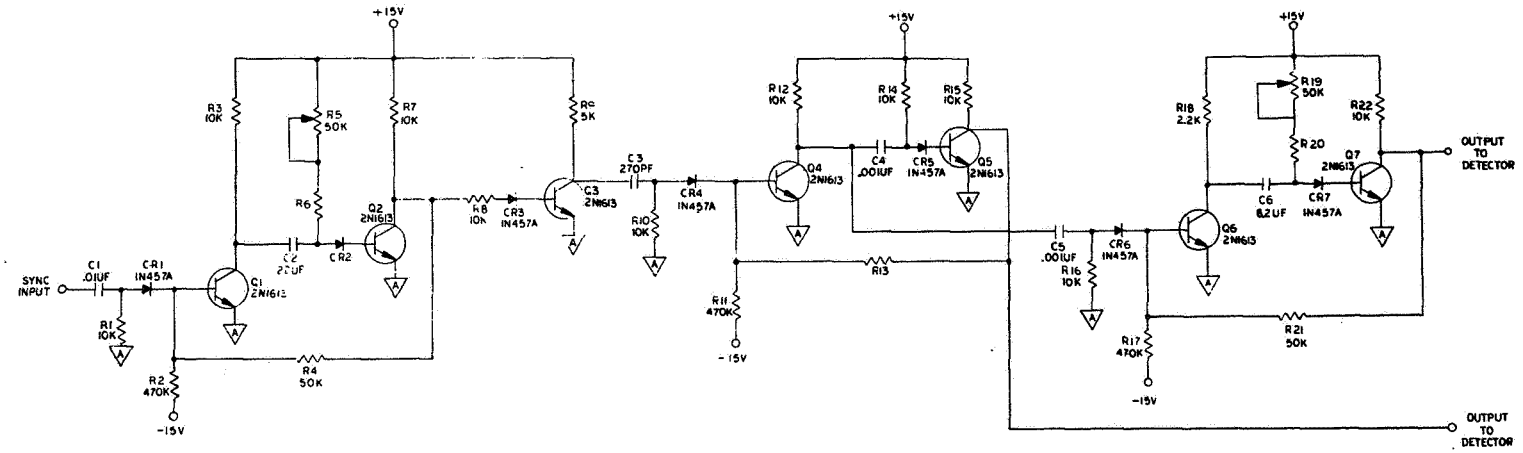

Figure 26. Synchronizer schematic.

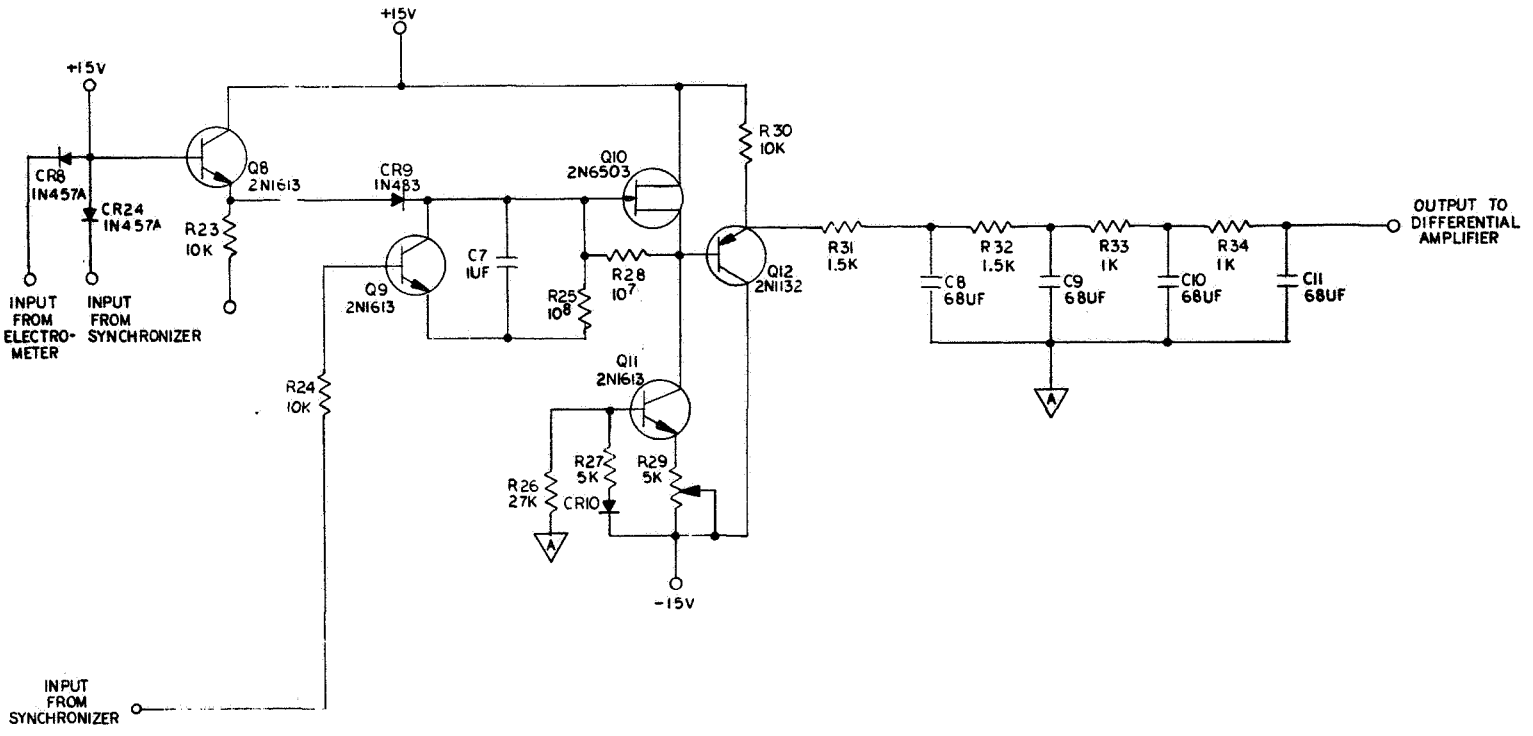

Figure 27. Detector schematic.

d. Differential amplifier. — The schematic of the differential amplifier is presented in Figure 28. The outputs of the two filter networks are fed through R54 and R55 into the differential amplifier. R57 and R58 are adjusted to provide the desired output voltage level.

e. High voltage power supply. — The power supply which furnishes high voltage to the cold cathode ionization gauge (see Figure 1) is a standard solid state high frequency oscillator type supply having the following specifications:

Power-Input:	- 24 $\pm$ 1.5 volts dc at 3 Ma. no load current
Output:	4 kV, adjustable $\pm$ 7.5 percent
Current:	0 - 10 μ amps
Stability:	$\pm$ 0.5 percent under all specified combinations of line, load and temperature
Ripple:	0.0015 percent of output voltage peak-to-peak
Temperature:	-25°C to +65°C
Regulation Response Time:	2 ms or less from no load to full load

Potting will provide for easy high voltage connection and insulation.

Power supply to be rf shielded

Power supply to be short-circuit protected

E. Packaging

The overall packaging concepts for the different versions of the yaw attitude sensor are illustrated in Figures 29, 30, 31, 32, and 33. It should be noted that packaging of the rotary valve version and the flexure-pivot valve version of the yaw attitude sensor system have been grouped together. These two valves are sufficiently similar to permit the use of a single design to accommodate either valve.

In each design, the mechanical cycling valve, cold cathode ionization gauge and magnet and the electronics will be mounted within a metal frame of low weight and high rigidity. The electronics will be of modular form and will be fastened to the assembly so as to be easily removable. The cold cathode gauge and magnet will be magnetically shielded with a light weight laminated box fabricated of layers of soft iron, netic, and co-netic material. The electromagnetic drive units for the mechanical cycling valves will be similarly shielded.

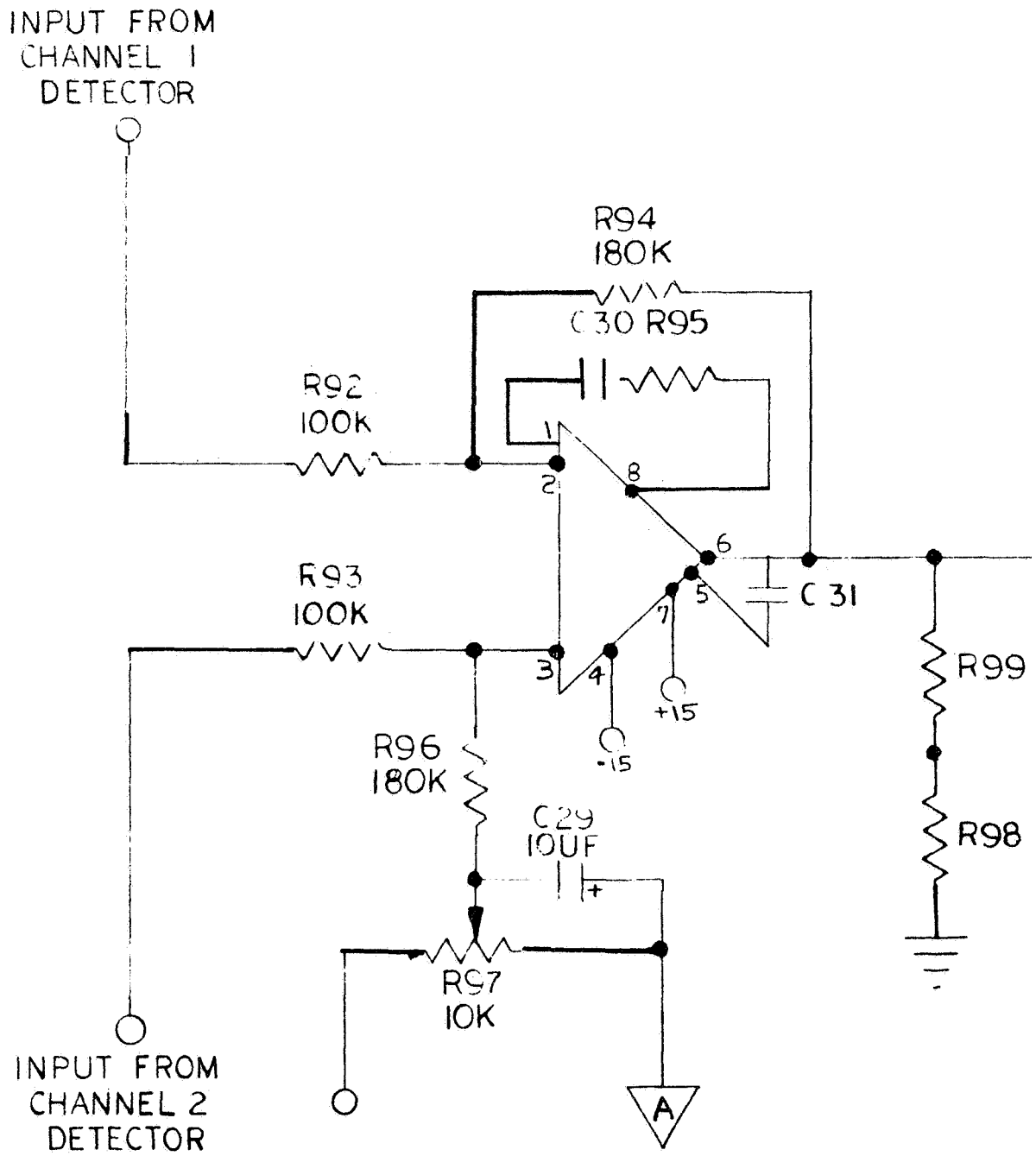

Figure 28. Differential amplifier schematic.

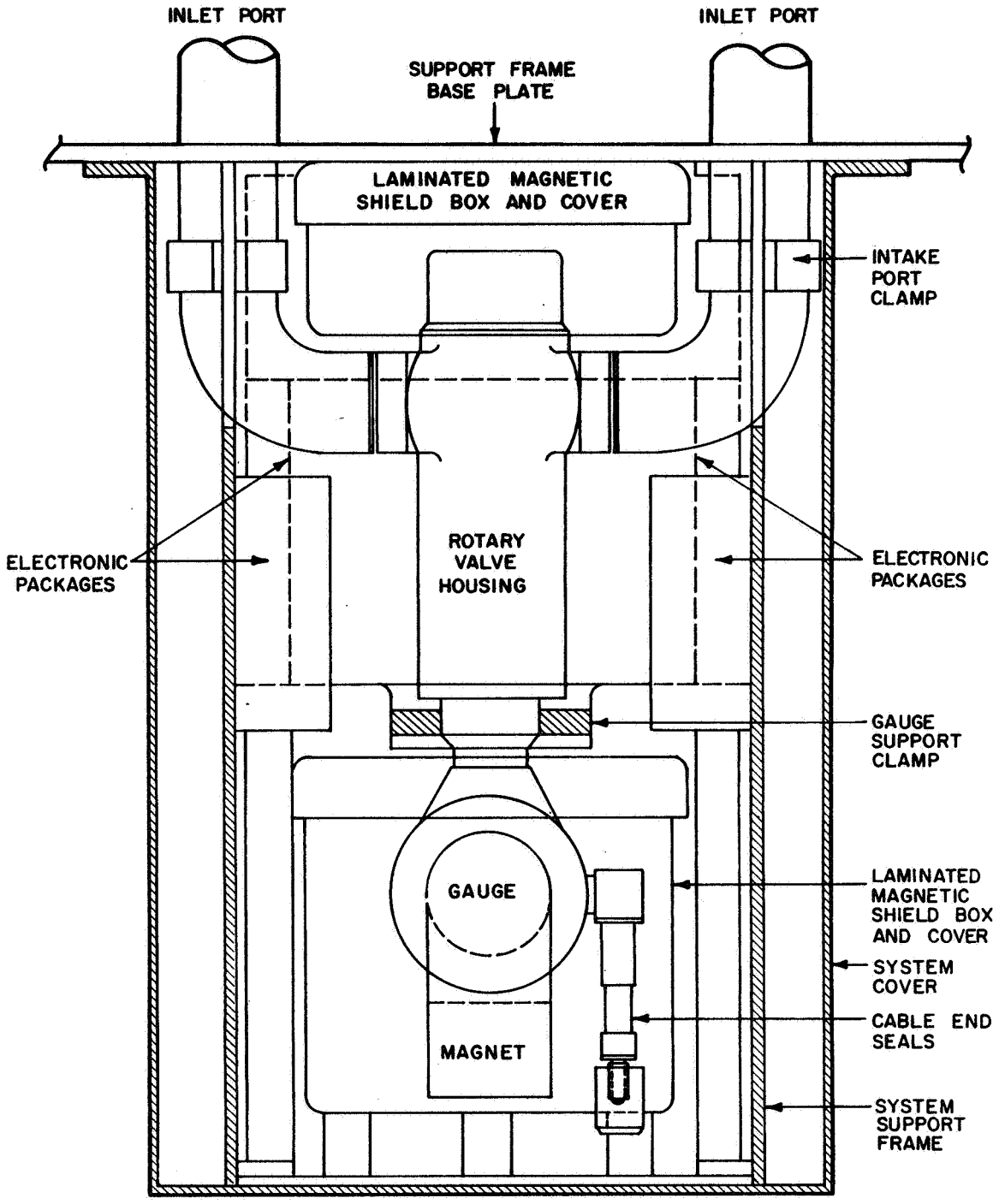

Figure 29. Front view of rotary valve and flexure-pivot valve version of yaw attitude sensor package.

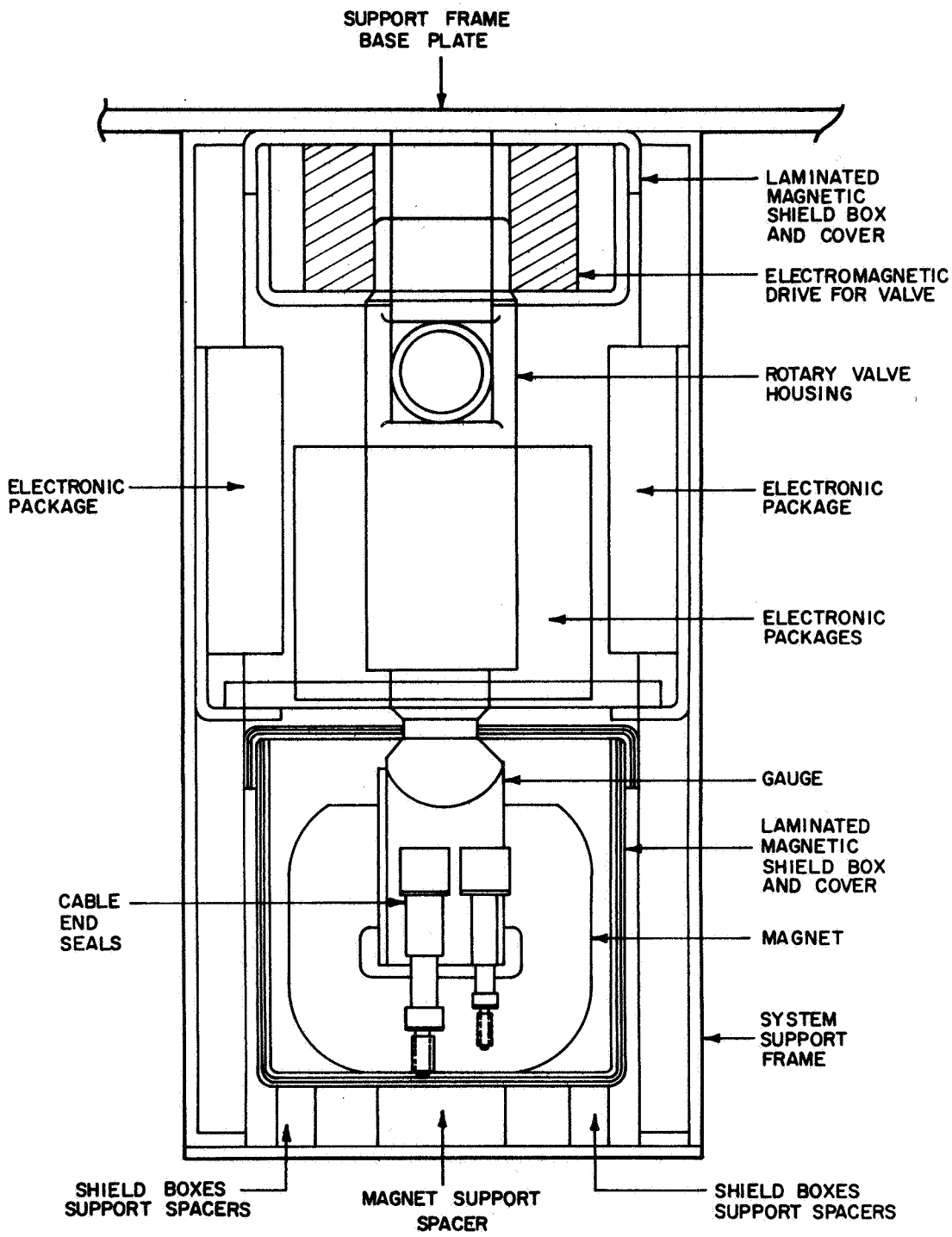

Figure 30. Side view of rotary valve and flexure-pivot valve version of yaw attitude sensor package.

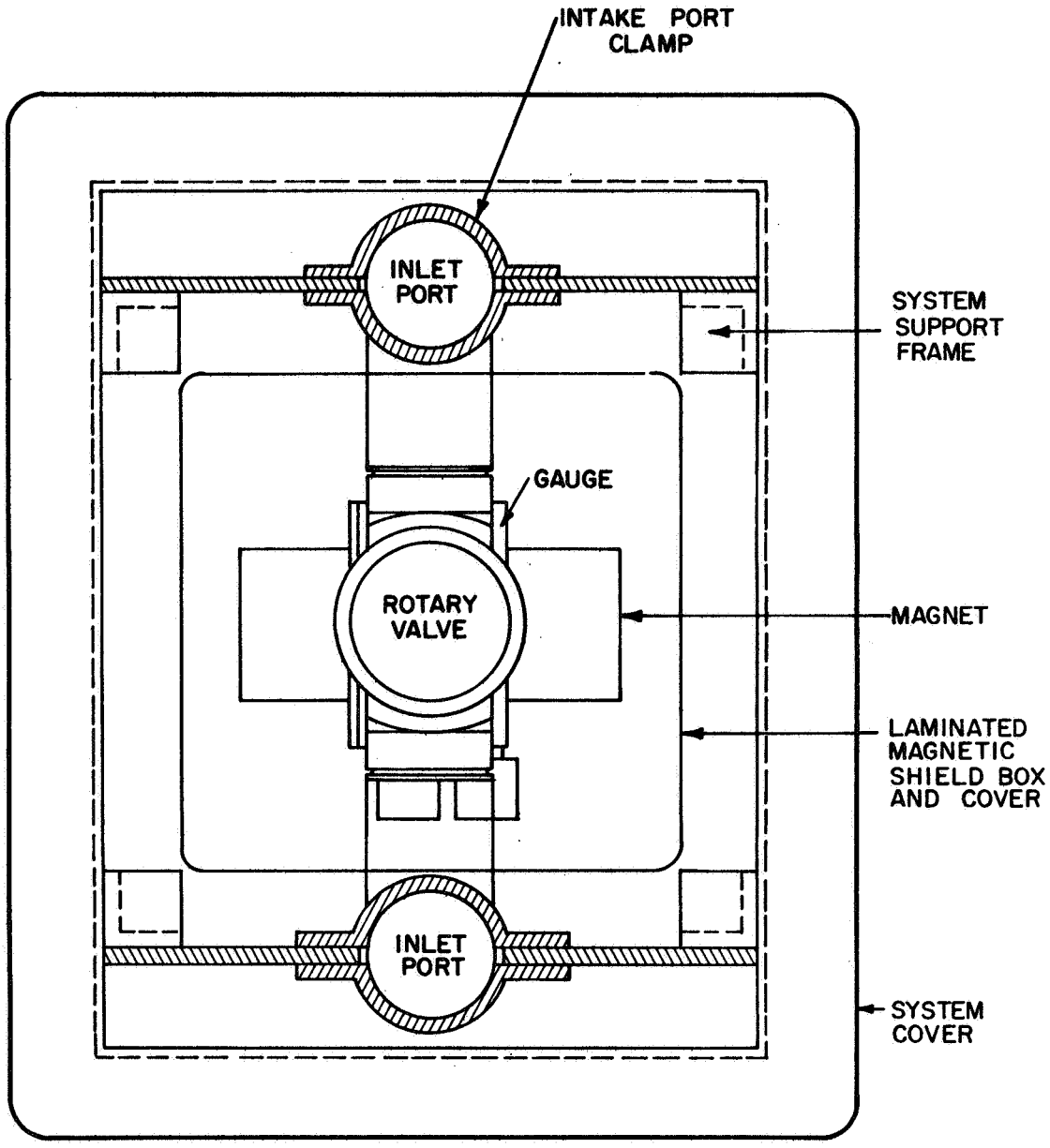

Figure 31. Top view of rotary valve and flexure-pivot valve version of yaw attitude sensor package.

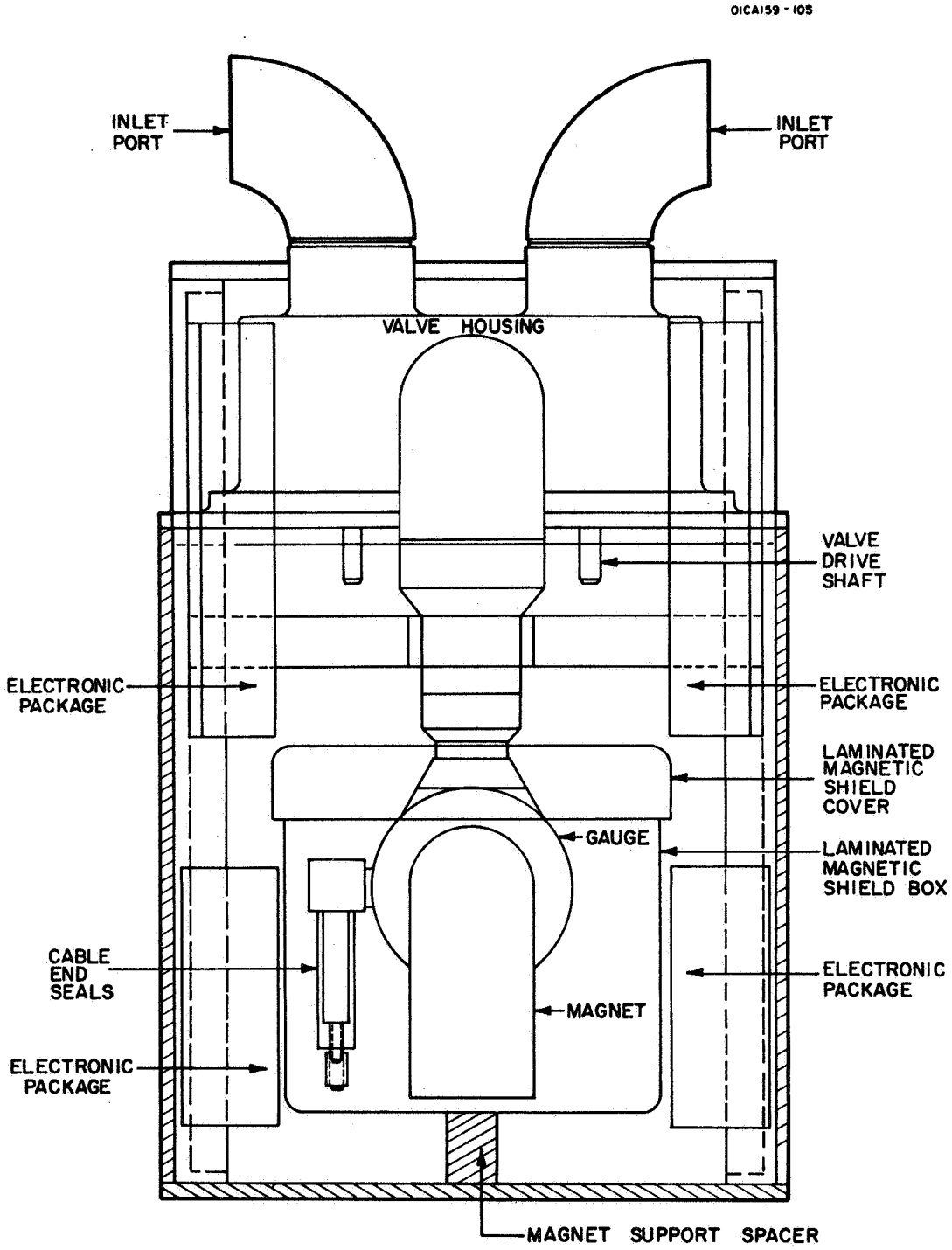

Figure 32. Front view of linear reciprocating valve version of yaw attitude sensor package.

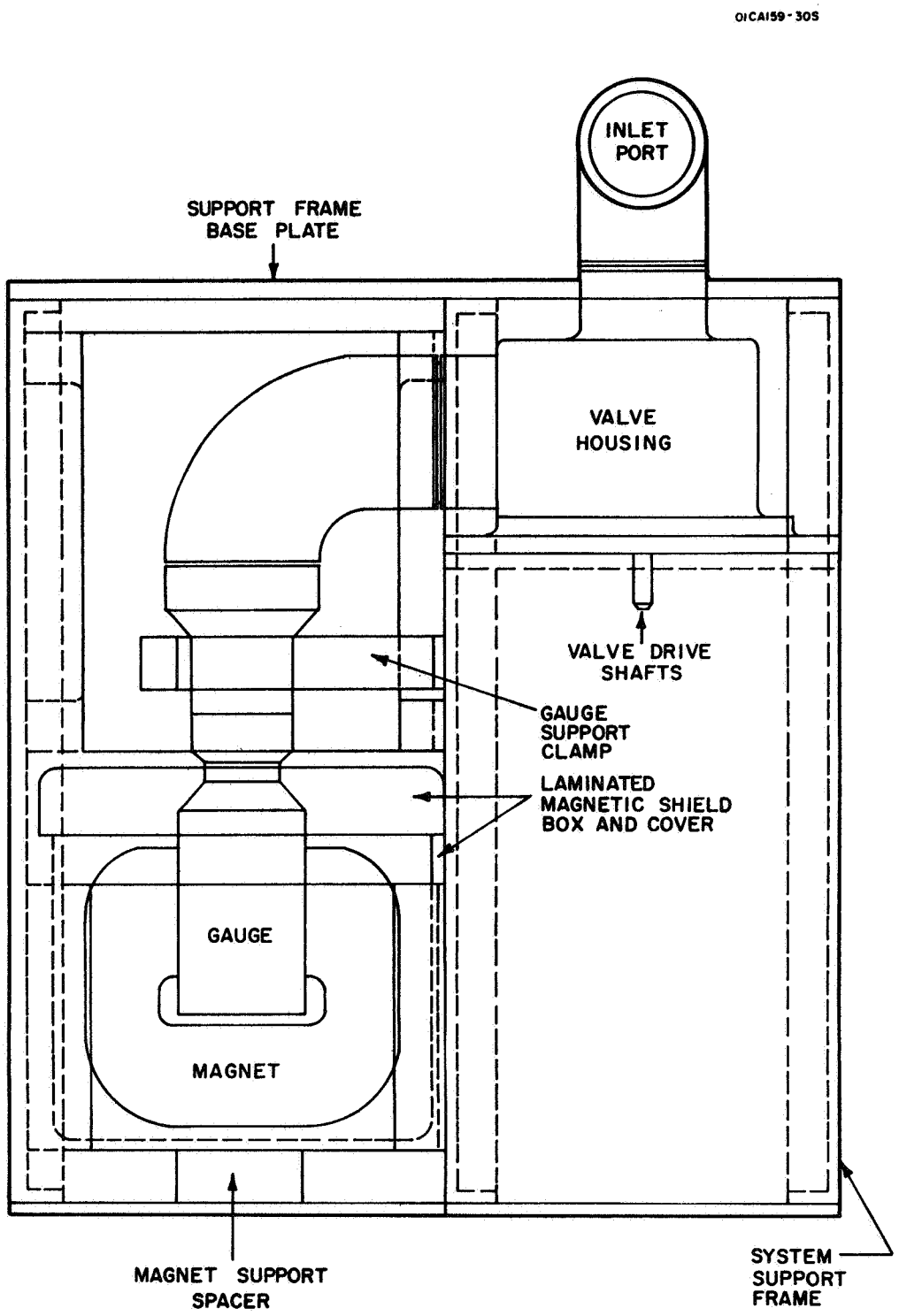

Figure 33. Side view of linear reciprocating valve version of yaw attitude sensor package.

The support frame of aluminum angle and plate will be mounted to a solid base plate which will provide a mounting surface to the vehicle and an attachment point for the two gas inlet tubulation ports. A protective cover that is mounted to the base plate will provide protection against damage by handling, extra magnetic and electric shielding, and will also permit the entire package to be pressurized if desired. An electrical connector to the package will be mounted in the protective cover.

In addition to the basic requirement that the various components, subsystems, harness, etc., of the electronic system must be held together in some firm spacial relationship, the package design must consider constraints imposed upon it by the following: (1) shock and vibration, (2) heat flow apportionment and operating temperatures, (3) weight and volume apportionment, (4) radiation, and (5) electromagnetic interference and susceptibility.

1. Shock and vibration. — The problem of providing electronic package designs to survive the shock and vibration environment imposed during launch conditions is best understood by referring to the transmissability curve for a simple spring-mass system shown in Figure 34. The above data are presented in Figure 35.

In general, all components of a system can be represented by a simple lumped spring-mass system as shown, since all components have compliances and mass. These components are mounted on a structure which is caused to accelerate periodically and randomly so that the base structure will become the source of vibrational energy and the forcing function can be thought of as acting at the mounting surface or interface of the component.

The concern in packaging for vibration hardness is to reduce, as much as possible, the deflection of the component as measured at its mass center. Deflection can cause modulation of circuit parameters, fatiguing of support structure, and in extreme cases, rupture of internal parts and structure.

The deflection, X, is shown as a function of frequency in the familiar curve of Figure 35. At low frequencies the mass center of the component follows the input or base structure deflection. As the frequency nears $\sqrt{K/m}$, or resonance, the deflection amplifies and becomes greater than the input or base deflection. This amplification is a function of the energy sinking or heat generating property of the component, shown as B, Figure 35, due to flexure. For frequencies above $\sqrt{K/m}$ the deflection decreases rapidly and approaches zero.

The philosophy used in designing support structure is to adjust $\sqrt{K/m}$ so that resonance lies above the input vibration spectrum of the launch vehicle by adjusting K so it is sufficiently large. Hence, stiffness is important in all component mounting. Care must be exercised in package

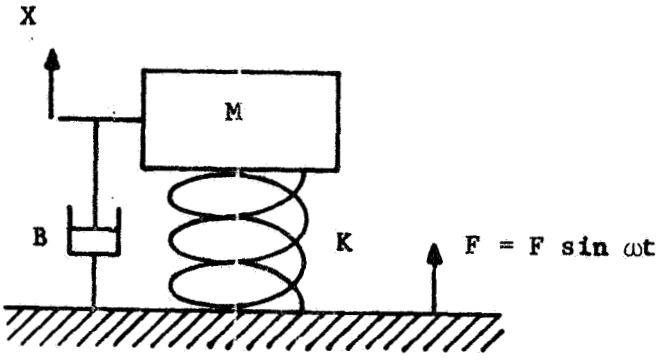

Figure 34. Schematic of simple mass-spring system.

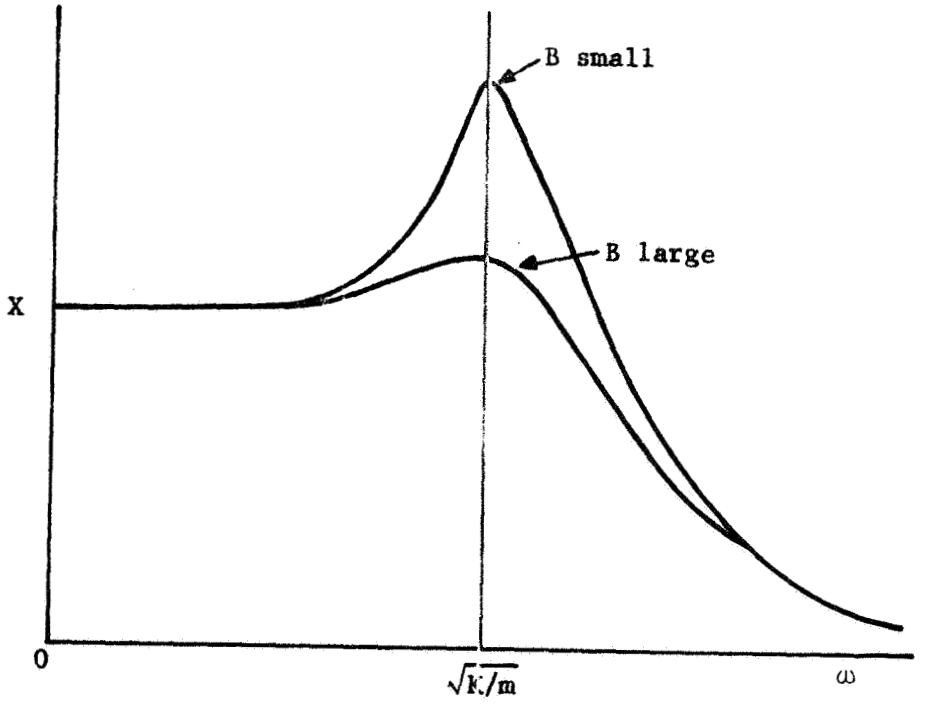

Figure 35. Transmissability curve for spring-mass system.

design so that by including stiffness, the mass of the overall component is not also increased, since the ratio K/m is the controlling parameter. From this ratio, the familiar aerospace structures parameter of strength-to-weight ratio is immediately derived. The design of instrument cases, circuit boards and other panel-type structures follows the same rules since a panel section is a compliant mass.

Conformal coatings and castings of thermal-setting plastics are generally beneficial in increasing the strength-to-weight ratio of component assemblies. In addition, these plastics (urethane, epoxy, polyester, etc.) are quite lossy and provide good energy sinking or damping (large B). The use of transistorized, miniaturized circuitry is particularly suited for vibration hardening since their total mass is relatively low. This is even more pronounced with the use of integrated thin film circuits. These circuits coated or potted in plastic provide vibration hardness which will endure any known launch environment including gun launches (50,000 g).

Instrument cases can be either cast or welded, of fairly thick light weight beryllium, aluminum, or magnesium if complete shielding is required. The thickness parameter must be adjusted to obtain sufficient strength to avoid panel flutter. Here again, strength-to-weight is important and too much thickness may increase the mass and reduce the panel resonant frequency. If the case does not require complete shielding, lighter stock may be used which is lightened and stiffened in strategic areas by means of flanged cutouts or "lightening holes."

F. Test System

The vacuum test system was designed to furnish two independent gas pressures that can be used according to the "two-chamber simulation method" described in the previous chapter for testing the yaw attitude sensor over a wide range of pressure. The yaw attitude sensor system cold cathode ionization type pressure (vacuum) gauge and its associated mechanical cycling valve connect to the test system so that either port or tubulation of the valve can communicate with a higher or lower pressure.

As can be seen from the schematic drawing of Figure 36, the system is a "dry" pumping system in that no oil diffusion or mercury diffusion pumps are used. The presence of pump oil in a vacuum system can furnish lubrication to moving parts, such as ball bearings, and can thus invalidate the results of experiments designed to determine the operating characteristics of these moving parts in a true space vacuum environment.

The test system provides two identical test chambers, each chamber being pumped by separate ion pumps, titanium sublimation pumps, and zeolite sorption pumps. Nude ionization gauges of the Bayard-Alpert

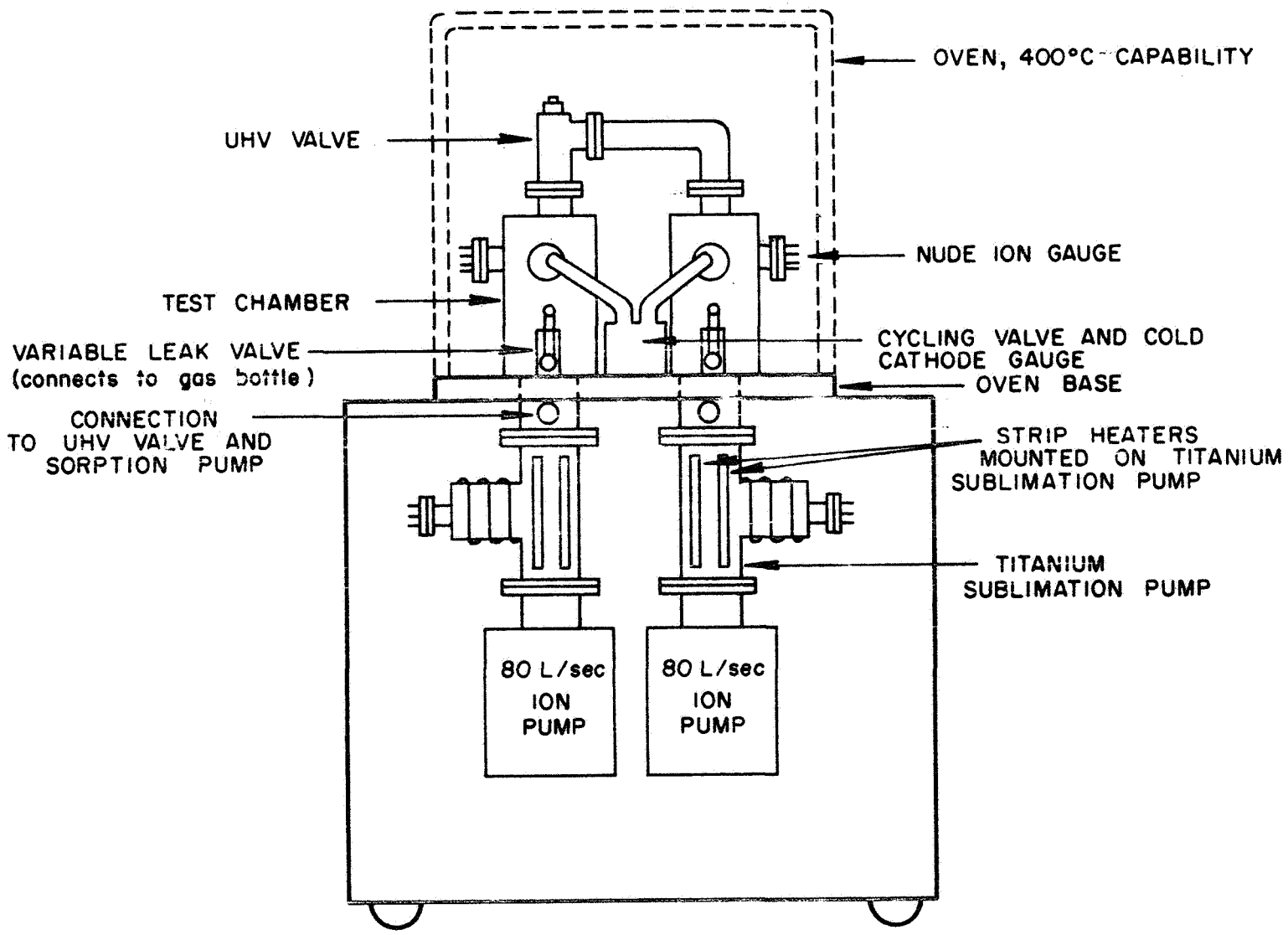

Figure 36. Vacuum test system for the velocity vector sensor.

variety measure the pressure in each test chamber. A variable leak valve connected to each test chamber permits the pressure in each chamber to be adjusted independent of the pressure in the adjacent chamber. The two chambers can be connected together by means of an ultra-high vacuum (UHV) valve. Connection of the two chambers makes it possible to equalize the pressures in the chambers when required to obtain a zero pressure differential at the input of the mechanical cycling valve. The use of this valve also permits the readings of the test chamber nude ionization gauges to be compared. A high temperature bakeout oven is furnished for baking the test chambers, the mechanical cycling valve, the cold cathode ionization gauge and all of the vacuum components located above the oven base. Bakeout is required when low background pressures of the order of 10^{-9} to 10^{-10} torr are to be attained. The system was designed to permit the connection of 1 liter bottles of pure gas to the variable leak valves of each test chamber. Zeolite-type sorption pumps, which are chilled with liquid nitrogen prior to operation, are used to pump down each test chamber and its associated ion pump and titanium sublimation pump from atmospheric pressure to approximately 10^{-3} torr, at which pressure the ion pumps and titanium pumps can be turned on.

The test system was designed to be housed in a mobile cabinet. All of the vacuum components including the pumps, valves, gauges and test chambers are mounted on and within a single "vacuum console" cabinet. All of the electronic control units that are required for the operation of the pumps and gauges are mounted in a separate mobile electronics rack. Cooling water connections as well as electrical connections are required for the vacuum console. The bakeout oven can be easily installed and removed from the vacuum console. All valves and control units are accessible from the front of the two cabinets.

The sizes of the vacuum pumps were selected on the basis of their compatibility with the yaw attitude sensor, especially the mechanical cycling valve and its connecting tubulations. The pumps are large enough to provide a rapid pump-down and also handle the outgassing load that would be developed during bakeout.

4. CONSTRUCTION

A. Mechanical Cycling Valves

The three mechanical valves were constructed in accordance with the general designs discussed in the previous chapter. All of the valves were constructed primarily from 304 stainless steel so that they would be suitable for high vacuum, or even ultra-high vacuum, operation. The 304 stainless steel was generally hydrogen annealed to remove stresses before the final finish machining was performed on those parts having small tolerances and close spacing to adjacent parts. Figure 37 shows the comparative sizes of the three mechanical cycling valves.

1. Rotary valve. - In the rotary valve, the balance of the rotor is of importance. It was decided to make the wall thickness of the rotor lighter at a position opposite the aperture to achieve at least a static balance. The drive rotor was fastened to the top of the valve rotor by pinning. The drive rotor contained four small permanent magnets that were sealed and welded vacuum tight within it. The gold-plated ball bearings that support the valve rotor were lightly spring loaded in the axial direction with the use of a Bellville type spring washer. The amount of loading applied to the bearings is critical since too heavy a loading will cause the bearings to bind. It can be seen from the illustration of Figure 16, that the valve rotor can be easily installed and removed from the flanged end of the valve simply by removing the Tru-arc type retaining ring.

The two side arm tubulations to the valve housing are welded in position, as is the demountable flange at the bottom of the housing. Great care must be taken in all welding operations since the parts can be distorted by the intense and uneven heat distribution. The usual procedure is to provide adequate heat sinking as close to the welded seam as possible.

Major component parts of the rotary valve, with the exception of the drive rotor, are shown in the exploded view photograph of Figure 38. The rotary valve is the smallest and simplest of the three valves that were constructed. It has the highest ratio of open-to-closed vacuum conductance. As mentioned earlier, its chief drawback was the erratic behavior of the gold-plated ball bearings, which seemed to depend critically on the amount of axial loading on the bearings. A second difficulty that was experienced with this valve was the problem of starting the valve, that is, putting the rotor into operation. This difficulty was primarily due to the type of electromagnetic drive that was used.

The smooth operation of the rotary valve depended to some extent on the orientation of the valve. In particular, the valve worked better in the vertical than in a horizontal position. Presumably, the forces acting on the bearings varied with the direction in which gravity caused the rotor

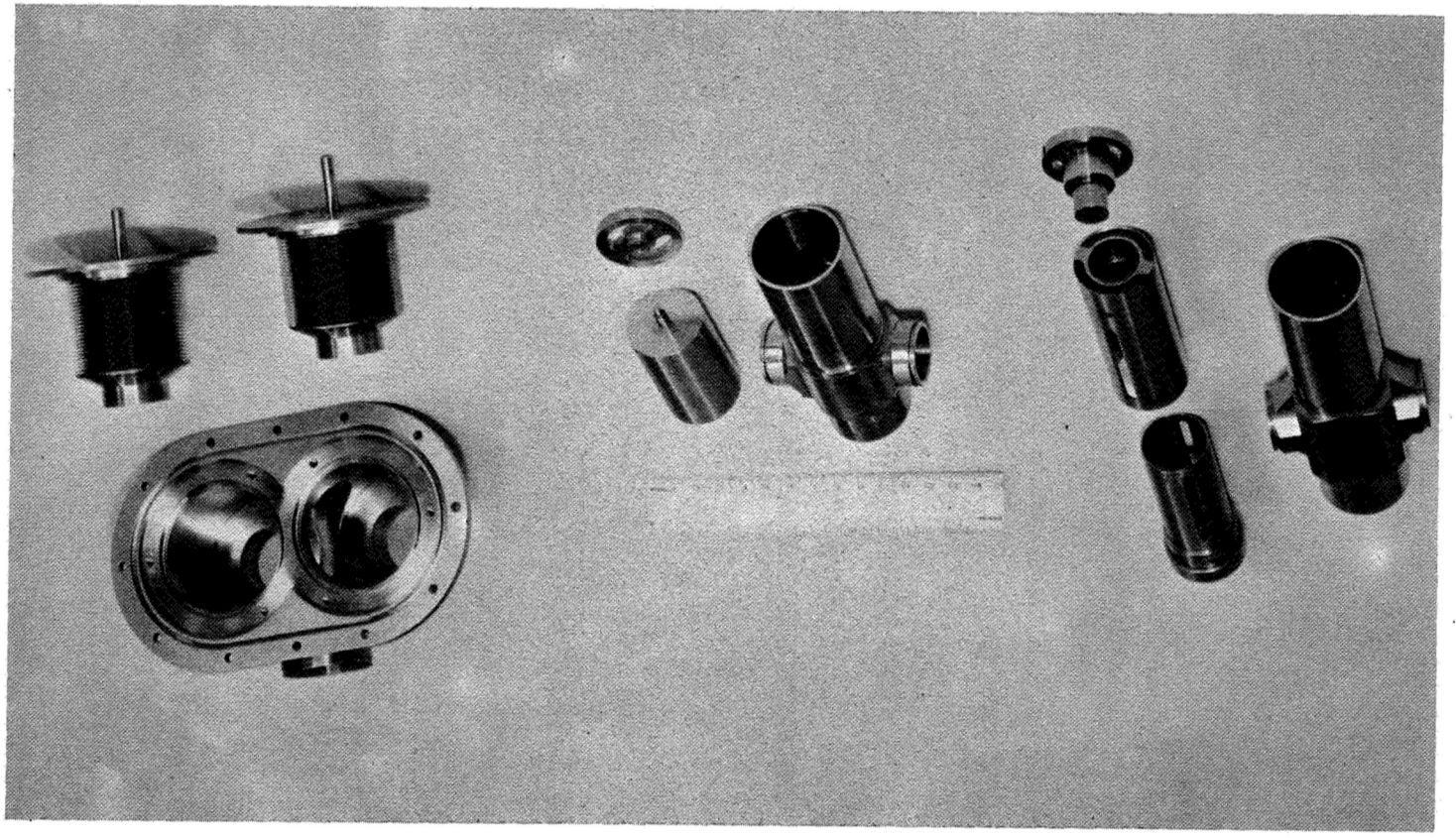

Figure 37. Photograph of comparative sizes of the three mechanical cycling valves.

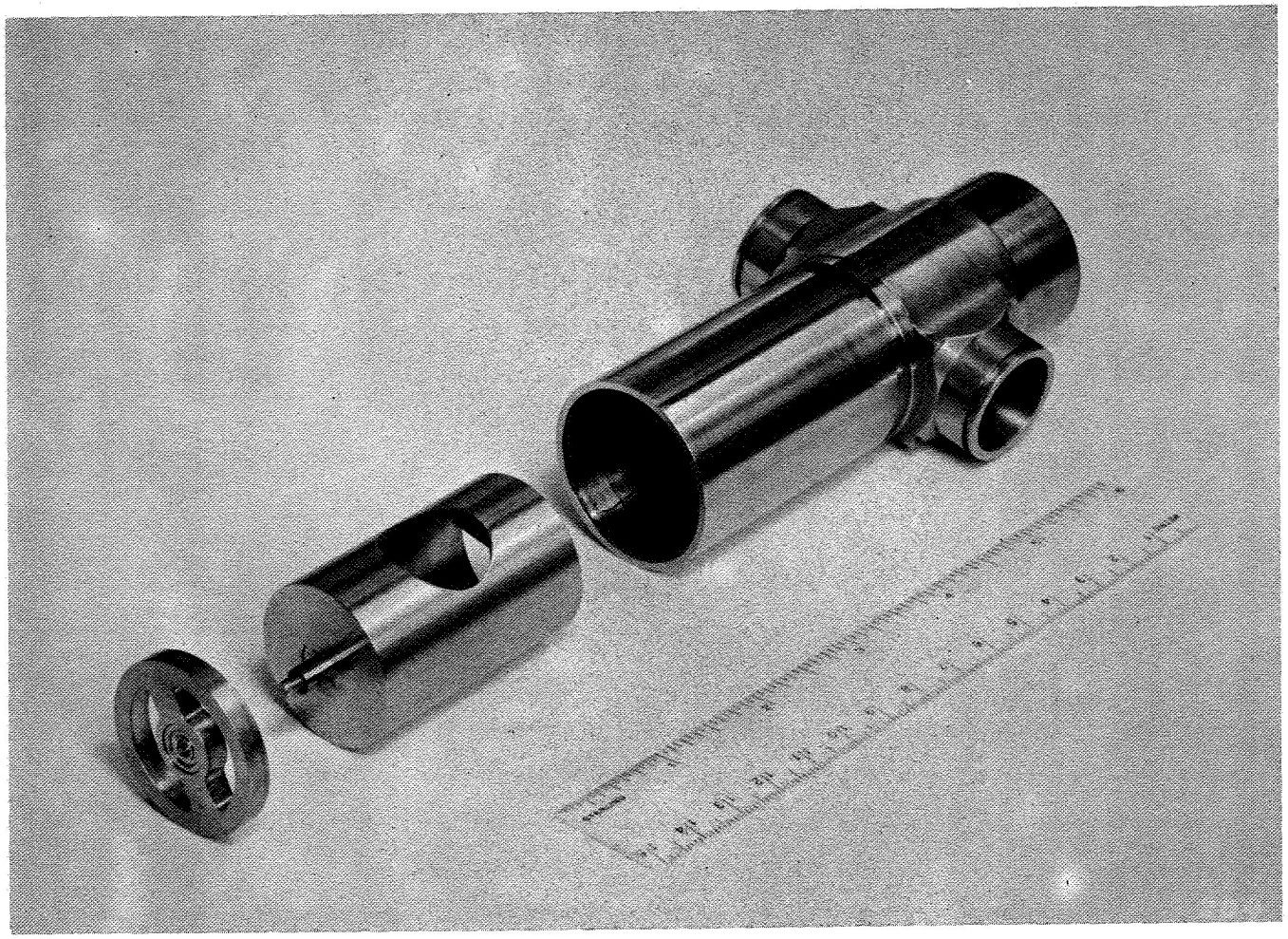

Figure 38. Photographic exploded view of the rotary valve.

to load the bearings. The physical clearance between the o.d. of the rotor and the i.d. of the housing had to be greater than the radial "play" or tolerance of the bearings to prevent the rotor from rubbing on the housing with the valve in a horizontal position.

2. Linear reciprocating valve. - The construction of the linear reciprocating valve was only partially completed during the project. As can be seen from Figure 37, this valve is comparatively large and bulky; and it is the heaviest and most complex of the valves. The attainment of true alignment of the poppets and the ports required careful machining and assembly. The total travel of the bellows enclosed poppet assembly was of the order of 3/8 inch. Of the total amount of travel, the poppet was designed to have a 1/8-inch clearance when open and a 1/4-inch overlap when closed. With this arrangement, the valve would have both ports closed during a portion of each cycle. The valve was designed to have each poppet in the fully closed position with the bellows at its nominal free length (that is, neither compressed nor extended). The bellows were then compressed during each opening cycle. Welded metal bellows have a maximum lifetime when used only in compression.

Toward the end of the project year, it became apparent that there would be neither sufficient funds nor time to complete the linear reciprocating valve and build a suitable drive mechanism for it. It was decided to concentrate attention on the rotary valve and the flexure-pivot valve.

3. Flexure-pivot oscillating valve. - The flexure-pivot oscillating valve is perhaps the most unique of the three valve designs. The two cylinders which are used in a counter-rotating configuration must be accurately ground to close tolerances on their diameters. The alignment and concentricities of the flexure pivot bearing mountings are especially critical in this double rotor design since any angular tilt of either rotor will cause rubbing.

The slit openings of each rotor have been made as long and narrow as possible in order to accomplish two objectives. The first objective is to provide the largest possible aperture for the "open" position of the valve. The second objective is to reduce the total amount of angular travel as much as possible in order to lengthen the lifetime of the flexure pivots. As can be seen in the photographs of Figures 37 and 39, the tubulations to the valve housing have been deliberately flared in order to accommodate the use of long slit openings in the rotors. The flared tubulation housing of the flexure pivot valve is more difficult to machine than the ordinary tubulation housing of the rotary valve. The requirement for long slit openings also increases the overall length of the valve as compared to the length of the rotary valve, for example.

Whereas the rotary-valve housing is open at only one end, the flexure-pivot valve housing is open at both ends. The bearing holder for the upper flexure-pivot becomes the sealing cap for the top of the valve housing with an end weld to minimize distortion and to permit the bearing holder to be easily machined off if the valve is to be disassembled.

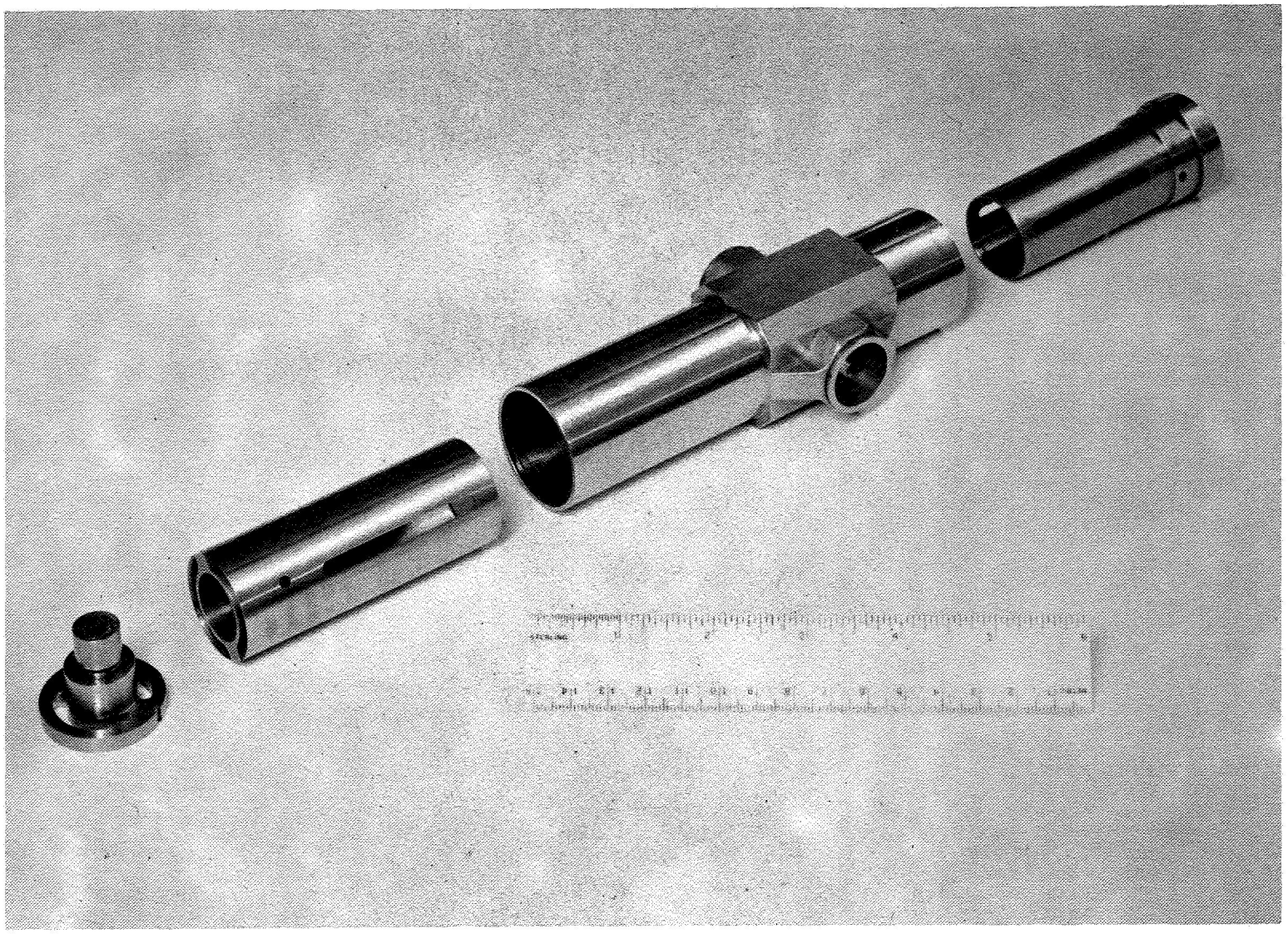

Figure 39. Photographic exploded view of the flexure-pivot oscillating valve.

At the end of each of the two slotted rotors, pure nickel magnetic drive rotors were installed. These drive rotors are acted upon by the external magnetic field of the electromagnetic drive unit. The drive rotors have the largest possible outer diameter to minimize the air gaps that will exist between the pole pieces of the electromagnetic drive and the drive rotor.

As can be seen in Figure 20, the lower slotted rotor (at the end at which the gauge will be attached) is the outer rotor while the upper slotted rotor is the inner rotor. Ideally, these two rotors should be designed and constructed so that they both have the same moment of inertia and, hence, the same resonant frequency when used with identical flexure pivots. The two rotors that were constructed do not have quite the same moment of inertia. Since their average diameters are different, the two rotors must necessarily have different masses.

The rotor diameters and slit widths were designed to provide valving action with an angular movement of ±15 degrees for each rotor. In the relaxed position, there is no overlap of the slits and the valve is effectively closed at both inlet ports. This is a sort of "fail-safe" provision in case the electromagnetic drive unit fails. With both ports closed, the valve would yield a zero or null signal at the output of the yaw attitude sensor. The two ports are opened alternately when the rotors reach the extreme positions of their angular travel.

One other unusual feature of this valve that should be mentioned is the center shift of that portion of each flexure-pivot bearing that is attached to one of the rotors. The center shift of the bearings used for a ±15 degree angular motion is estimated to be about 2 mils. The spacing between the rotors must be adequate to allow for this shifting of the centers.

4. Electromagnetic drive units for valves. - Two electromagnetic valve drive units were constructed as illustrated in Figures 17, 21, and 40. A single unit was built to operate the rotary valve while two separate units were constructed to operate the two rotors of the flexure-pivot valve. Only the flexure-pivot valve drive units are shown in the photograph of Figure 40. The cases that surround the pole pieces, yoke, and coils are magnetic shielding boxes that are made up of alternate layers of soft iron, insulating glass-epoxy sheet, netic and conetic material.

The electromagnetic drive units were of an experimental nature. Both units used high permeability Armco soft iron for the pole pieces and the yokes. The pole pieces and the yokes were not laminated in order to simplify the design. Since the valves would be operated at low cycling rates of less than 10 c/s, it was decided to accept the hysteresis and eddy current losses that developed.

The two pole pieces of the rotary valve electromagnet were "shaded" by cutting a deep slot near one edge of each pole face and by wrapping a

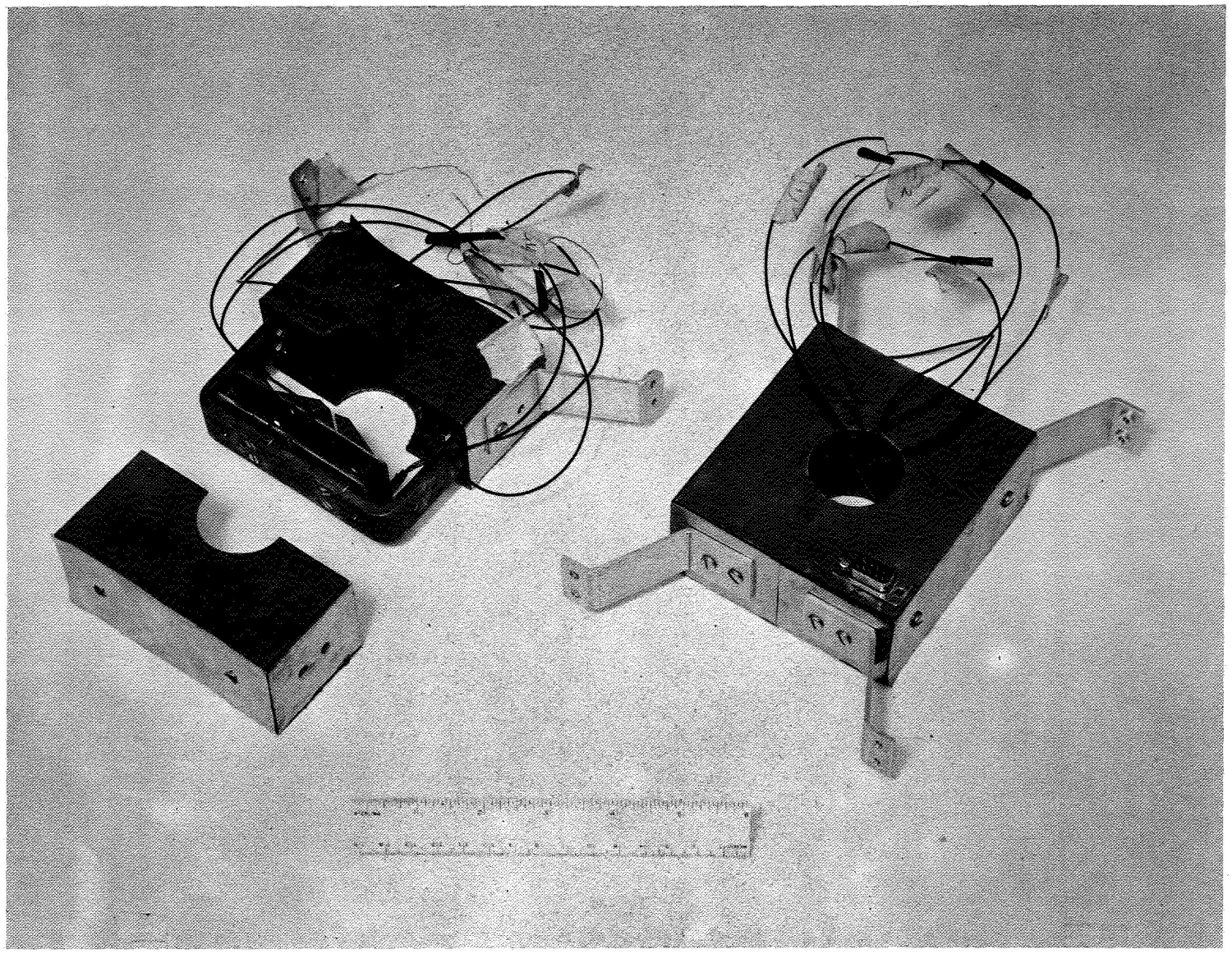

Figure 40. Photograph of the flexure-pivot valve electromagnetic drive units.

868

single turn of copper sheet around the small secondary pole piece that was formed. This electromagnet was adjusted by tightening the four screws that joined the pole pieces to the yoke so that the pole pieces were a press fit over the top of the rotary valve housing. The two coils were wound with enamel-coated copper magnet wire. The coils could be connected either in series or in parallel depending on the power supply that was used to energize them.

The pole pieces of the flexure pivot valve electromagnet are of an unusual shape, as can be seen in the illustrations. The intent was to concentrate the magnetic field in the regions where the nickel drive rotors would be located when the rotors were at either end of their angular travel positions. Diametrically opposite coils of this electromagnet could be connected either in series or in parallel. The rectangular configuration of the yoke and its two-piece construction were selected for simplicity of construction and ease of adjustment. More compact arrangements of the pole pieces, the coils, and the yoke are possible. In the overall design, the flexure-pivot valve electromagnets, together with their magnetic shield boxes, would be mounted to the metal framework of the system package; and they would not be supported by the valve.

B. Electronics

Photographs of the various electronic units are shown in Figures 41 through 44. Not included in these illustrations is the electronic drive circuit of the flexure-pivot valve. The development of this drive circuit had only been carried through to the breadboard stage.

The high voltage power supply, as shown in the upper left of Figure 41, was a potted, sealed unit fabricated by a subcontractor to GCA Corporation specifications. All other electronic units were built by the GCA Corporation. The design of the individual electronics packages was coordinated with the overall system packaging.

All qualified components were used in the final construction of the electronics. As can be seen from the photographs, specially designed printed circuit boards were used for mounting the components. The printed circuit boards were mounted to rigid aluminum base plates that were designed for each separate electronics package. Removable aluminum covers were built to shield and protect each separate electronic package. Since the two yaw-attitude sensor systems that were constructed were "engineering models," no potting was provided for any of the newly designed electronics in order to facilitate future testing.

Subminiature connectors were used for all input and output connections. Trimpots were used for all adjustable resistances. Fixed resistors were either carbon composition types or RN 60 oxide film types. Threaded mounting holes were provided on each base plate.

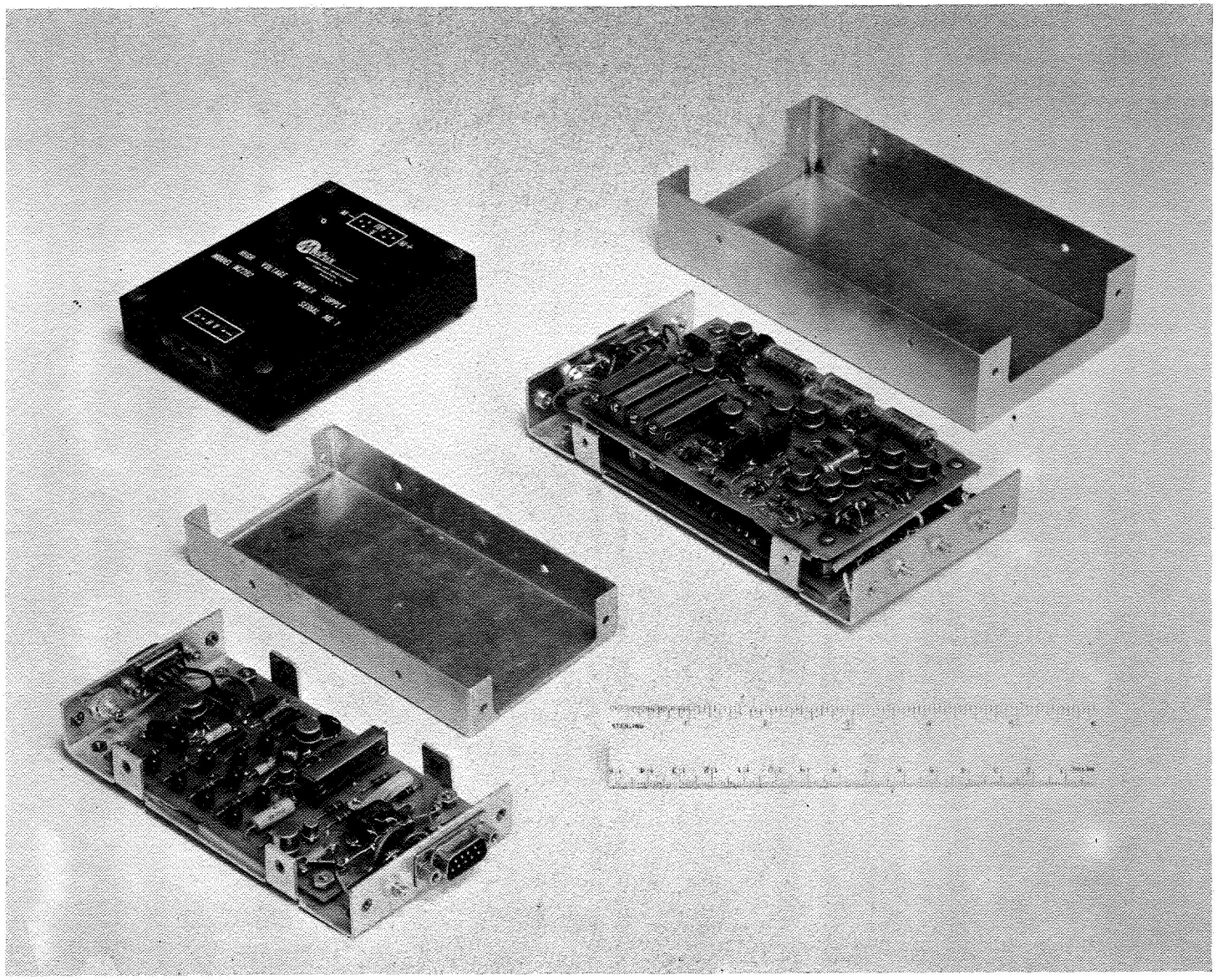

Figure 41. Photograph of electrometer amplifier, high voltage power supply and synchronous detector-differential amplifier.

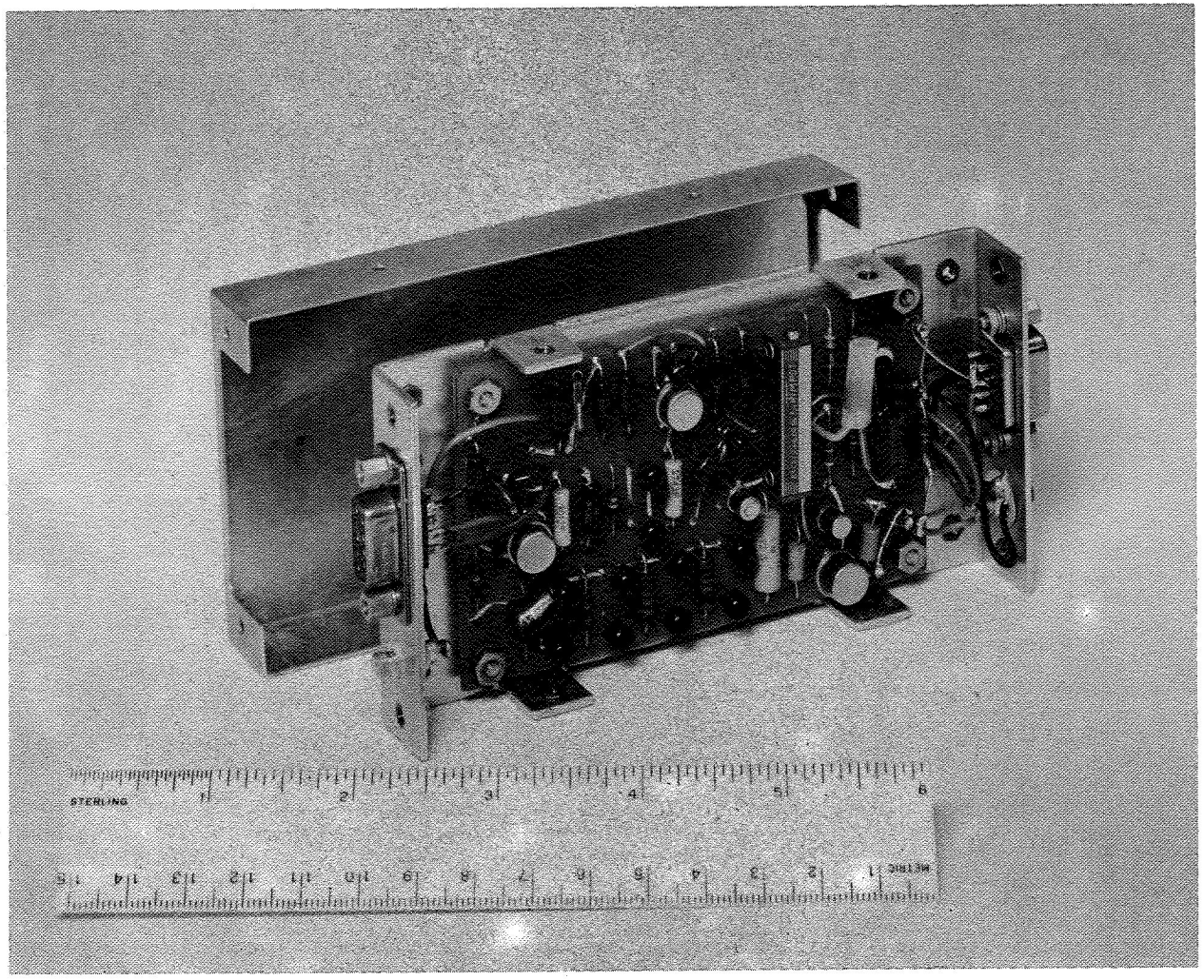

Figure 42. Photograph of the electrometer amplifier.

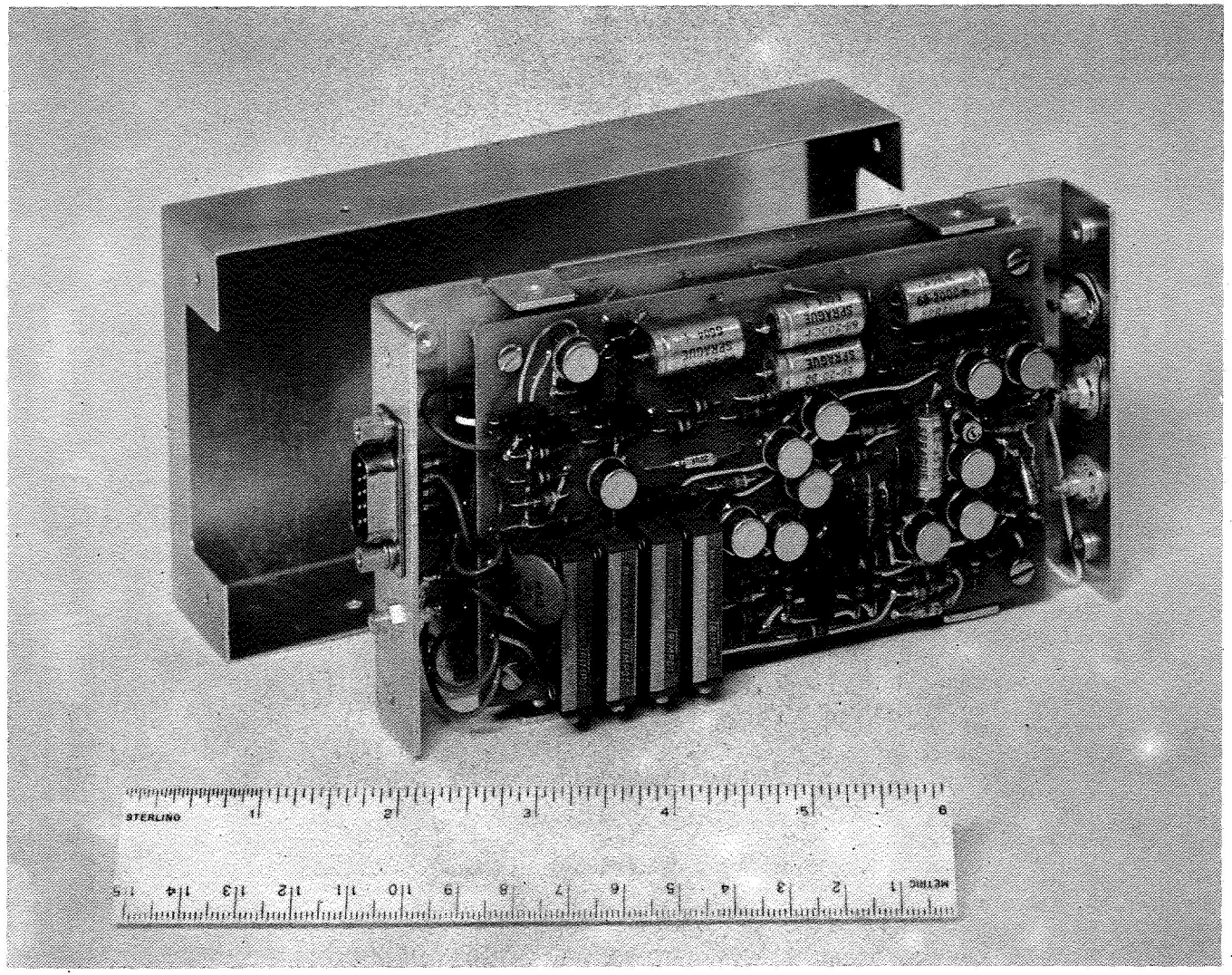

Figure 43. Photograph of the synchronous detector-differential amplifier.

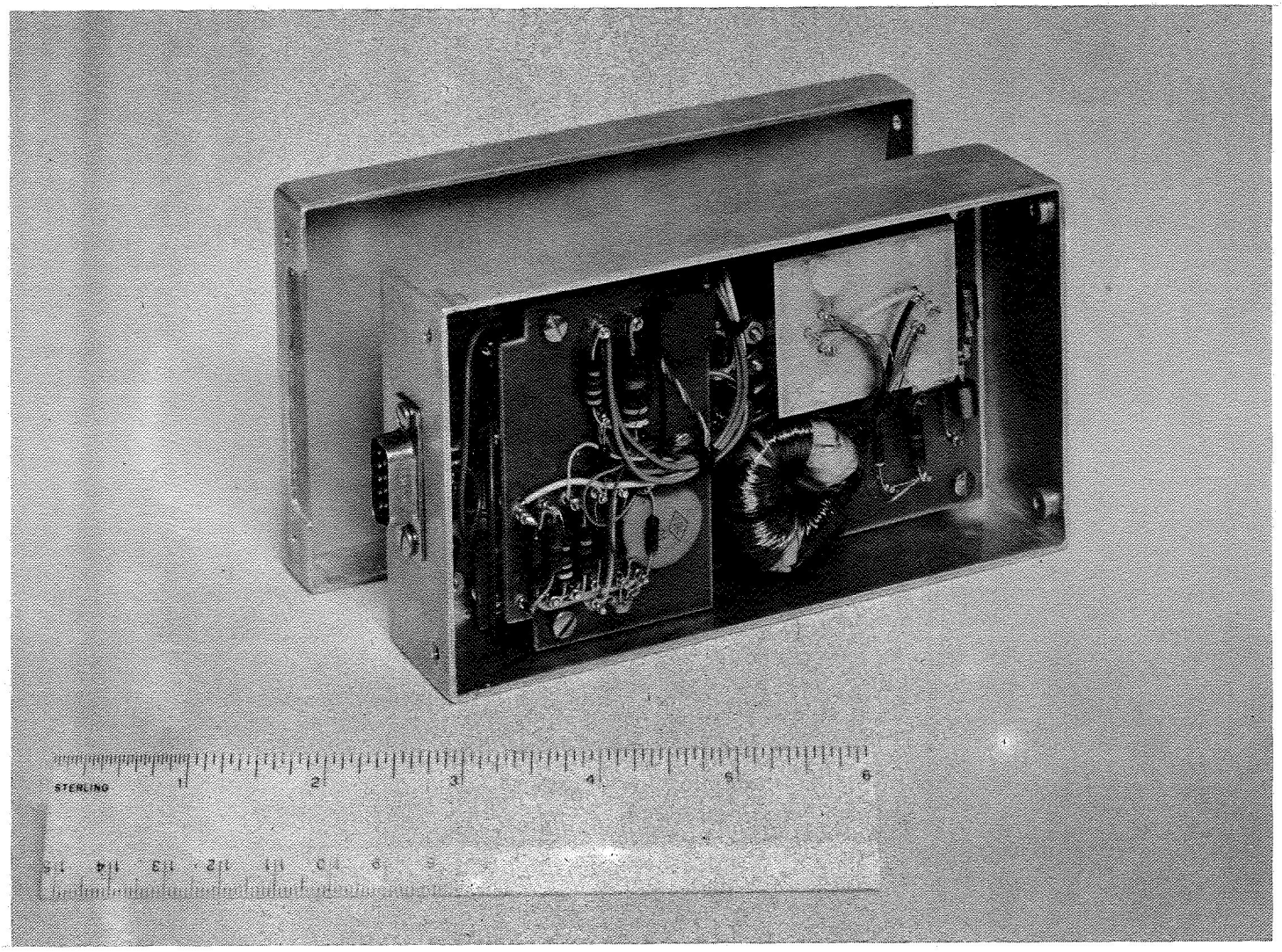

Figure 44. Photograph of the dc-to-dc converter.

The dc to dc converter accepted the vehicle input voltage of -24 volts dc and delivered output voltages of +15 volts dc and -15 volts dc as required by the remainder of the electronics. The toroidal coil of the flux oscillator is clearly visible in Figure 44.

C. Packaging

After it was decided to stop the construction of the linear reciprocating valve, the system packaging problem became much simpler. As mentioned earlier, the rotary valve and flexure-pivot valve were sufficiently alike so that a single package could be designed to accommodate either.

The support frame of aluminum angle was designed to achieve a "unit body" construction. The basic "box-like" support frame structure was welded together, as shown in Figure 45. Mounting brackets were fastened in removable fashion to the support frame. One pair of mounting brackets was used to hold the ionization gauge magnet and its laminated magnetic shield box at the bottom of the support frame. In Figure 45, this shield box and magnet are shown in position. The laminated shield box has a split top cover that fastens to the top open edge of the box. This split cover is not shown in the figure. Other pairs of mounting brackets are used to support the various electronic packages along the inner side walls of the support frame. The truss-shaped support brackets shown separately near the ruler are used to support the ionization gauge and the lower part of the mechanical cycling valve. The ionization gauge and cycling valve occupy the central part of the support frame. The cycling valve is supported by brackets that clamp the extended tubulations just before they pass through the split base plate. The base plate was split on the engineering models for convenience in installing and removing the cycling valve and gauge. The split base plate and the protective cover are shown at the right in Figure 45. The cover is made of welded sheet aluminum, and its rectangular flange (covered with paper tape in the illustration) mates with a rectangular O-ring groove located on the underside of the base plate.

The system package is relatively heavy and bulky as presently constructed and there is considerable waste space within the support frame. Other package configurations can undoubtedly reduce the overall system volume and weight.

D. Test System

The vacuum test system that was constructed is shown in the photograph of Figure 46. The vacuum console is shown at the left while the electronics rack is at the right. The front door of the oven has been removed to permit the test chambers to be seen. The rotary valve, which is flanged to an ionization gauge and magnet, is connected to the two test chambers via short horizontal tubulations. These tubulations are

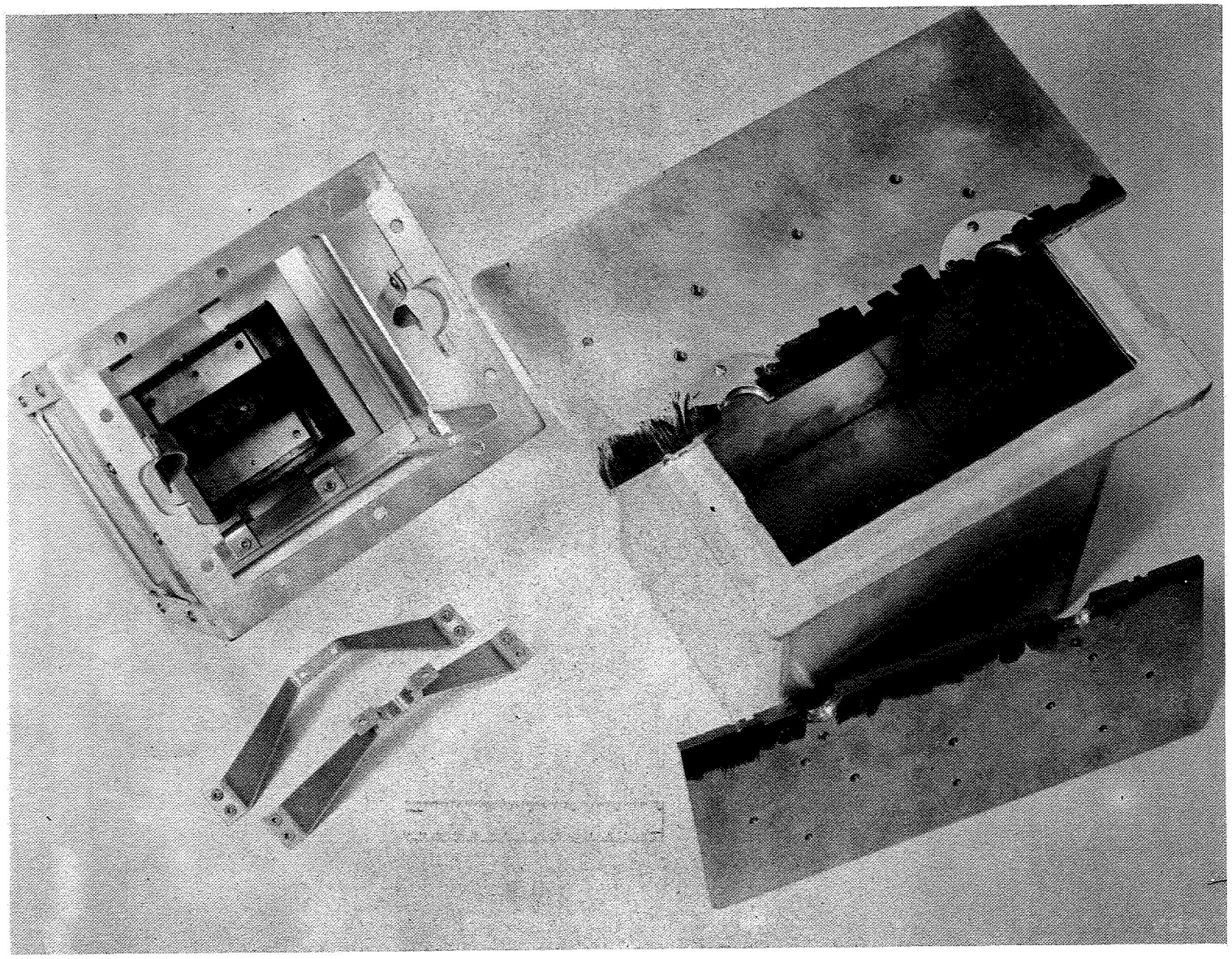

Figure 45. Photograph of the support frame and split base plate.

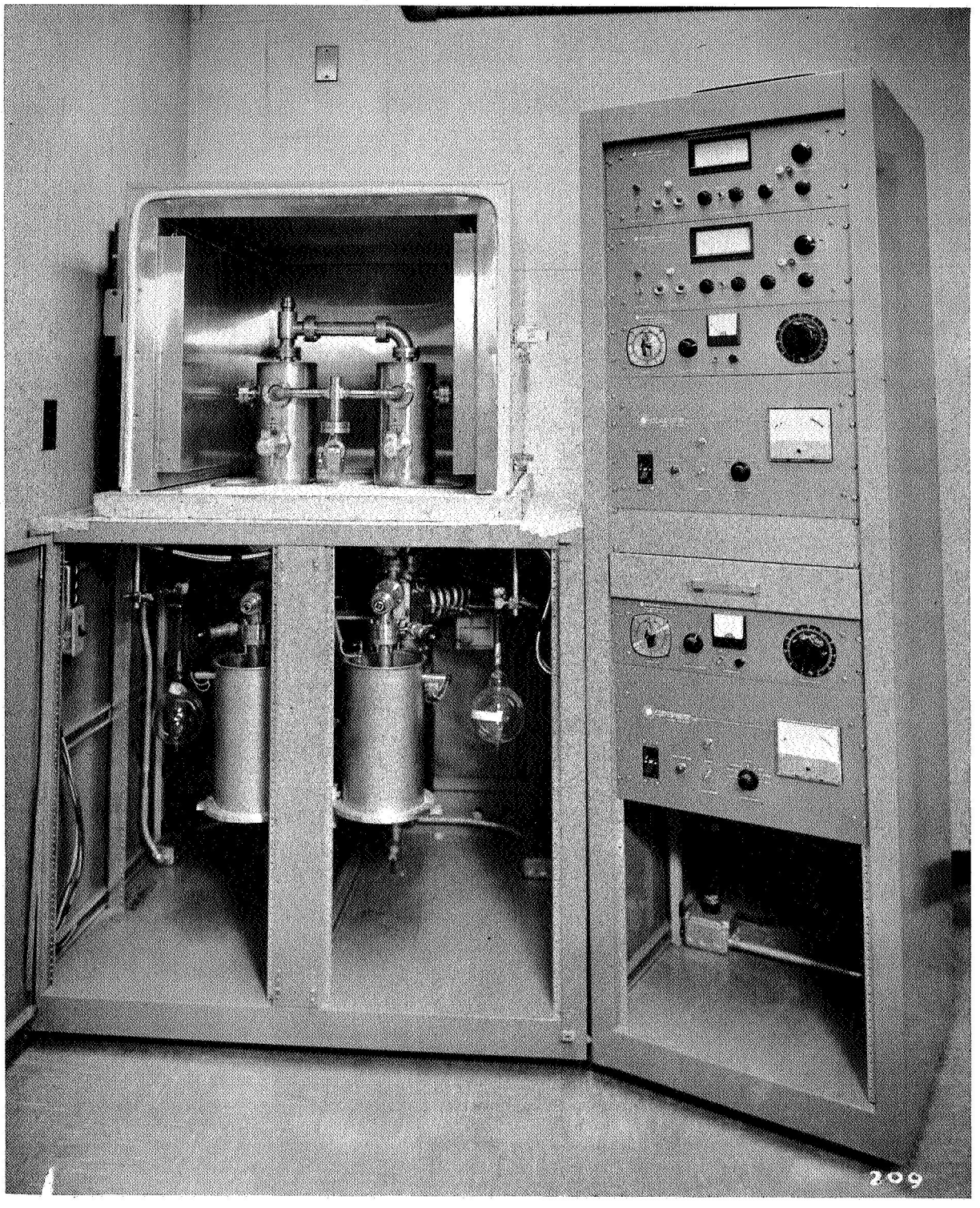

Figure 46. Photograph of test system.

flanged so that they can be conveniently demounted from the test chambers. At the lower front of each test chamber are the variable leak valves. These valves connect with the 1-liter glass gas bottles that are located below the top of the vacuum console. The connecting gas lines are made of copper and kovar. At the outboard sides of each test chamber one can see the flanged nude Bayard Alpert ionization gauge bases. The valve at the top of the left-hand test chamber is the ultra-high vacuum (UHV) valve that can be used to connect the chambers together.

The oven and the test chambers rest on the oven base, a 2-inch thick slab of marinite. The oven base, in turn, is fastened to the top of the vacuum console cabinet. The titanium sublimation pumps and the 80 liter/sec ion pumps are suspended from the bottoms of the two test chambers, and so the entire weight of the vacuum components is carried by the top of the cabinet. The titanium sublimation pumps are angled diagonally toward the back of the cabinet. The electrical connections to these pumps run conveniently through the back of the cabinet and over to the control units on the electronics rack. The ion pumps cannot be seen in the photograph since they are located directly behind the two sorption pumps that are at the front central part of the cabinet. The flanges that join the sorption pumps and their isolation valves (UHV valves) have special venting valve flanges. The venting valves may also be used for leak checking. Varian Millitorr type high pressure ionization gauges were installed at the lower end of each test chamber below the cabinet top. These latter gauges can measure pressures as high as 10^{-1} torr, and are useful during the initial stage of vacuum pump-down. Convenience electrical outlets were provided at each side of the cabinet. Removable hinged doors were present at both the front and back of the vacuum console cabinet.

The electronics rack was a standard 78-inch high enclosed rack having a hinged, louvered door at the rear. The two uppermost units mounted in the rack were the dual ionization gauge control units. Each of these units is capable of operating one low pressure Bayard Alpert type gauge and one high pressure Millitorr type ionization gauge. The third unit from the top was the right-hand titanium sublimation pump control unit while the fourth unit was the right-hand ion pump control. Below this ion pump control was a convenience desk-type pull-out drawer that could be used for storage of parts and writing. Below the pull-out drawer was the left-hand titanium sublimation pump control. The last and lowest unit was the left-hand ion pump control. Many electrical outlets were provided inside the rack.

The oven itself was a 7-kW ducted, forced air unit. The temperature within the oven could be controlled within a few degrees to temperatures as high as 500°C. The oven had front and rear doors and could be placed in position or removed by two people.

5. TESTS AND RESULTS

A. Mechanical Cycling Valves

1. Rotary Valve. - Only two of the three mechanical valves that were designed were fabricated completely and placed in operation. The linear reciprocating valve was not completed. The rotary valve was operated to a much greater extent than the flexure-pivot valve, primarily because the rotary valve drive circuit was completed much earlier.

The rotary valve was placed into operation with the use of two different types of driving mechanism. The first valve drive mechanism was the experimental electromagnetic drive shown in Figure 17. The second valve drive mechanism consisted of a small U-shaped permanent magnet external to the valve that coupled magnetically to a pure nickel rotor within the valve.

For the first valve drive mechanism, the drive rotor consisted of either a pure nickel rotor or a permanent magnet rotor. The pure nickel rotor was used with the second valve drive mechanism. The nickel rotor was essentially a rectangular bar of pure nickel with a central hole. The nickel rotor slipped over the top shaft of the rotary valve rotor and was fastened securely with set screws. The U-shaped magnet spacing was large enough to slip over the top of the rotary valve housing so that the nickel rotor tended to complete the magnetic circuit.

The U-shaped permanent magnet was mounted on a Bodine Model NSH-12R variable speed motor connected to a Minarick Electric Company Model SH-12 speed control. The motor with the attached U-shaped magnet had to be mounted rigidly since there was a strong attraction between the permanent magnet and the rotor. Unless there was trouble with the gold plated ball bearings of the valve, the valve rotor generally followed the rotational motion of the external magnet quite well. The external magnet drive was quite flexible in that the valve could be conveniently opened and closed by hand and could be cycled at very low speeds with the use of the geared-down variable speed motor. Schematic drawings of the external magnet drive and the nickel drive rotor are presented in Figure 47.

The first valve drive mechanism, (i.e., the electromagnetic drive) operated well with either the nickel rotor described above or with a permanent magnet rotor. The latter rotor consisted of a stainless steel disk approximately 1-1/4 inches in diameter and 1/4 inch thick. Four blind holes about 3/16 inch in diameter were drilled into the disk from the cylindrical side wall. However, instead of being drilled radially inward toward the center of the disk, these four holes were drilled so as to form an inscribed square within the circular rotor. Small round permanent bar magnets were inserted in the blind holes and then sealed with stainless steel plugs that were welded at the cylindrical surface. The construction of this rotor is shown in Figure 47.

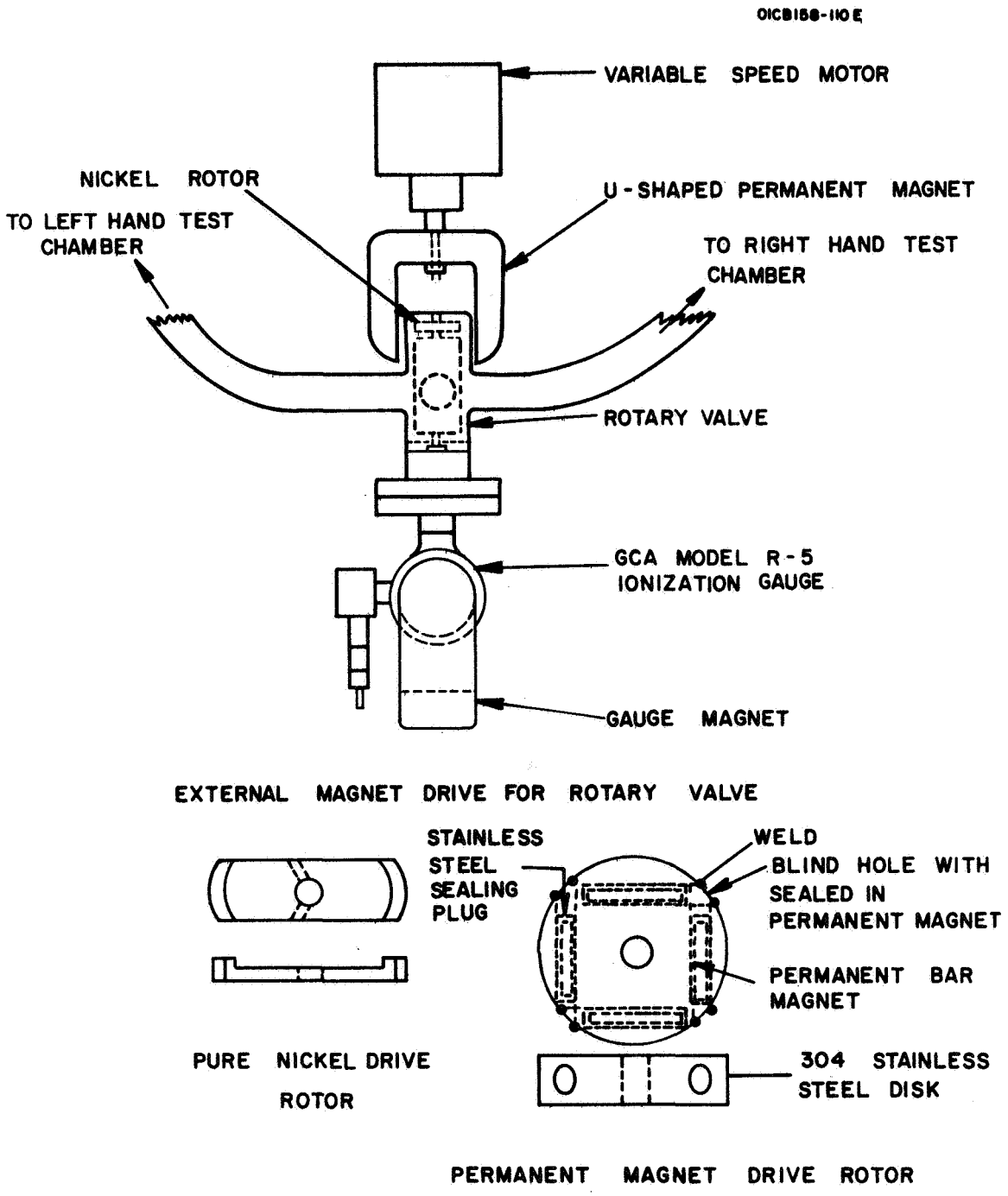

Figure 47. Rotary valve drive rotors and external magnet drive.

It was found that the two-pole experimental electromagnetic drive unit would turn either of the two drive rotors in synchronism with the driving current through the electromagnet coils once the drive rotors were started. Tests of the valve drive circuit capability were made on the bench in atmospheric air. The valves were open (the pressure sensor was not attached) and the rotation of the valve rotor could be seen through the open tubulations to the valve body or housing. If the valve rotor was started by hand, it would gradually come up to speed and lock-in with the rotation frequency of the electromagnetic drive.

The nickel drive rotor would not start by itself under any conditions. On the other hand, the permanent magnet drive rotor seemed to start by itself, but the starting phase was very erratic and unpredictable. In ten starting experiments, for example, the rotor started five times in less than 3 minutes and the other five times at much longer time intervals.

In an attempt to improve the starting characteristic, small coils were wound around the shaded poles and the phase of the current to these shaded poles, relative to the current phase through the main coils, was varied. It was found that the starting was still erratic, unpredictable, and unreliable. It was concluded that a two-pole electromagnetic drive was not suitable and that a four-pole electromagnetic drive would be necessary. A pure nickel drive rotor could be used with the latter type of electromagnetic drive.

During the experimentation with the rotary valve drive circuits, and in later experiments with the rotary valve connected to the vacuum test system and evacuated, it was found that the axial loading on the gold plated ball bearings and the orientation position of the valve critically affected its operation. For example, the valve might operate well in a vertical position but not in a horizontal position. If the Bellville type washers used to axially load the bearings were too heavy (too strong a spring constant), the valve rotor would not move when placed under vacuum, although it would move at atmospheric pressure.

Another difficulty was noticed after the rotary valve had been driven by the external magnet drive for periods of time of the order of an hour. The valve becomes quite warm to the touch, partly because the U-shaped magnet dragged on the housing occasionally. At some point in time, the rotor would stop its rotation, as though the bearings had "seized." Light tapping of the housing generally freed the rotor. It is believed that high temperatures may have developed at the bearings or differential temperatures developed between the rotor and the housing to increase the axial loading on the bearings.

The results of a closely related parallel study that was made of the operating characteristics of ball bearings in a vacuum environment

will be presented next. This study was performed under contract to Honeywell, Inc. The same type of gold-plated ball bearings that were used in the rotary valve were used in this study.

In connection with a comparative study of the relative merits of a rotary valve and a flexure-pivot oscillating valve, an experimental study was made to determine the operating characteristics of ball bearings in a vacuum environment. It was known from previous work that high speed operation of ball bearings in vacuum often led to catastrophic failure of the bearings within a comparatively short time [9,10,11]. The objective of the experiments was to determine low speed characteristics of gold-plated ball bearings operating in a vacuum.

As illustrated in Figure 48, a butterfly test valve was constructed to make use of gold-plated ball bearings. The valve assembly was fabricated primarily of non-magnetic 304 stainless steel. The central circular flat vane of the valve was fastened to cylindrical shafts which, in turn, were mounted to the inner races of the ball bearings. The outer races of the ball bearings were supported and held fixed in position by bearing retainer blocks. Nickel cylinders (drive rotors) were pinned to the ends of the vane shafts. An external permanent magnet was used to couple magnetically to one of the nickel drive rotors as shown in the vacuum test system sketch of Figure 48. A small variable speed motor was used to rotate the permanent magnet, and the rotational motion of the magnet was thus transferred to the circular vane of the valve. The clearance between the circular vane and the surrounding cylindrical housing was 0.003 inch so that any axial movement of the vane by this amount would cause the vane to bind or rub on the housing.

The butterfly test valve was designed to mount within a 6-inch o.d. by 4-inch i.d. Conflat demountable UHV flange. The location of the valve within the test system is shown in Figure 48. The test system was an all-stainless UHV-type system that used cryogenic sorption pumping in the forevacuum and getter ion pumping of the test chamber. This mode of pumping is important since there were no pumping fluids or organic vapors within the system which could furnish lubrication to the ball bearings. Put another way, an all-dry pumping system of this type is essential if there is to be a realistic simulation of the space environment.

A window was provided at the test chamber so that the operation of the valve in vacuum could be observed. A nude-type Bayard Alpert ionization gauge was used to monitor the degree of vacuum in the test chamber. A General Radio Company Strobotac was used to measure the rotational speed of the butterfly valve as shown in the schematic drawing.

The various tests that were performed with the experimental arrangement described above are summarized in Table 4. The first test showed that the butterfly valve had the same rotational speed as the driving permanent magnet for speeds up to 3,010 rpm. The second test, with the

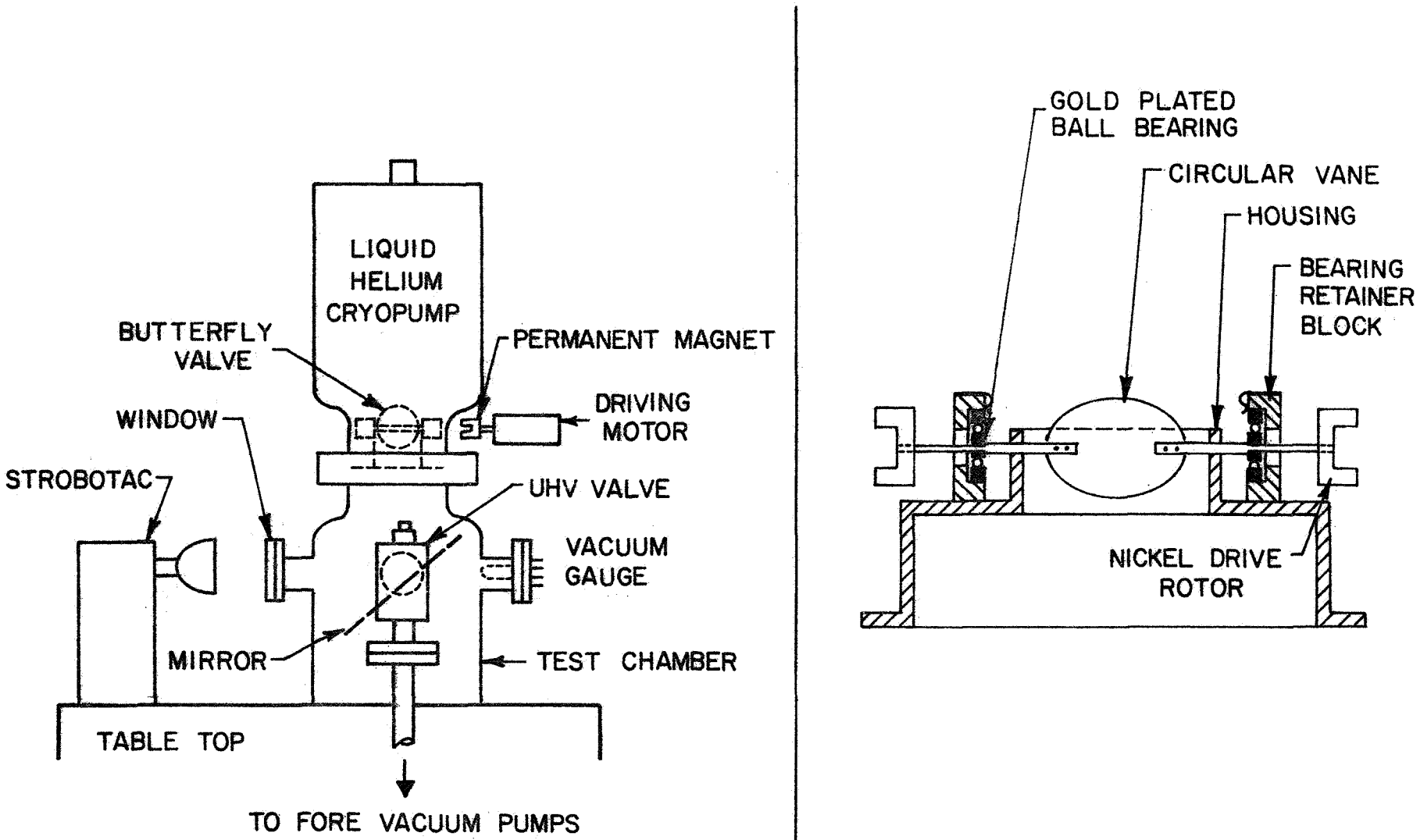

Figure 48. Butterfly test valve schematic.

TABLE 4

BALL BEARING TESTS

TEST	RESULTS
1. MEASURED THE ROTATIONAL SPEED OF THE DRIVING MAGNET AND THE BUTTERFLY VALVE, WITH THE VALVE IN A VACUUM.	1. THE VALVE HAD THE SAME SPEED AS THE DRIVING MAGNET.
2. STARTED THE VALVE OPERATING AT 3,010 RPM IN A VACUUM OF 4.7×10^{-6} TORR.	2. THE VALVE OPERATED FOR LESS THAN 15 HOURS, 46 MIN. EXAMINATION SHOWED THAT THE VALVE VANE COULD MOVE AXIALLY BY 0.005 INCH AND THUS COULD RUB ON THE HOUSING.
3. REMOVED MOST OF THE AXIAL MOVEMENT BY REPOSITIONING THE BEARING RETAINER BLOCKS. THE VALVE OPERATED WELL IN AIR.	3. THE VALVE WOULD NOT OPERATE IN VACUUM. SUSPECT THAT REMOVAL OF AXIAL PLAY IN THE BEARINGS CAUSED BINDING UNDER VACUUM CONDITIONS.
4. INSTALLED NEW BALL BEARINGS AND ALIGNED THEM FREE OF AXIAL LOADING BY USING A JIG.	4. THE VALVE RAN SMOOTHLY IN VACUUM AT SPEEDS BETWEEN 400 AND 600 RPM FOR 13 DAYS, WHEN THE TEST WAS ENDED. VALVE MOTION CREATED AN AUDIBLE SOUND.
5. AFTER OPERATION FOR 13 DAYS AT SPEEDS BETWEEN 400 AND 600 RPM, THE VALVE SPEED WAS INCREASED TO 1500 RPM.	5. THE VALVE RAN NORMALLY FOR ABOUT 2-1/2 HOURS. AT THAT TIME THERE WAS A POWER FAILURE IN THE BUILDING. WHEN POWER WAS RESTORED ABOUT 1 HOUR LATER, THE VALVE WOULD NOT START, EVEN AFTER 4 OR 5 ATTEMPTS.
6. WITHOUT DISTURBING THE VALVE, AIR WAS ADMITTED TO THE VACUUM CHAMBER.	6. THE VALVE STARTED ALMOST AT ONCE IN AIR AND RAN SMOOTHLY.

valve operating at a high speed of 3,010 rpm, showed that any loosening of the valve mounting support structure or any increase in the allowable radial or axial movement of the inner race of the ball bearings (as would occur with wear of the bearings) could lead to binding where small clearance gaps are present. The third test demonstrated the critical nature of ball bearing alignment in vacuum. An improperly aligned ball bearing may work in a normal atmospheric environment but will not operate in vacuum. In vacuum service, ball bearings must be positioned so that there is essentially no axial loading. If the butterfly test valve were rotated through 90 degrees so that the bearings supported the weight of the vane and shafts, their behavior in vacuum would be different. Of course, in an orbiting satellite, the gravitational force is balanced so that there would be no radial or axial loading of the bearings.

The fourth test performed demonstrated that properly aligned ball bearings would operate for an extended period of time (13 days in this instance) at low speeds of the order of 500 rpm. This test at low speeds was terminated only in order to try higher speed operation of the bearings. When there was an accidental power failure in the building, it was learned that the valve could not be restarted after having been motionless for about one hour. Possibly, the dwell time of 1 hour caused some "sticking" or incipient "cold welding." In any event an effective increase of friction prevented the valve from starting in vacuum, but did not prevent it from starting in air. The implications of this experiment for a valve that must be stopped and started repeatedly in vacuum are clear. Although the torque that could be magnetically coupled to the butterfly valve rotor was undoubtedly small, some earlier experimentation with ball bearings in vacuum confirmed this general behavior and showed that very large torques were necessary to free a "frozen" bearing of this kind.

2. Flexure-pivot valve. - Before describing some of the tests that were made with flexure-pivots and with the flexure-pivot valve, it would be useful to describe the characteristics of flexure pivots in greater detail.

The flexural-pivot bearing (also called flex-pivot or flexure-pivot), as furnished by the Bendix Corporation, consists of two concentric cylinders, one cylinder for each side of the suspension. These two cylinders are coupled together with flat cantilever leaf springs as shown in Figure 49. A photographic view of one half of a flexural pivot can also be seen in Figure 39 at the far left.

Designing with flexural pivots is similar to designing with other bearings; that is, radial and thrust loading and bearing lifetime must be considered. Unlike ordinary bearings, however, the suspension does not require lubrication. For small deflections, the flexural pivot has essentially an infinite lifetime since wear surfaces have been eliminated. Larger deflections result in a finite but predictable lifetime since spring fatiguing due to large amplitude deflection causes eventual failure.

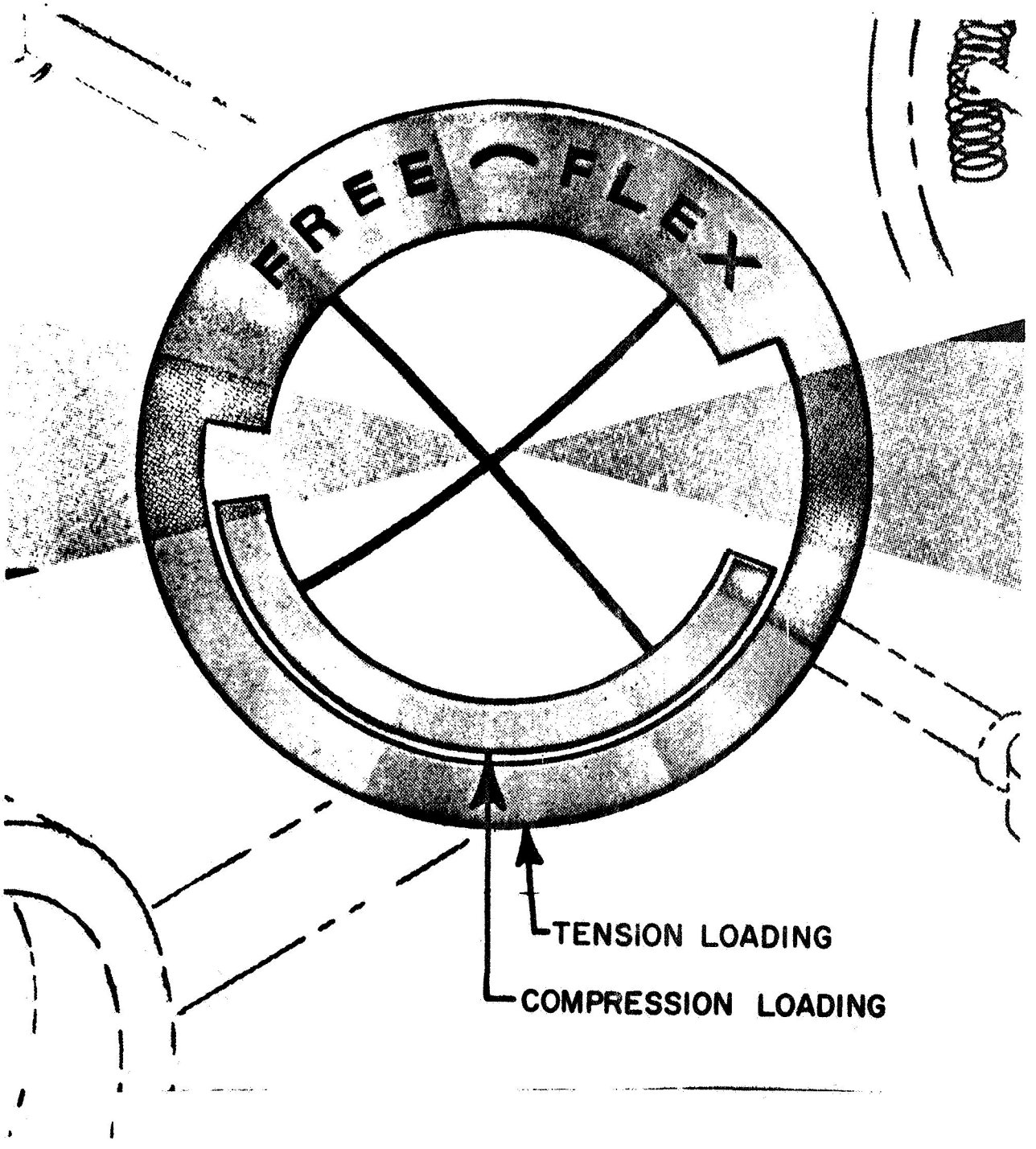

Figure 49. Flexural-pivot bearing.

A unique property of flexural pivots that must be understood is the shift in the axis of rotation with flexural angle. This shift is caused by the shortening of the leaf spring cord distance due to their arc shape under deflection. Such a shift of the center axis will affect the flexure pivot valve design in that adequate clearance must be provided. Figure 50 shows this center shift.

Another characteristic property of flexural pivots is the hysteresis of the leaf spring zero-torque position. The hysteresis is a function of deflection as shown in Figure 51. The hysteresis of the flexural pivot is a tendency of the leaf springs to permanently deform in the direction of bending. The spring, upon being deflected, does not return to its original starting point, and, under oscillation, it has a zero torque position which also oscillates. For a deflection of $\pm$ 33 percent (10 degrees out of a possible 30 degrees) of rated deflection, the curve of Figure 51 gives a hysteresis angle of less than 0.06 degrees, which is a change in deflection of only 1/2 percent.

Figures 52 and 53 show families of life curves for varying levels of deflection versus radial loading for Series 800 flexural pivots. These curves are valid for pivots other than the 800 series provided that the percent of rated deflection is entered as the ordinate value. Figure 49 illustrates how the flex-pivot may be placed either in tension or compression. For the flexure pivot valve, the two rotors will be balanced and in the zero-g environment of flight there should be neither radial compression nor tension applied to the bearings. As is apparent from the figures, the life of a flexural pivot bearing is a function of leaf spring stressing.

At the time that the gold-plated ball bearing tests were carried out for Honeywell, Inc., a series of life tests were made of Bendix 5016-800 flexural-pivots. The element of lowest reliability in a yaw attitude sensor system appears to be the mechanical cycling valve, and in the flexure-pivot valve, the pivot itself becomes the questionable element.

To provide a means of cycling the flexural-pivots for life testing, a motor-driven bell-crank mechanism was constructed as shown in Figure 54. A total of ten pivots were tested at a given time in this jig. The bell-crank driven reciprocating slide which engaged forked levers attached to the free end of each flex-pivot was used to generate a pure torque input to each unit. These levers were statically balanced so that earth g-loads could not generate radial loading. The bell-crank position was adjustable so that the flex-pivot could be operated at either $\pm$ 15 degrees or $\pm$ 12 degrees. The frequency of cycling was 15 Hz, which was just below the natural frequency of the pivot loaded with the forked arm.

The test jig was loaded with ten flexural-pivots and was operated for a total of 1.4×10^6 cycles at a deflection of $\pm$ 15 degrees or $\pm$ 50 percent of rated deflection. At this count, the pivots were examined, and a total of four pivots had failed due to a fracture in one of their three

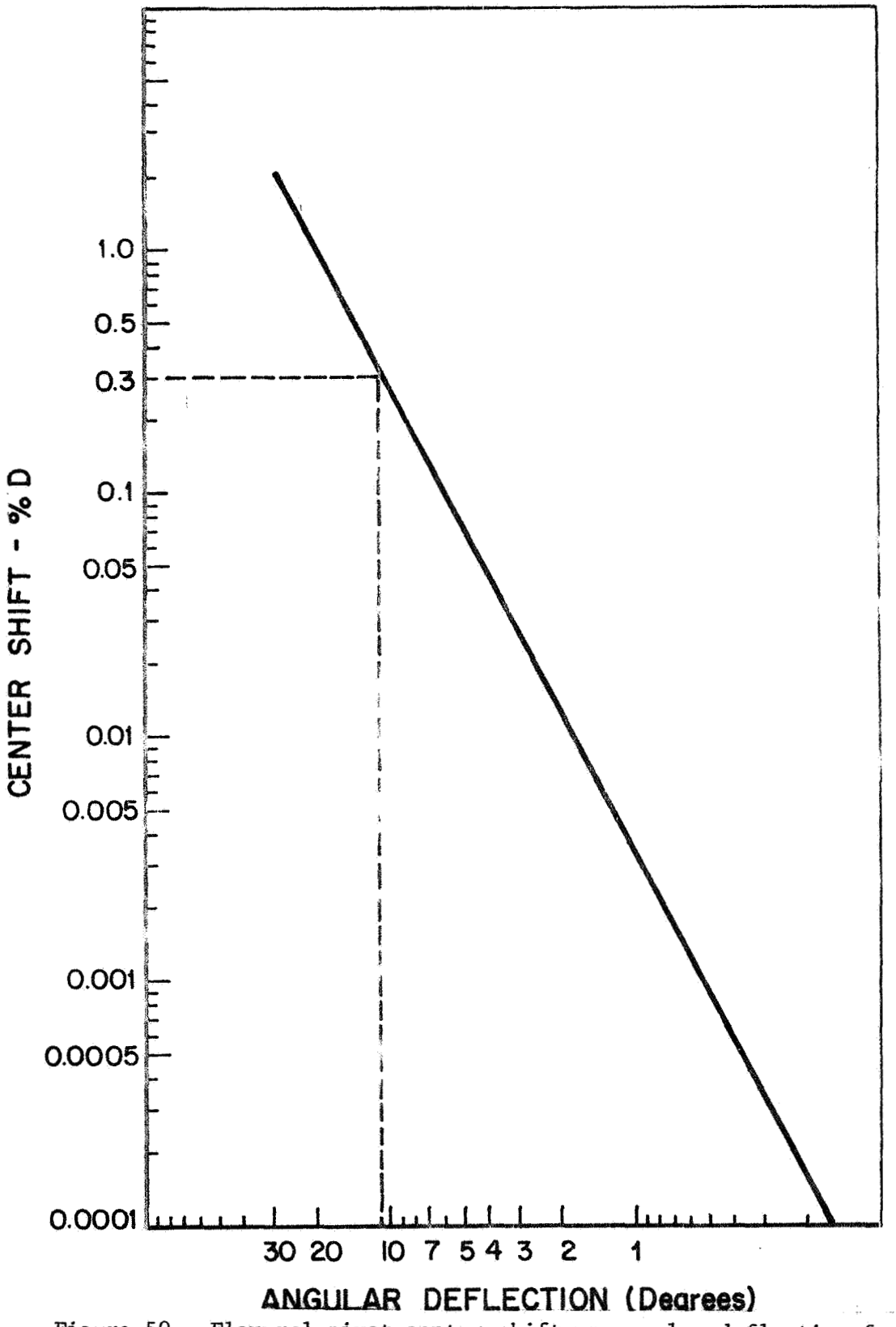

Figure 50. Flexural-pivot center shift vs angular deflection for cantilever and double end supported flexural pivots under no-load conditions.

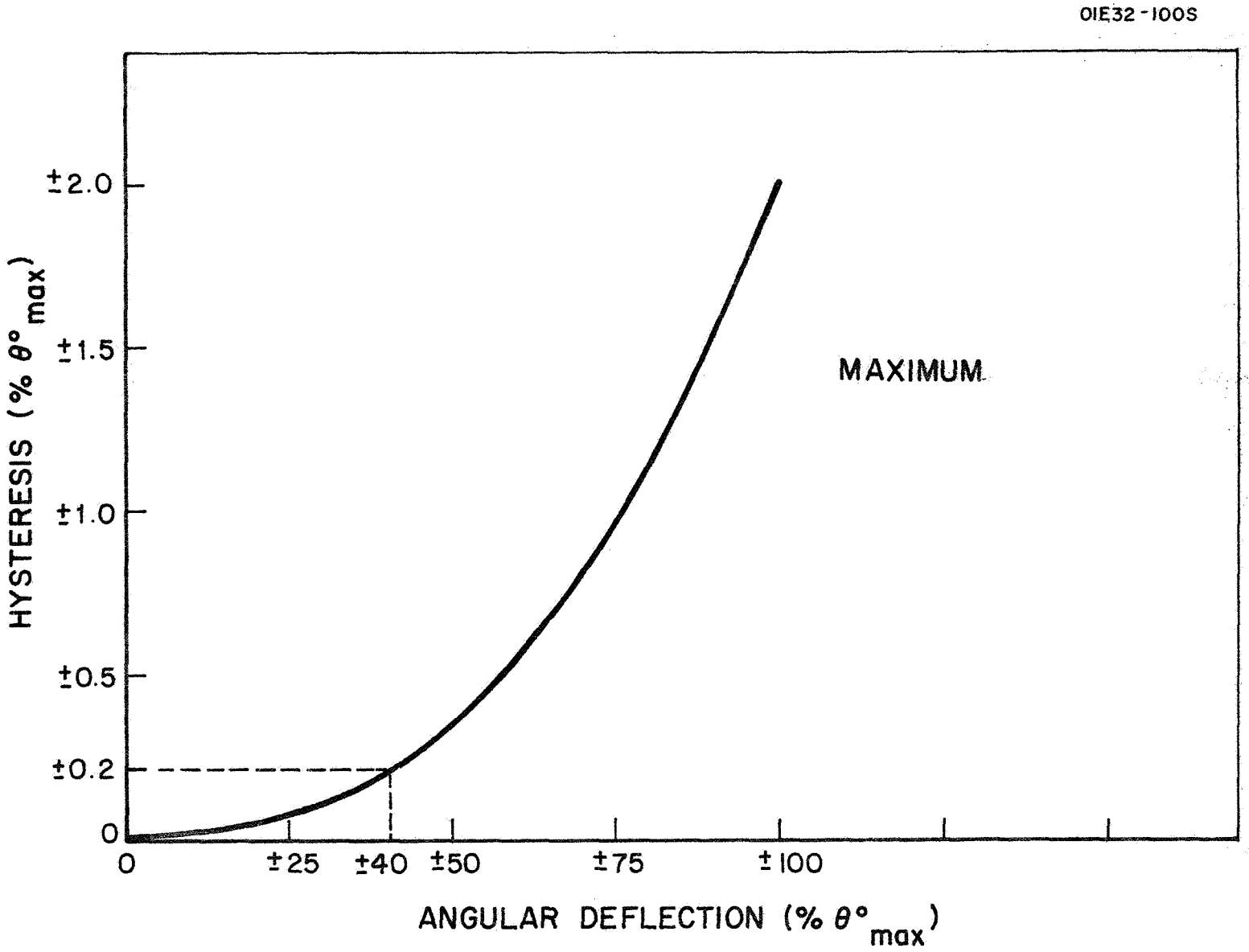

Figure 51. Flexural pivot hysteresis vs angular deflection for cantilever and double end supported flexural pivots under no-load conditions.

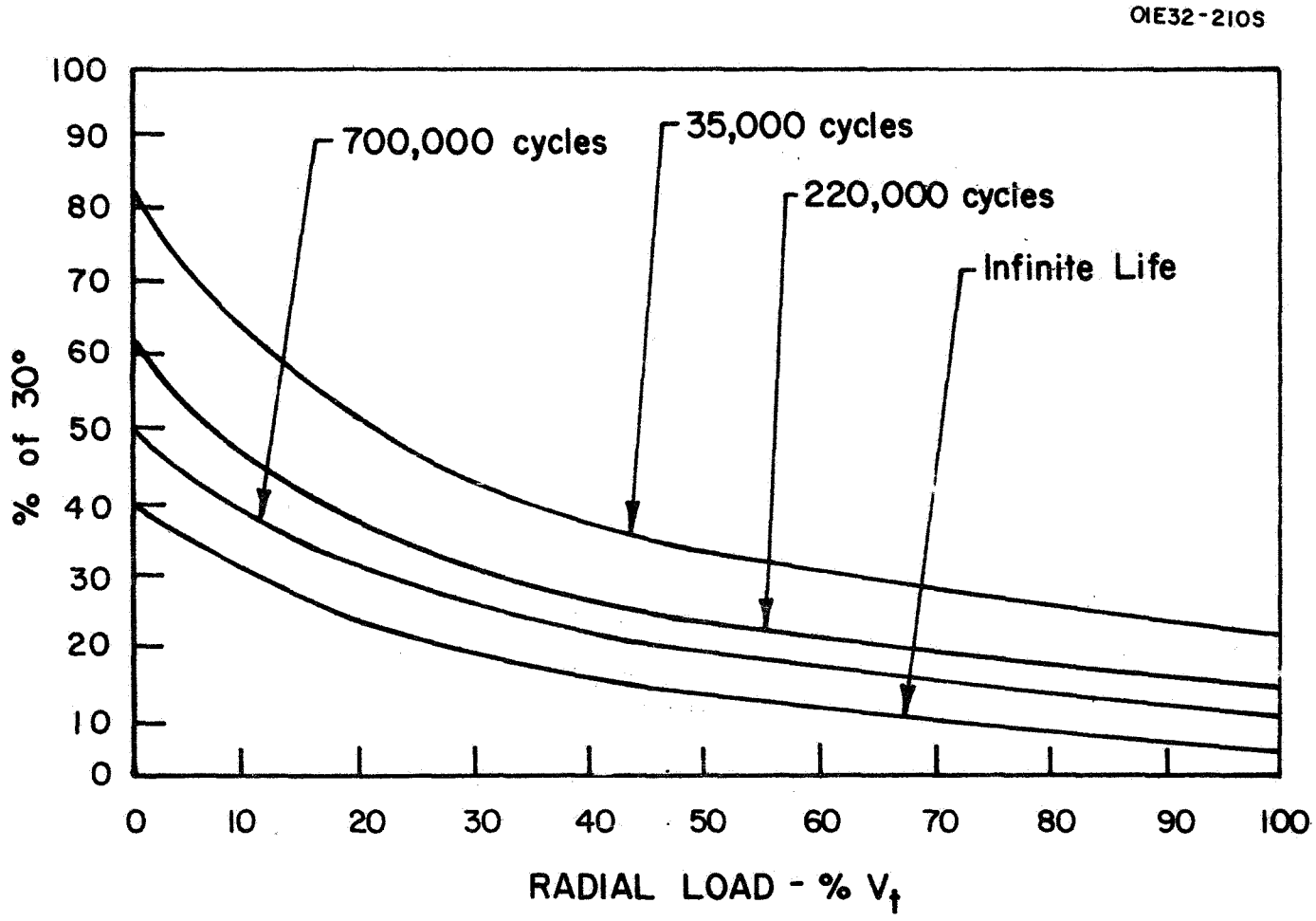

Figure 52. Flexural pivot predicted life for radial tension loading.

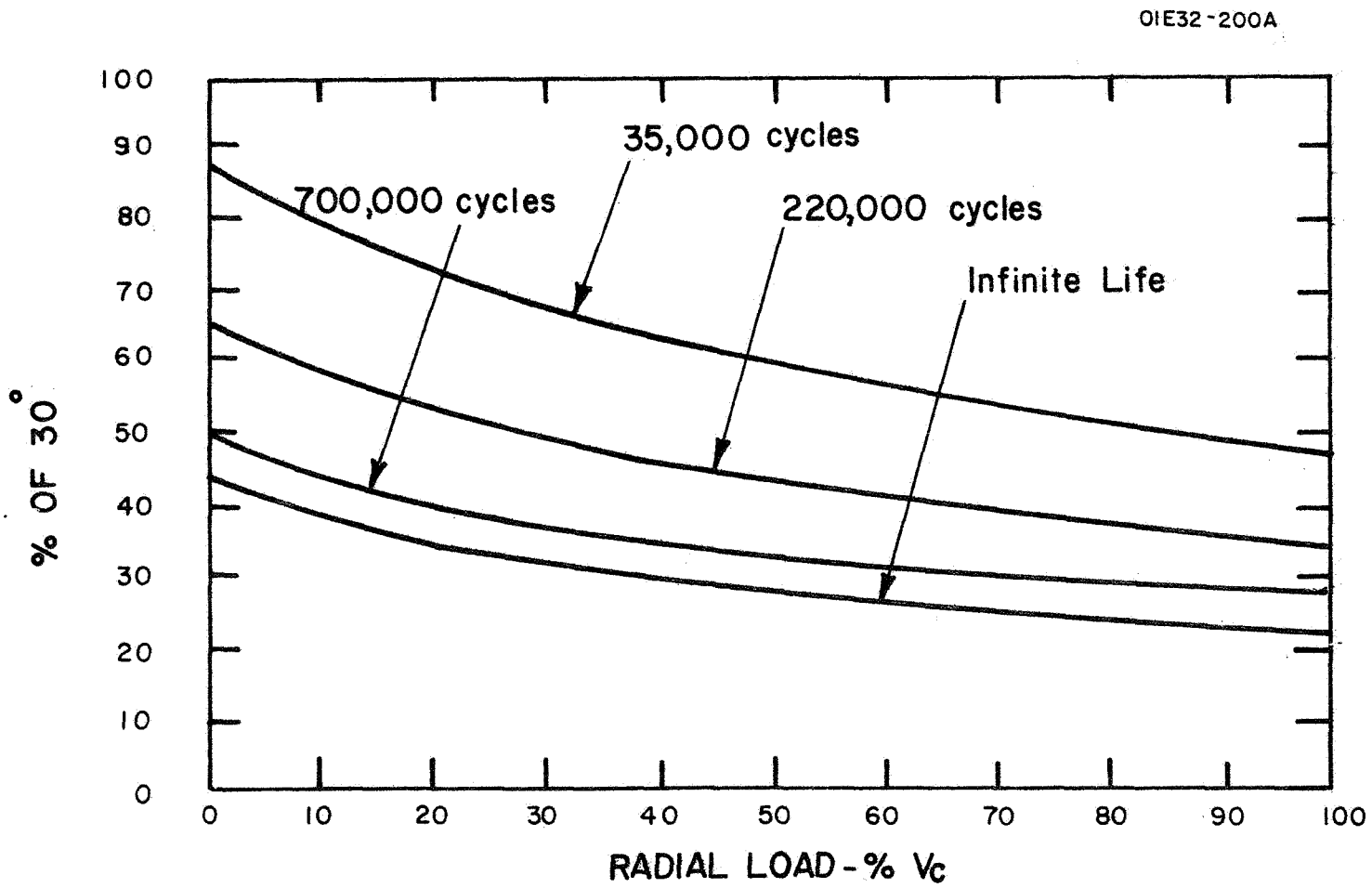

Figure 53. Flexural pivot predicted life for radial compression loading.

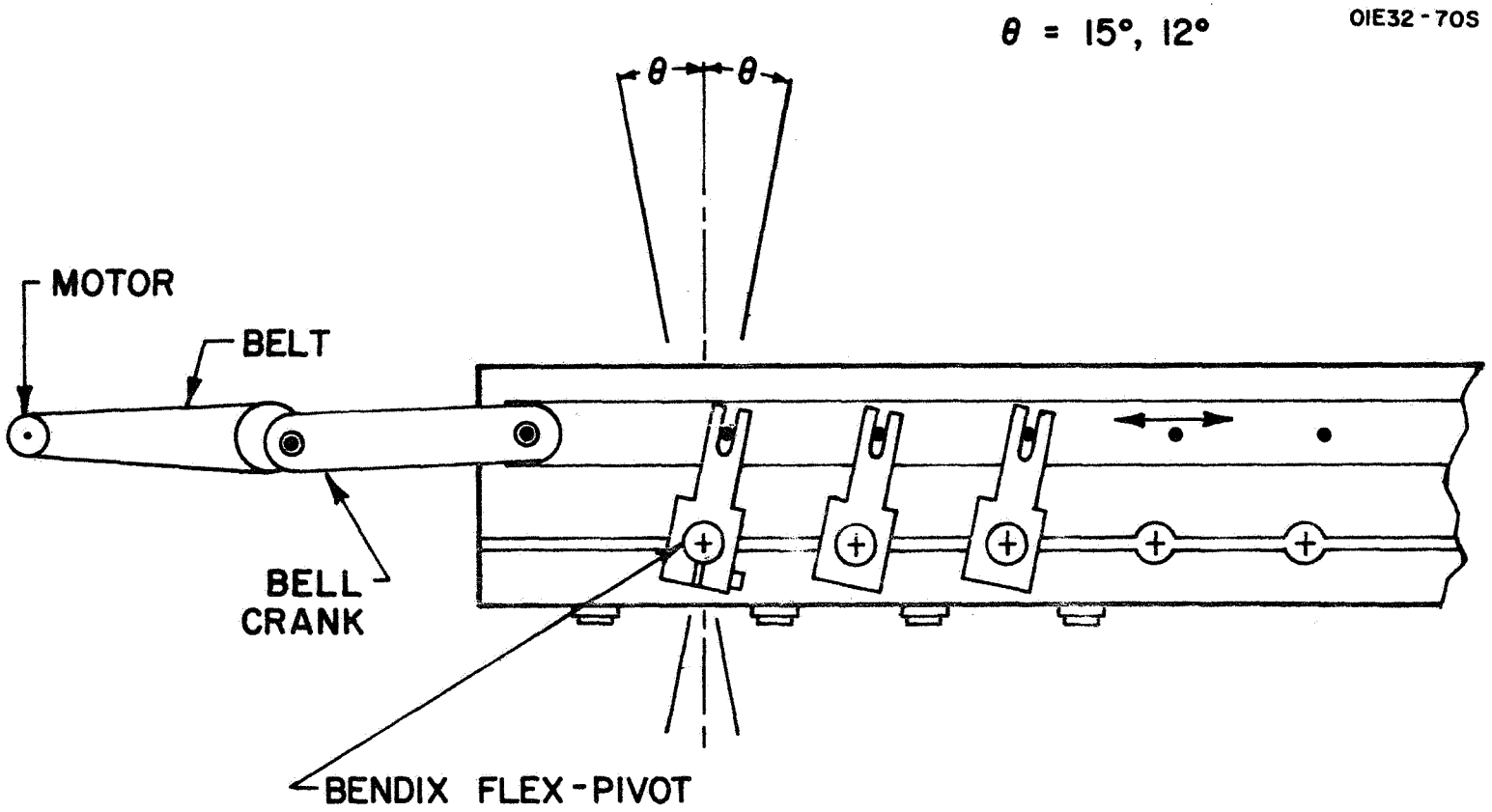

Figure 54. Flexural pivot life test jib.

leaf springs. These failures occurred during the night over a 4-hour period, and, therefore, the cycle count at the last inspection prior to this period or 1.17×10^6 was used as the life count for all four pivots. These pivots are shown in Table 5 as samples Nos. 4, 5, 7, and 8. At a total count of 6.4×10^6 cycles, another pivot failed in the same manner as the other four, that is, one of the three leaf springs fractured. This unit is shown as Sample No. 3 in Table 5.

At a total count of 1.1×10^7 cycles, the deflection angle was changed to $\pm$ 12 degrees or $\pm$ 40 percent of rated deflection, and five new pivots were installed. These new units are shown in Table 5 as Samples Nos. 11, 12, 13, 14, and 15. The five surviving samples, Nos. 1, 2, 6, 9, and 10, of the 15-degree test were retained in the fixture for the 12-degree test. A total of 56.2×10^6 cycles were accumulated to date on Samples Nos. 1, 2, 6, 9, and 10 without failures. (Table 5 reports the total cycles as of 20 October 1966.) Samples Nos. 11 through 15 accumulated a total of 30.2×10^6 cycles to date without failure.

Table 6 shows the results of various tests that were performed by the flexural pivot vendor (Bendix). These tests were made of random samples taken from production lots. Not all samples were of the type 800 series as noted by the rated deflection. However, since the life of the pivot is based upon leaf-spring stressing, the significant parameter is the test deflection taken as a percentage of rated deflection. Samples tested at deflections of $\pm$ 40 percent or below show an accumulated cycling of over 30×10^6 which is considered the burn-in run for an infinite-life unit.

A detailed discussion of the test results follows.

(a) GCA Samples No. 4, 5, 7, and 8. - These units accumulated 1.17×10^6 cycles at 50 percent rated deflection before failure. Referring to Figures 52 and 53, the predicted life for zero radial loading is 7×10^5 cycles. Examination of these units under a microscope revealed a stress-raising nick in the fracture of one of the samples indicating a fault in manufacture. All four samples were returned to the vendor for inspection and metallurgical analysis. The vendor report revealed nothing negative in either fabrication or metallurgy, and pointed out that the units were expected to fail at 7×10^5 cycles.

(b) GCA Sample No. 3. - This unit failed at an accumulated cycling of 6.4×10^6, and since the predicted life of the test deflection of 50 percent is 7×10^5, the sample yielded an excess life of 5.7×10^6 cycles.

(c) GCA Samples No. 1, 2, 6, 9, and 10. - These units accumulated 1.1×10^7 cycles at 50 percent rated deflection and 4.52 cycles at 40 percent rated deflection and are still operating, yielding an excess life of 10.3×10^6 cycles. At 40 percent rated deflection these same samples have accumulated an additional 45.2×10^6 cycles.

TABLE 5

GCA TEST RESULTS FOR BENDIX 5016-800 FLEXURE PIVOTS

TEST SAMPLE NO.	RATED DEFLECTION	TEST DEFLECTION	PREDICTED LIFE	TOTAL CYCLES	REMARKS
1	$\pm 30^{\circ}$	$\pm 15^{\circ}$	7×10^{5}	1.1×10^{7}	PLACED IN $\pm 12^{\circ}$ JIG
2	"	"	"	"	"
3	"	"	"	6.4×10^{6}	FAILED
4	"	"	"	1.17×10^{6}	FAILED
5	"	"	"	"	"
6	"	"	"	1.1×10^{7}	PLACED IN $\pm 12^{\circ}$ JIG
7	"	"	"	1.17×10^{6}	FAILED
8	"	"	"	"	"
9	"	"	"	1.1×10^{7}	PLACED IN $\pm 12^{\circ}$ JIG
10	"	"	"	"	"
1	$\pm 30^{\circ}$	$\pm 12^{\circ}$	INFIN.	4.61×10^{7}	STILL OPERATING
2	"	"	"	"	"
6	"	"	"	"	"
9	"	"	"	"	"
10	"	"	"	"	"
11	"	"	"	2.02×10^{6}	"
12	"	"	"	"	"
13	"	"	"	"	"
14	"	"	"	"	"
15	"	"	"	"	"

TABLE 6

BENDIX TEST RESULTS FOR BENDIX 5016-800 FLEXURE PIVOTS

TEST SAMPLE NO.	RATED DEFLECTION	TEST DEFLECTION	PREDICTED LIFE	TOTAL CYCLES	REMARKS
1	$\pm 15^{\circ}$	$\pm 10^{\circ}$	100,000	270,000	FAILED
2	"	"	"	1,029,600	"
3	"	"	"	1,617.840	"
4	"	"	"	210,600	"
5	$\pm 30^{\circ}$	$\pm 12.6^{\circ}$	30,000,000	30,049,200	NO FAILURE
6	"	$\pm 20^{\circ}$	100,000	307,800	FAILED
7	"	"	"	648,000	"
8	$\pm 15^{\circ}$	$\pm 10^{\circ}$	"	324,720	"
9	$\pm 30^{\circ}$	$\pm 20^{\circ}$	"	146,800	"
10	"	$\pm 12.6^{\circ}$	30,000,000	16,912,800	NO FAILURE
11	"	$\pm 20^{\circ}$	100,000	924,480	FAILED
12	"	"	"	351,360	"
13	$\pm 15^{\circ}$	$\pm 6.3^{\circ}$	30,000,000	2,138,171,904	THIS PIVOT STILL ON TEST
14	"	$\pm 7.5^{\circ}$	5,050,000	34,320,000	FAILED
15	"	"	"	30,320,000	"
	"	$\pm 11.25^{\circ}$	159,000	162,800	"
	"	$\pm 15^{\circ}$	25,000	145,400	"
16	$\pm 7.5^{\circ}$	$\pm 3.75^{\circ}$	5,050,000	6,730,000	"
17	"	$\pm 5.6^{\circ}$	159,000	172,200	"

(d) GCA Samples No. 11 through 15. - These units operating at 40 percent rated deflection accumulated 30.2 x 10^6 cycles and were still operating. Vendor reports indicate that units burned in to 30 x 10^6 cycles will yield essentially infinite life.

(e) Bendix tests. - Samples No. 5 and 13 are units tested at 40 percent rated deflection and should yield an infinite life. Test results show that no failure occurred after 30 x 10^6 cycles which is considered by the vendor to be the burn-in life to assure infinite life. Unit No. 13 is still operating with over 2 billion cycles logged to date.

Sample No. 10 was tested at 40 percent rated deflection and accumulated 16.9 x 10^6 cycles, under the normal burn-in, but nevertheless did not fail.

All the other samples show actual life-to-failure well in excess of predicted life.

In view of the test results, the flexural pivot is considered to be a satisfactory device for use as a yaw attitude sensor valve rotor suspension. All failures have occurred well in excess of predictions for two different stress levels, 50 percent and 40 percent rated deflection. An added margin of reliability can be expected if the final design further reduces stressing to 33 percent of rated deflection.

Failures experienced in the GCA tests show that only one spring fails of the total of three springs in a unit. The failures were not catastrophic since the other two springs maintained the integrity of the suspension, the only degradation due to a failure being a change in flexural-pivot spring constant.

A change in flexural-pivot spring constant will reflect itself into the valve design as a shift in the natural frequency of the rotor-flexural pivot assembly, and since the rotor is always operated at resonance, this change in frequency will affect only the electronic system bandpass requirement. Bandwidth requirements to accommodate a spring failure are given as follows: The natural frequency of the rotor assembly is

$$\omega_n = \sqrt{K/I}$$

where

K = the total flex-pivot spring constant and is equal to $6K_1$

K_1 = the spring constant of one leaf spring

I = the second moment of the rotor about its cylindrical axis.

For small changes in K, the bandwidth is given by

$$\Delta\omega = \frac{1}{2}\sqrt{\frac{1}{KI}}\ \Delta K$$

or

$$\frac{\Delta\omega}{\omega} = \frac{1}{2}\frac{\Delta K}{K}$$

since $K = 6K_1$ and $\Delta K = K_1$

$$\frac{\Delta\omega}{\omega} = \frac{1}{12} = 8.4 \text{ percent.}$$

Therefore, a bandpass of ω_n (+ 0, - 10 percent) will provide for non-degraded performance in the event of a flex-pivot failure of the type experienced in the tests reported above.

The conclusions can be made that all available evidence indicates that the life of a flex pivot is predictable with high confidence and that in the event of a failure of a flex pivot, proper design of the valve will enable continued non-degraded performance.

The flexure-pivot valve was operated in air on several occasions but was never operated under vacuum. Because of the single-ended support of each of the two counter rotating rotors, the valve was always operated in a vertical position. The electromagnetic drive units shown in Figure 21 were powered either by commercial low frequency oscillators or by a breadboard-flight type flux oscillator.

It was found that the displacement of the rotors was negligibly small unless the driving frequency coincided with the natural resonant frequency of each rotor. Since the two rotors had different moments of inertia due to differences in mass and mass distribution, their resonant frequencies were not the same. The lighter inner cylinder had a mass of 100.04 grams and resonated at 8.0 cps. The heavier outer cylinder had a mass of 106.25 grams and resonated at 7.6 cps. Presumably, the flexure-pivot support bearings of the two rotors were identical. Each cylinder required about 4 or 5 watts of power. There is no reason why the mass of the outer cylinder cannot be reduced in any future design of a two-rotor flexure-pivot valve. For the present valve design, it would be more convenient to add mass to the lighter inner cylinder to reduce its resonant frequency to 7.6 cps. This could easily be done with the use of weighting washers that would fit inside the inner rotor at a position near the flexure-pivot bearing housing.

B. Electronics

In the early stages of the system development, it was necessary to develop a system to simulate the signal input to the electronics as realistically as possible. This same type of simulation system could be used in place of the vacuum test system whenever purely electronic difficulties were to be investigated.

The simulation system consisted of a rotating shaft on which an opaque disk was mounted. A photocell was used to detect the light modulation created by a modulation pattern that was cut in the rotating disk. The output signal of the photocell was amplified and used to modulate the high voltage (from 1.7 to 6.3 kV) output of a laboratory type high voltage power supply. The modulated high voltage was applied to the anode of a GCA Model R5 cold cathode ionization gauge that had been sealed off under vacuum and which had a residual pressure in it, when operating, of about 10^{-9} to 10^{-10} torr.

Figure 55 is a schematic of the circuit used to measure the high voltage modulation, while Table 7 shows the amount of high voltage modulation that was obtained with the use of the simulation equipment. The actual gauge output currents that corresponded to the high voltages shown depended on the pressure within the sealed-off ionization gauge.

In order to better understand the nature of the electronics that process the output signal of the pressure sensor, a brief description of the circuits will be given first, followed by a presentation of waveforms that were monitored at important points in the circuit.

As shown in the block diagram of Figure 56, the modulated gauge output current is processed by the logarithmic electrometer and the other electronic functional units in the usual way. Two magnetic reed switches are mounted near the rotating disk. As a magnetic shield is rotated between the switches and fixed magnets, a synchronized switching occurs. The closure of switch number one generates a sync pulse which triggers one-shot multivibrator No. 1A. This multivibrator provides a variable delay to effect phase synchronization between the sync pulse and the simulated modulation. This stage will not be required in the final equipment. The output of multivibrator 1A triggers multivibrator 1B which discharges the peak detector stage capacitor and also triggers multivibrator 1C. The peak detector is discharged by the leading edge of the 1B output pulse, while 1C is triggered by the trailing edge. Multivibrator 1C has a period equal to the "on-time" of port No. 1 and opens gate No. 1 for that period of time. With gate No. 1 open, the signal can flow from the inverter stage into the peak detector network. The same sequence of stages is duplicated for the other port. Two filters are provided to smooth the outputs of the peak detectors and provide a dc signal to the differential amplifier. The output of the differential amplifier provides yaw data to the spacecraft telemetry.

Figure 57 is a compilation of waveforms existing at the various positions marked by letters in the block diagram of Figure 56. These waveforms are a reduction of oscilloscope photographs. The input signal simulation technique described above was used to furnish the gauge signal and the synchronizing pulses.

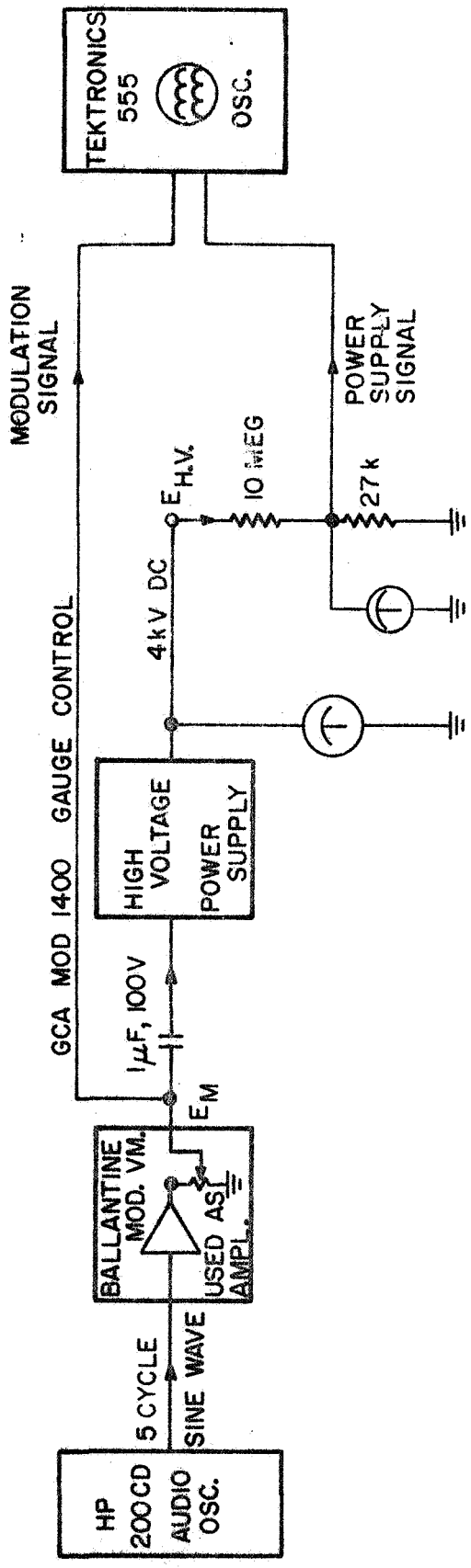

Figure 55. High voltage modulation test circuit.

TABLE 7

HIGH VOLTAGE POWER SUPPLY OUTPUT VOLTAGES
AND THE CORRESPONDING INPUT MODULATION

Modulation Input E_m (Volts, peak-to-peak)	0.25	0.5	0.75	1.0	1.5	2.0
High Voltage Output, $E_{H.V.}$ (Min. and Max. kV)	3.82 to 4.18	3.39 to 4.61	3.09 to 4.91	2.78 to 5.22	2.47 to 5.52	1.7 to 6.3

Note: The unmodulated output voltage of the high voltage power supply was 4.0 kV

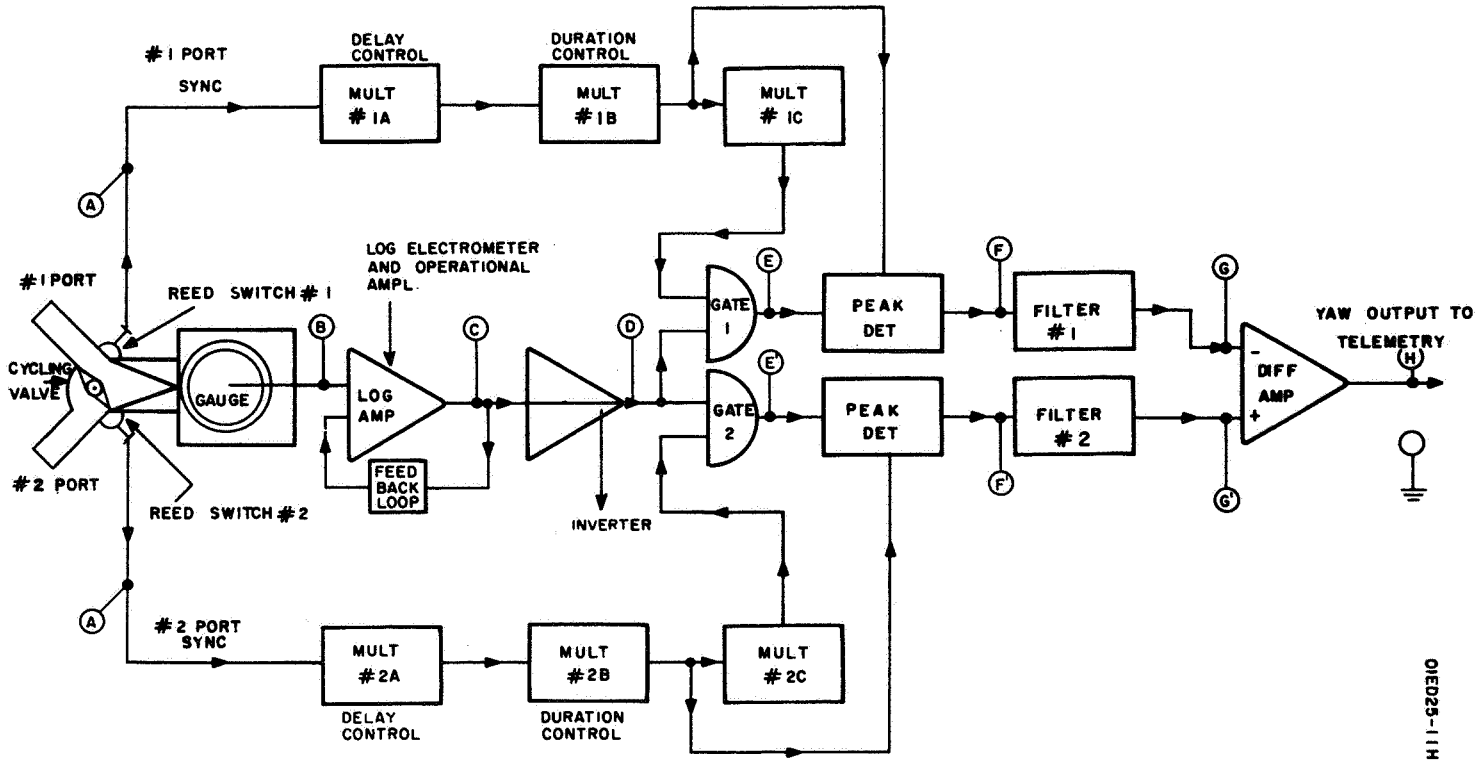

Figure 56. Block diagram of yaw attitude sensor electronics.

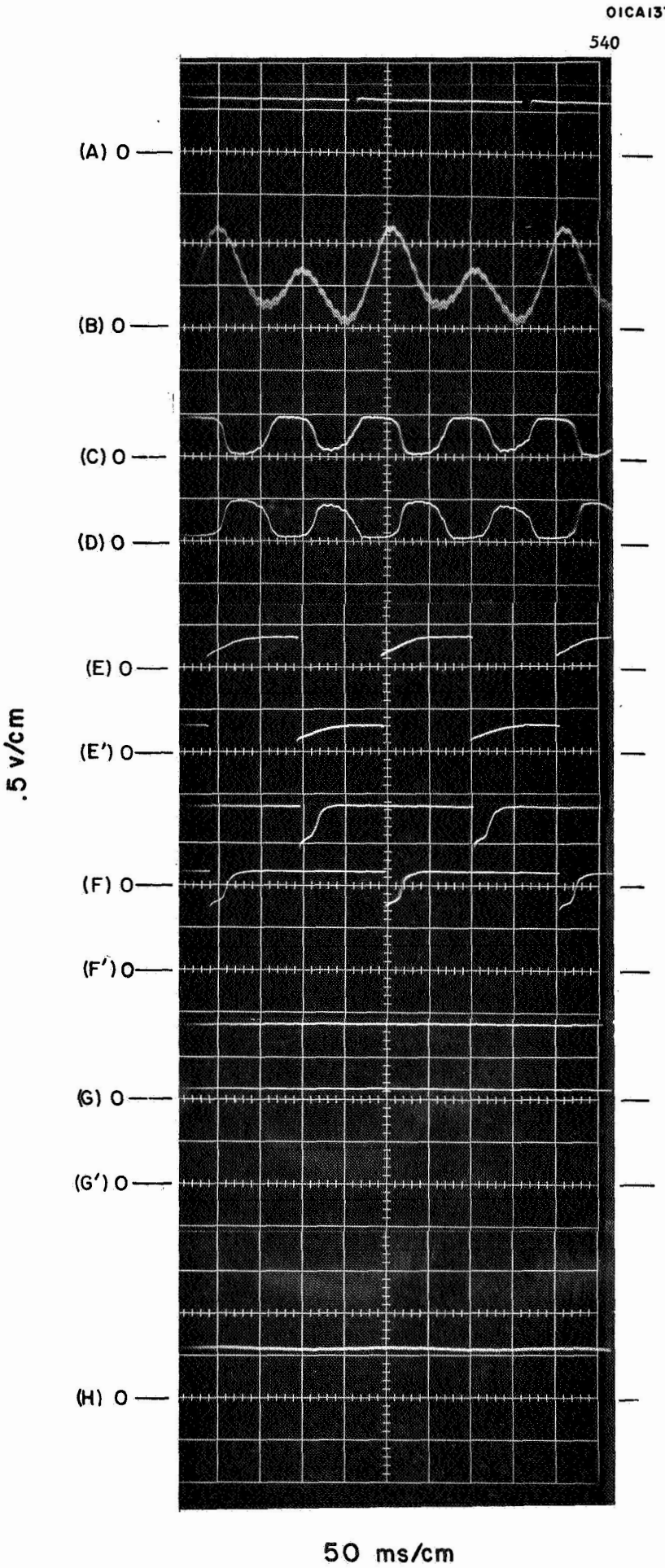

Figure 57. Typical operational waveforms of yaw attitude sensor electronics.

The top trace (A) of Figure 57 was the pulse that synchronized the entire electronics. This pulse was generated by the closing of a magnetic reed switch. The closing time would normally be determined by the position of the mechanical cycling valve. In this instance the pulse was generated by a magnet attached to the shaft on which the modulating disk was mounted. As the magnet was rotated 360 degrees, or one complete turn, it passed a reed switch which closed, and was held closed during the short duration of passage.

The second trace (B) shows the signal generated to modulate the 4 kV power supply. The difference in amplitude of the first and second half cycles simulated the difference in pressure at the two valve tubulations. This signal was generated by rotating a predetermined shaped disk through a light beam focused onto a photodiode. The waveform shown was the actual output of the photodiode.

The third trace (C) shows the negative going output of the electrometer, and the fourth trace (D) shows the inverted signal out of the inverter.

The reason for inverting was the need for a positive signal to process. The difference in amplitude of the first and second half cycles is shown on the negative side on the top trace and on the positive side on the bottom trace.

The fifth and sixth traces (E) and (E′) respectively, show the gate "on" and "off" time. The on and off time of each gate was timed so that one half of the cycle was fed into the No. 1 input, and the other half cycle was fed into the No. 2 input. The first one-shot multivibrator adjusted the delay of the sync on each input such that the gates were turned "on" during their respective periods. The second one-shot multivibrator determined the duration of sample time (or "on" time width). The photo shows the "on" and "off" time corresponding to each respective half cycle.

The seventh and eighth traces (F) and (F′) respectively, show the voltage during discharge and charge time. The storage circuitry was discharged and allowed to change at a rate corresponding to the sync timing of the timing circuits.

The ninth and tenth traces (G) and (G′) respectively, show the dc output of the No. 1 and No. 2 filters (or the inputs of the differential amplifier).

The eleventh trace (H) shows the output of the differential amplifier. A slight ripple was present which indicated that the filtering was not complete. When the final switching and voltage levels have been determined, the filtering will be improved to eliminate the output ripple.

C. Magnetic Shielding Measurements

The strongest magnetic field that is present in the yaw attitude sensor system is the one which derives from the permanent magnet used with the cold cathode ionization gauge. The magnetic field in the air gap of this C-shaped magnet has a nominal value of about 1050 gauss, but some magnets have magnetic fields as strong as 1300 gauss.

Using a magnet that had a measured air gap field of 1300 gauss, measurements were made of the fringing field at various distances from the center of the air gap. It was found that at a distance of 12 inches from the air gap, the magnetic field strength was approximately 83,000 gamma (830 milligauss or 0.83 gauss). Since it was desired to reduce the magnetic field at this position to about 100 gamma, it was necessary to provide shielding that would decrease this fringe field by a factor of about 1000.

Several series of experiments were performed to shield the magnet with various high permeability materials. It was found that the best results for three layers of shielding material were obtained by using a soft Armco iron shield immediately adjacent to the magnet and surrounding this shield with one of netic material. A final third shield of co-netic magnetic shielding material formed the third and outermost layer. (Netic and co-netic magnetic shielding alloys are manufactured by the Magnetic Shield Division of Perfection Mica Company, Chicago, Illinois.) Netic is a non-retentive alloy that is non-shock sensitive and suitable for high level attenuation. Co-netic is a high permeability alloy developed for maximum attenuation at low flux density.

It was found that three complete layers of shielding material entirely surrounding the magnet reduced the magnetic fringe field to about 1000 gamma at a position 12 inches from the center of the magnet air gap. If one end of the three cylindrical shield cans (the end opposite the position at which the magnetic field measurement was made) was left open, the residual magnetic field increased to about 2500 gamma showing the effect of openings and holes in the shielding structure.

It was decided to build an experimental shielding box to surround the permanent magnet and thus reduce the magnetic field to a manageable level. It was felt that any additional shielding required could be done at the cover of the complete package.

The shield box was rectangular in shape. The innermost layer was 0.020 inch thick soft iron. A glass epoxy laminate about 0.025 inch thick was cemented over this inner shield and a layer of netic material about 0.006 inch thick was cemented to the outside of the insulating laminate. A second glass epoxy laminate was cemented over the netic material and a final outer layer of 0.006 inch thick co-netic material was cemented over this second insulating laminate. Mounting holes were provided at the bottom of the box and cutout notches for the high voltage

and gauge output current connections were provided at the upper edge of the open box. A split cover made up with the same laminated structure was fitted to the open top portion of the box. The cover had a central hole about 1 inch in diameter through which the gauge tubulation passed.

Careful measurements were made of the residual magnetic fringe field of an ionization gauge magnet placed within the rectangular shield box described above. A Bell model 240 gaussmeter was used to make these measurements. The earth's magnetic field was carefully balanced out and the residual field was measured at six points along three mutually perpendicular axes that passed through the center of the magnet air gap. The measurements along the axis of the air gap (dipole axis) yielded fields of 40 and 50 milligauss. The measurements transverse to the axis but in the plane of the C magnet yielded fields of 15 and 30 milligauss. The measurements along the remaining transverse axis yielded fields of 38 and 40 milligauss. Since the maximum permissible magnetic field is 1 milligause, an additional 50-fold attenuation would be required.

D. Test System Operation

The test system was carefully leak-checked with a helium mass spectrometer type leak detector prior to being placed in operation. It was found that a few of the copper gasketed flanges had to be tightened before the system was vacuum tight.

The zeolite-type sorption pumps must be baked overnight prior to being chilled with liquid nitrogen. These pumps have built-in calrod-type heaters which have been connected to standard 115-volt snap switches mounted within the cabinet. Due to the position in which the Hoke type venting valves were mounted, it was necessary to provide thermal sheilding (asbestos sheets covered with aluminum foil) around these valves to prevent their overheating during the sorption pump bake-out. The sorption pump UHV valves should be closed during bake out, but the venting tubes must be left unstoppered.

After the sorption pumps have been baked, they are allowed to cool down by natural radiation and convection or they may be force-cooled with a fan, air gun, or stream of compressed air. At the end of the bake out interval (before cooling), the venting tubes at the outboard sides of the sorption pumps must be stoppered. When the sorption pumps are no longer warm to the touch, liquid nitrogen may be poured slowly into the annular space between the outer shell and inner core of the pump. At this time (or somewhat later, if desired), the UHV sorption pump valves may be opened so that pumping of the complete system can begin.

It takes approximately 20 or 30 minutes for the pressure in the test system to be reduced below 10^{-1} torr. At this time, the high pressure millitorr ionization gauges that are located just below the top of the cabinet may be turned on. The dual range ionization gauge

control units located at the top of the electronics rack are turned on (main power on) and the current emission controls are set at 0.1 Ma (yellow lettering). The "pressure gauge" switches are set to the "Log" position for logarithmic scale readings. The filament "on" buttons may now be pressed to turn on the gauges and read the system pressures. The yellow pilot lights marked "Hi" will light up when the gauges are turned on. Pressures are read with the central toggle switches in the up or "pressure" position. With these toggle switches in the down or "emission" position, one reads the filament emission of the gauge filaments. The filament emission for the high pressure gauges is 16μA, a reading of 1.6 on each meter. The emission current may be adjusted with the "high adjust" control. The pressures may be read more accurately on the linear scales provided by the "pressure range" controls. The electrometers contained within these control units should be zeroed occasionally by placing the pressure range switches in the "short" position and adjusting the "zero" controls. The uppermost control unit in the electronics rack is connected to the right-hand high pressure gauge.

When the pressure gauges indicate that the pressures have decreased below 1×10^{-3} torr, the ion pumps may be turned on. To do this, the meter range switches are placed in the "Log" position, the metal toggle switches are placed in the up or "start" position and the on-off snap switches are moved upwards to the "on" position. The red high voltage pilot lights will turn on and the meters will read far up scale in the region where the logarithmic scales have a black band. The voltage on the ion pumps may be read by switching the "meter range" switches to the KVx2 scale. The high voltage will be relatively low initially, but will increase slowly as the ion pump begins to operate. The pressure readings of the high pressure gauges should be watched closely during this starting period. If the pressures start to rise continuously above 10^{-2} torr, the ion pumps can be turned off and the sorption pumps allowed to reduce the pressure again to 1×10^{-3} torr and below. The pressure rises momentarily to the 10^{-2} torr region when the ion pumps are turned on because the gas discharge within the pumps outgasses the internal pump surfaces. When the ion pumps really begin to pump, there will be a rapid decrease of pressure into the 10^{-5} and 10^{-6} torr regions.

The titanium sorption pumps must be connected to a source of water and a drain before they are operated. They should not be operated unless the pressure is about 1×10^{-4} torr or less. To operate them, the percentage timer is placed in the "100 percent on" position and the filaments are first outgassed at currents of 30 to 35 amperes (the filament adjust control is used to set the filament current) for one minute. After the pressure has decreased, the pump may be operated by increasing the filament current to between 35 and 48 amperes. The pressure will start to decrease as the titanium sublimation occurs and the pump begins to operate. The titanium sublimation pumps are generally operated only in combination with the ion pumps.

Any time that the system pressure is in the 10^{-4} torr region or lower, the low pressure ionization gauges that are located on the test chambers may be turned on. This is done by first turning off the high pressure gauge filaments (push the filament "off" buttons) and then switching the emission control knob to the 10 Ma position (blue lettering). The filament "on" buttons can then be pressed to turn on the low pressure gauges and the blue pilot lights will light. As before, the meters will read the pressure when the central toggle switches are in the up or "pressure" position. With these switches in the down or "emission" position, the meters should read 4 Ma emission current. If they do not, they can be adjusted by means of the "low adjust" knob. The pressure range scales for the low pressure gauges are marked in blue.

Without any bake-out of the test chambers, the system was pumped down from atmospheric pressure several times. Typically, the system pressure would go into the 10^{-7} torr region the first day of pumpdown, into the 10^{-8} torr region the second day of pumpdown, and into the 10^{-9} torr region after about a week of pumping. The titanium sublimation pumps were not used. All of the low pressure pumping was done by the 80 ℓ/s ion pumps. It is expected that with a bake-out of the test chambers and ion pumps, the system ultimate pressure would go into the 10^{-10} torr region. The lowest pressure obtained without bake-out was about 4×10^{-9} torr.

The two leak valves that connect to the fronts of the test chambers were connected to 1 liter glass bottles of pure nitrogen gas. It was found that these valves exhibited a smooth fine control of the gas flow into each test chamber. It was possible to adjust the pressure in each chamber with great precision, as indicated by the low pressure gauge readings. There was a small amount of pressure drift observed after a leak valve was adjusted. It is believed that the drift was caused by a shift in the equilibrium pressure within the ion pump and consequent small changes in its pumping speed and not by any changes in the gas flow entering the chamber.

It was found that the two test chambers did not pump down to the same ultimate pressure. The left-hand chamber consistently pumped down to a lower pressure than the other chamber. Since the working pressure of the system was usually a decade or so above the ultimate pressure level, the difference in ultimate pressures represented a chamber gas composition difference of about 5 percent.

It was found experimentally that the UHV valve located at the top of the left-hand test chamber did not equalize the pressures in the two chambers when it was opened as long as the 80 ℓ/s ion pumps were operating. When the ion pumps were turned off (the leak valves being closed), the system pressure tended to rise slowly and approach an equilibrium value asymptotically. At this time, the pressures in the two chambers were believed to have been equalized.

E. Pressure Cycling Experiments with the Rotary Valve

In order to test the operation of the rotary valve under vacuum and at the same time test the response of the GCA Model R5 cold cathode ionization gauge to a cycling pressure, the rotary valve was connected to the test chambers as shown in the photograph of Figure 46.

The Model R5 test gauge was connected to the rotary valve with a demountable flange. The two tubulations of the rotary valve were flanged so that they could be conveniently connected to the two pressure chambers of the test system. The rotary valve was driven by magnetic coupling via an external permanent magnet. The permanent magnet was rotated by a Bodine Model NSH-12R variable speed motor connected to a Minarick Electric Co. Model SH-12 speed control. The high voltage to the cold cathode gauge was furnished by a J. Fluke Model 408A power supply. The gauge output current was amplified by either a Keithley Model 415 fast response linear electrometer or a Keithley Model 412 logarithmic electrometer. The logarithmic electrometer was used when the range of pressures to be measured was greater than one decade. The output of the electrometer was recorded with either a Sanborn Model 150 strip-chart recorder or a Honeywell 906C Visicorder.

The results of the various pressure cycling experiments are displayed in Tables 8 through 11. Nitrogen gas was used as the test gas in all of the experiments. The same GCA Model R5 gauge and rotary valve were used for all the tests. Each table lists the maximum and minimum gauge currents for each cycling frequency. The frequency labelled zero represents the equilibrium gauge currents with the gauge connected to each of the two chambers for at least 5 or 10 minutes. The column labelled $I_{MAX} - I_{MIN}$, the difference between the maximum and minimum gauge readings, is the peak-to-peak amplitude of the oscillating gauge current. The reduction in this peak-to-peak amplitude from its largest value at equilibrium (zero frequency) represents an attenuation caused by the frequency dependence of the system response. The average gauge current for each frequency has also been listed in each table. The average gauge current is a measure of the dc current level (dc pressure level) and shows if the pressure oscillations have shifted to a higher or lower pressure level. For example, in Table 10, it can be seen that the average current has continuously increased with frequency. Here the corresponding continuous increase in I_{MAX} indicates either an outgassing process that increased with time or else a generation of gas within the rotary valve due to rubbing at the bearings or some other metal-to-metal contact points.

The data presented in Table 8 were obtained with a Keithley fast response model 415 electrometer. These data probably represent the most reliable of all the data taken, since the rotary valve was operating properly up through a frequency of 4 cycles per second. Notice that the maximum current decreased with increasing frequency for frequencies of 2, 3 and 4 cycles per second. At the same time, the minimum currents increased with increasing frequency. This represents the expected

TABLE 8

DATA AND RESULTS OBTAINED IN A TWO CHAMBER-CYCLING VALVE EXPERIMENT USING A GCA MODEL R5 COLD CATHODE GAUGE EXPOSED TO AN 8.5 TO 1 NITROGEN GAS PRESSURE RATIO

Pressure Oscillation Frequency (c/s)	I_{MAX} (Ampere)	I_{MIN} (Ampere)	$I_{MAX} - I_{MIN}$ (Ampere)	$\frac{I_{AVE}}{\frac{I_{MAX} + I_{MIN}}{2}}$ (Ampere)	Reduction in $I_{MAX} - I_{MIN}$ (Percent)	Remarks
0	9.75×10^{-8}	1.15×10^{-8}	8.60×10^{-8}	5.45×10^{-8}	0	Initial Equilibrium Levels
2	9.75	2.00	7.75	5.87	9.9	
3	9.10	2.20	6.90	5.65	19.8	
4	8.60	2.50	6.10	5.55	29.1	Gauge Anode Voltage of 2.0 kV
5	9.75	4.50	5.25	*7.12	38.9	
6	9.20	4.50	4.70	*6.85	45.4	

*These increases in the gauge readings are believed to be due to gas generated within the rotary valve at the higher cycling frequencies.

TABLE 9

DATA AND RESULTS OBTAINED IN A TWO CHAMBER-CYCLING VALVE EXPERIMENT USING A GCA MODEL R5 COLD CATHODE GAUGE EXPOSED TO A 25 TO 1 NITROGEN GAS PRESSURE RATIO

Pressure Oscillation Frequency (c/s)	I_{MAX} (Ampere)	I_{MIN} (Ampere)	$I_{MAX} - I_{MIN}$ (Ampere)	$\frac{I_{AVE}}{\frac{I_{MAX} + I_{MIN}}{2}}$ (Ampere)	Reduction in $I_{MAX} - I_{MIN}$ (Percent)	Remarks
0	1.00×10^{-7}	4.00×10^{-9}	9.60×10^{-8}	5.20×10^{-8}	0	Initial Equilibrium Levels
2	7.00×10^{-8}	6.3	6.37	3.81	*33.7	
3	7.00	8.0	6.20	3.90	35.4	Frequencies Changed in Steps
4	6.6	1.2×10^{-8}	5.4	3.9	43.8	
5	6.0	1.7	4.3	3.85	55.2	
6	6.0	2.1	3.9	4.05	59.4	Gauge Anode Voltage of 1.0 kV
7	6.0	2.5	3.5	4.25	63.5	
8	5.7	3.0	2.7	4.35	71.8	Frequencies Changed continuously; *log electrometer used here
9	5.5	3.2	2.3	4.35	76.1	
10	5.5	3.4	2.1	4.45	78.1	
11	6.0	4.5	1.5	5.25	84.5	

*The time constant of the logarithmic electrometer used in this experiment has probably affected the gauge current readings.

TABLE 10

DATA AND RESULTS OBTAINED IN A TWO CHAMBER-CYCLING VALVE EXPERIMENT USING A GCA MODEL R5 COLD CATHODE GAUGE EXPOSED TO A 1.63 TO 1 NITROGEN GAS PRESSURE RATIO

Pressure Oscillation Frequency (c/s)	I_{MAX} (Ampere)	I_{MIN} (Ampere)	$I_{MAX} - I_{MIN}$ (Ampere)	$\frac{I_{AVE}}{\frac{I_{MAX} + I_{MIN}}{2}}$ (Ampere)	Reduction in $I_{MAX} - I_{MIN}$ (Percent)	Remarks
0	2.6×10^{-8}	1.6×10^{-8}	1.0×10^{-8}	2.1×10^{-8}	0	Initial Equilibrium Levels
2	2.6	1.8	0.8	2.2	20	
3	2.9	2.2	0.7	2.55	30	Gauge Anode Voltage of 2.0 kV
4	3.2	2.7	0.5	2.95	50	Noisy Recorder Signals
5	3.3	2.8	0.5	3.05	50	

TABLE 11

DATA AND RESULTS OBTAINED IN A TWO CHAMBER-CYCLING VALVE EXPERIMENT USING A GCA MODEL R5 COLD CATHODE GAUGE EXPOSED TO A 1.2 TO 1 NITROGEN GAS PRESSURE RATIO

Pressure Oscillation Frequency (c/s)	I_{MAX} (Ampere)	I_{MIN} (Ampere)	$I_{MAX} - I_{MIN}$ (Ampere)	$\frac{I_{AVE}}{\frac{I_{MAX} + I_{MIN}}{2}}$ (Ampere)	Reduction in $I_{MAX} - I_{MIN}$ (Percent)	Remarks
0	1.27×10^{-6}	1.05×10^{-6}	2.2×10^{-7}	1.16×10^{-6}	0	Initial Equilibrium Levels
2	1.27	1.095	1.75	1.183	20.5	
3	1.27	1.145	1.25	1.208	43	Gauge Anode Voltage of 1.5 kV
4	1.27	1.182	0.88	1.226	60	
5	1.27	1.195	0.75	1.233	66	

behavior if the peak-to-peak amplitude is being limited by the time constant for gas exchange. Table 11 presents a somewhat different picture. Here the nitrogen pressure was relatively high and the pressure range for cycling was small. Apparently, the maximum pressure was attained in each cycle independent of the frequency but the minimum pressure (current) increased with increasing frequency. This kind of behavior indicates that gas exchange effects alone are not responsible for the attenuation but that desorption or re-emission of nitrogen gas prevented the gauge and valve from emptying completely at the higher frequencies.

One should note that different gauge anode voltages were used in the different experiments. It is expected that different gauge voltages will lead to different gauge pumping and re-emission characteristics and will thus change the response.

A study of the output recordings of such pressure cycling tests clearly shows any flaws that may be present in the operation of the valve. Any sticking or binding at the bearings shows up as an irregularity in the sinusoidal pattern. Rubbing of the rotor against the housing causes an increase in pressure as well as an irregularity in the pattern. Outgassing of the valve and gauge shows up as a rise in pressure when the valve is in its closed position (that is, when the valve is isolated from either test chamber). Pumping of the gauge is manifested as a decrease in pressure when the valve is in its closed position.

Pressure cycling experiments of this type, in addition to serving as a diagnostic tool for determining operating characteristics of the valve and pressure sensor, also serve to check the timing between the actual valve positions and the synchronizing pulses that are developed to indicate valve positions. The transfer function of the gauge and valve was obtained with this general experimental arrangement as indicated in Chapter 2.

F. Overall Test of the Yaw Attitude Sensor System

Using the rotary valve and GCA model R5 gauge connected to the test chamber as illustrated in Figure 46 and described in the previous section, the individual electronic components of the system were connected as shown in Figure 1. The valve synchronization pulses were obtained from a magnetic reed switch that was triggered by the external driving magnet. The valve was operated at a cycling frequency of slightly over 5 c/s as can be seen from Figures 58 through 74. The time scale for all of these oscilloscope waveforms was 20 ms/cm. The ordinate or voltage scale ranged from 1 to 5 volts/cm. The pressures in the two test chambers were adjusted to different levels and oscilloscope recordings were made of the gating pulses, logarithmic electrometer output pulses and the dc output voltages of the differential amplifier (the system output).

Figure 58 shows the synchronizing pulse that triggered the electronic gates. Figure 59 shows the output of the logarithmic electrometer over a single cycle with a test chamber pressure ratio of 8.4 to 1. Figures 60, 61, and 62 are grouped together since these waveforms were obtained with both test chambers at approximately the same pressure of 8×10^{-7} torr. The electrometer output of Figure 60 would be a straight line if both chamber pressures were identical. The vertical scale has been magnified here. Figures 63 and 64 are the output waveforms (dc outputs) of the differential amplifier for the case where the different pressures in the two chambers (the ratio of the two pressures was about 8.4 to 1) are interchanged. The two waveforms should be symmetrically disposed about the zero axis. It can be seen that the balance or zero position of the differential amplifier was off and had to be adjusted. In the next series of waveforms, Figures 65, 66 and 67, the pressure in both chambers was 4.5 to 10^{-7} torr. The zero dc output of the adjusted differential amplifier can be seen in Figure 67. The waveforms of the next series, Figures 68, 69, and 70 were taken with the right chamber at a pressure of 4.5×10^{-8} torr while the left chamber was 20 times greater at a pressure of 9.0×10^{-7} torr. The +1 volt output of the differential amplifier is shown in Figure 70. Finally, the last four waveforms can be grouped together since they were taken with approximately the same pressures in the two test chambers. The pressure in the right chamber was 9.2×10^{-7} torr while the pressure in the left chamber was 23 times less at a pressure of 4.0×10^{-8} torr. As can be seen from Figure 74, the dc output of the differential amplifier was now about -1.2 volts, somewhat greater in magnitude than the +1.0 volt output generated by the opposite pressure ratio of 20 to 1.

+20V

0

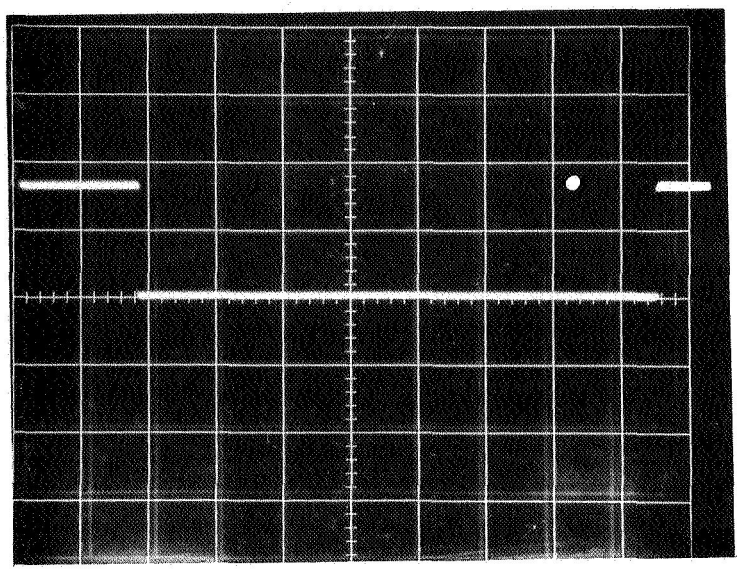

200 ms

-20V

Figure 58. Synchronizing pulse.

+4V

0

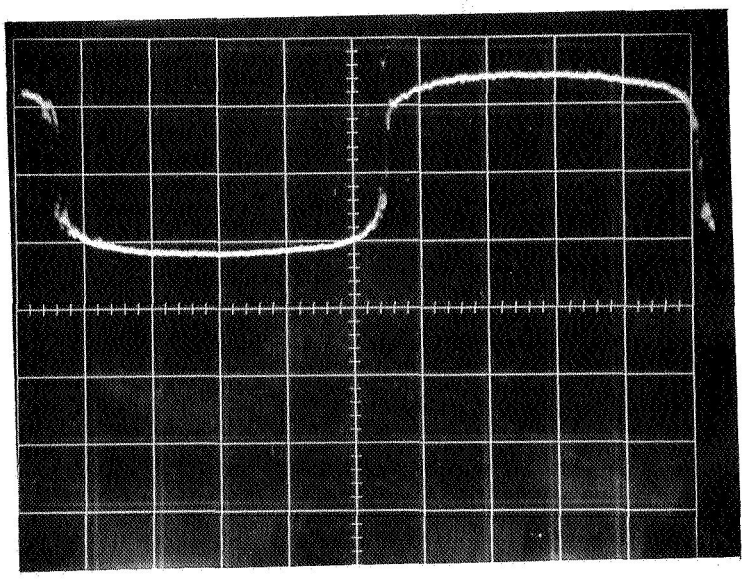

200 ms

-4V

Figure 59. Electrometer output.
Right chamber pressure = 1 x 10^{-7} torr
Left chamber pressure = 8.4 x 10^{-7} torr

+4V

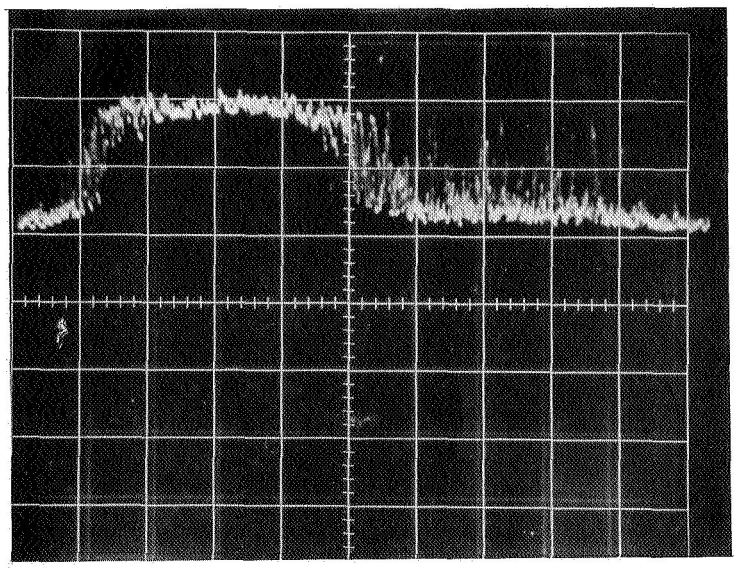

0

200 ms

-4V

Figure 60. Electrometer output.
Right chamber pressure = 8.2×10^{-7} torr
Left chamber pressure = 8.5×10^{-7} torr

+8V

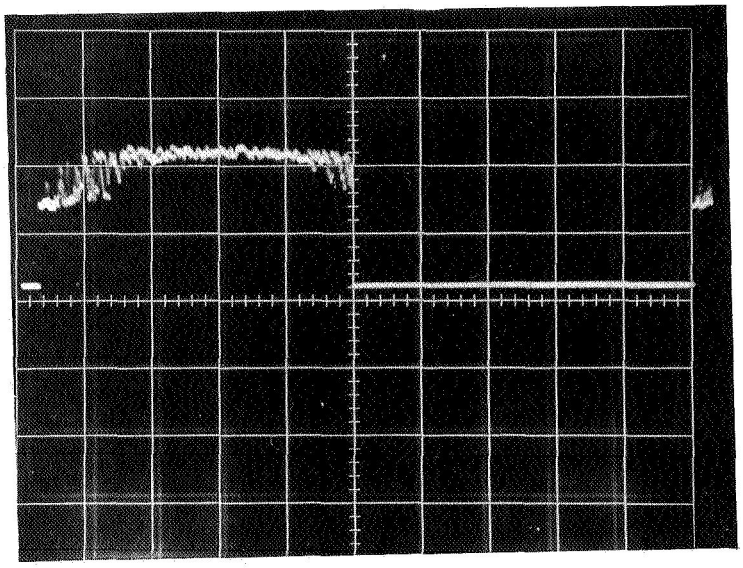

0

200 ms

-8V

Figure 61. Left chamber gate.
Right chamber pressure = 8.2×10^{-7} torr
Left chamber pressure = 8.5×10^{-7} torr

+8V

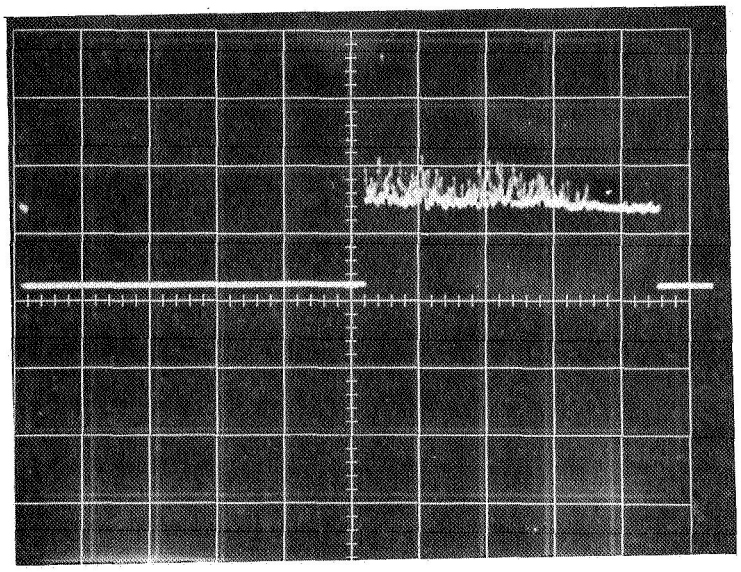

0

200 ms

-8V

Figure 62. Right chamber gate.
Right chamber pressure = 8.2×10^{-7} torr
Left chamber pressure = 8.5×10^{-7} torr

+4V

0 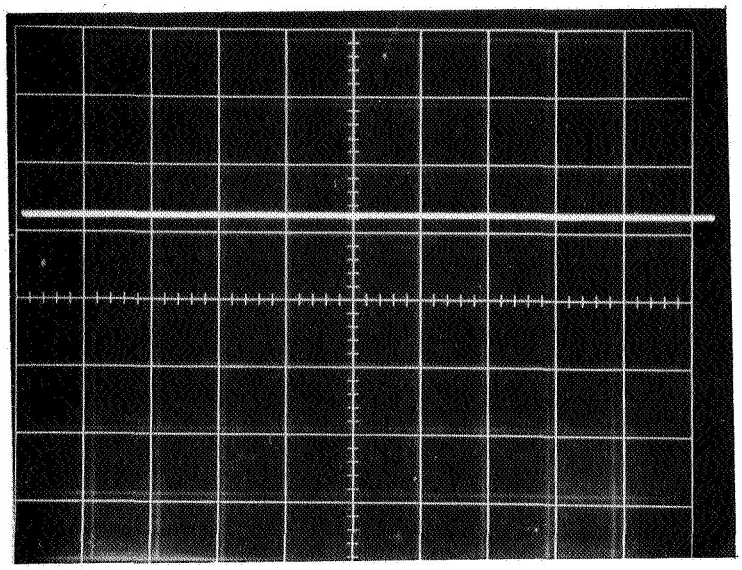 200 ms

-4V

Figure 63. Differential amplifier output.
Right chamber pressure = 1.0×10^{-7} torr
Left chamber pressure = 8.3×10^{-7} torr

+4V

0 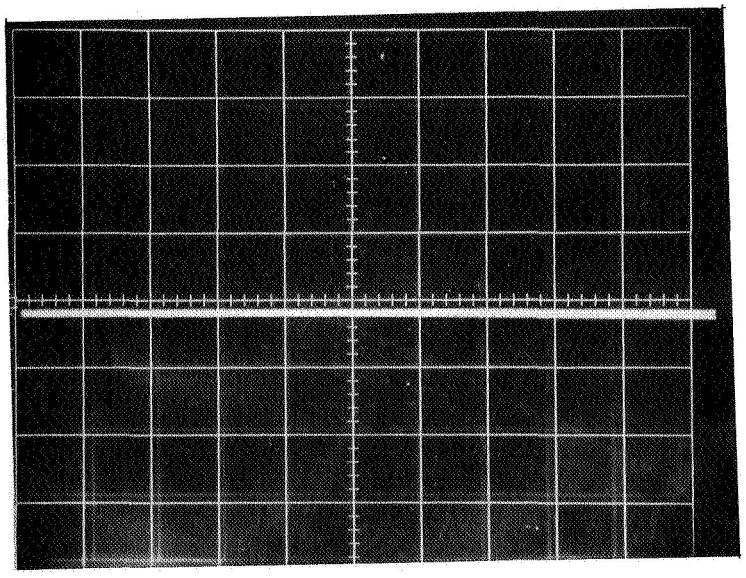 200 ms

-4V

Figure 64. Differential amplifier output.
Right chamber pressure = 8.4×10^{-7} torr
Left chamber pressure = 1.0×10^{-7} torr

+8V

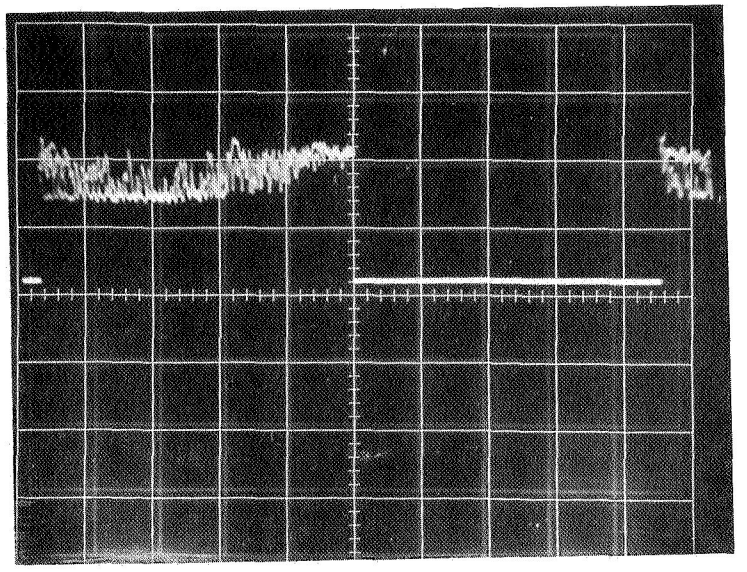

0

200 ms

-8V

Figure 65. Left chamber gate.
Right chamber pressure = 4.5×10^{-7} torr
Left chamber pressure = 4.5×10^{-7} torr

+8V

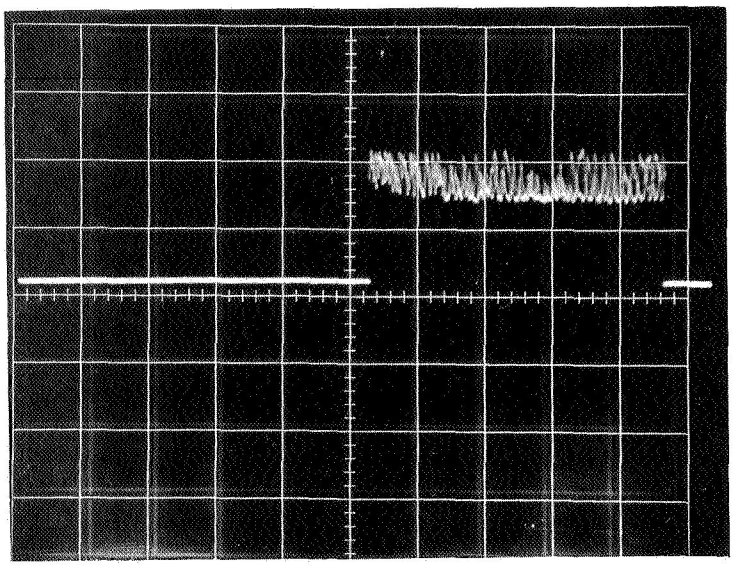

0

200 ms

-8V

Figure 66. Right chamber gate.
Right chamber pressure = 4.5×10^{-7} torr
Left chamber pressure = 4.5×10^{-7} torr

+4V

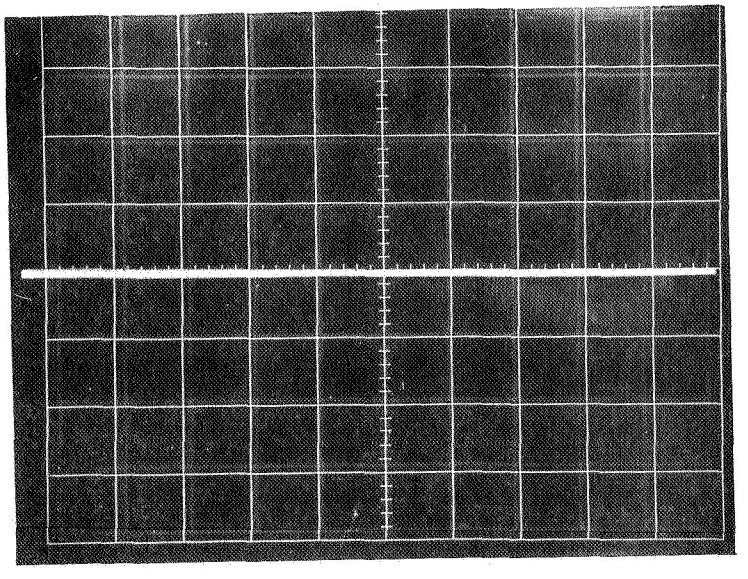

0

200 ms

-4V

Figure 67. Differential amplifier output.
Right chamber pressure = 4.5×10^{-7} torr
Left chamber pressure = 4.5×10^{-7} torr

+8V

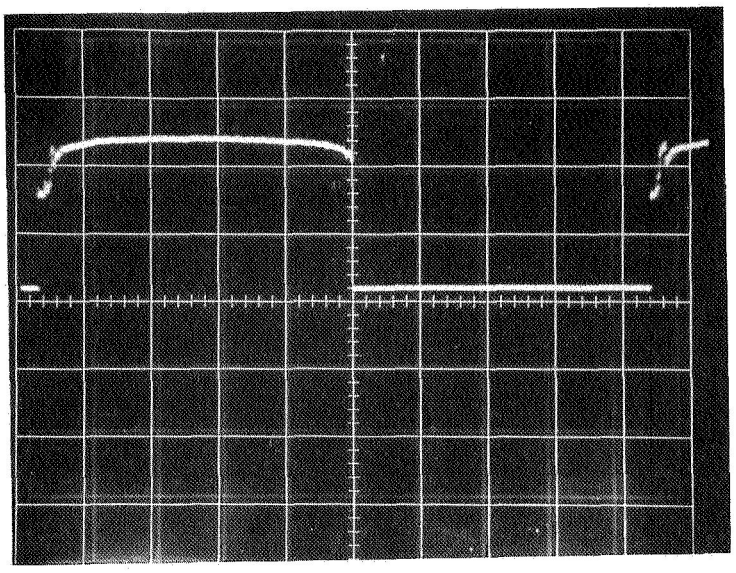

0

200 ms

-8V

Figure 68. Left chamber gate.
Right chamber pressure = 4.5×10^{-8} torr
Left chamber pressure = 9.0×10^{-7} torr

+8V

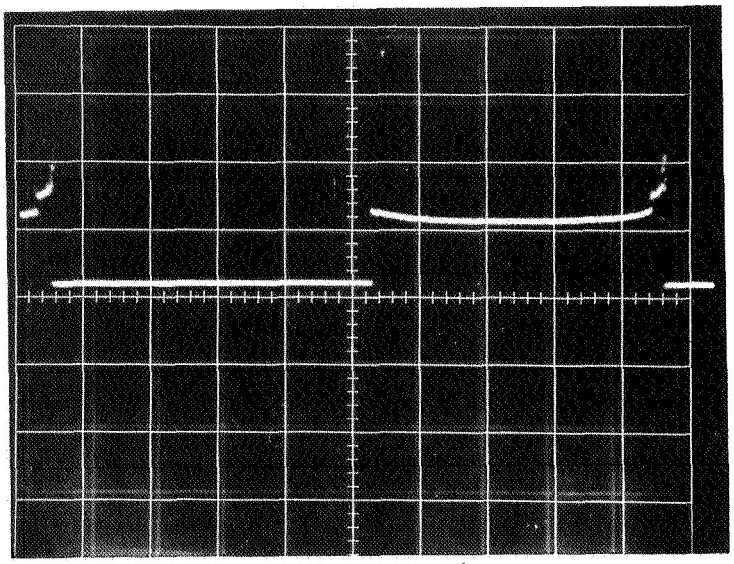

0

200 ms

-8V

Figure 69. Right chamber gate.
Right chamber pressure = 4.5×10^{-8} torr
Left chamber pressure = 9.0×10^{-7} torr

+4V

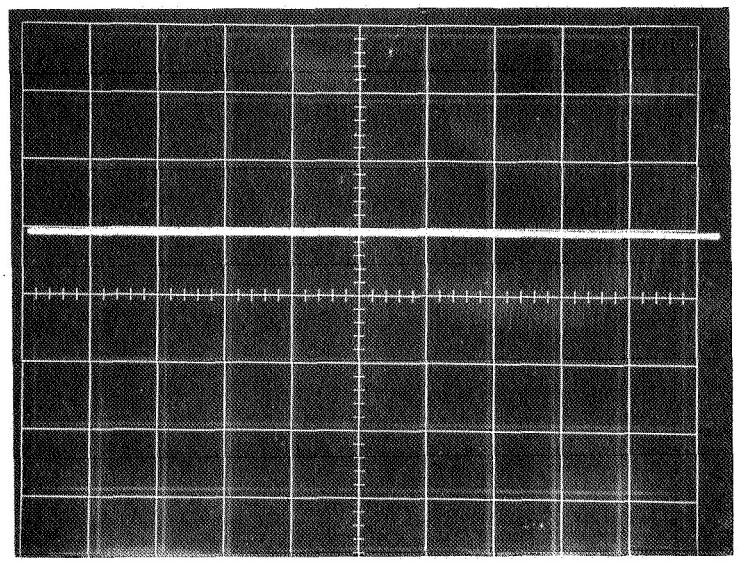

0

200 ms

-4V

Figure 70. Differential amplifier output
Right chamber pressure = 4.5×10^{-8} torr
Left chamber pressure = 9.0×10^{-7} torr

+8V

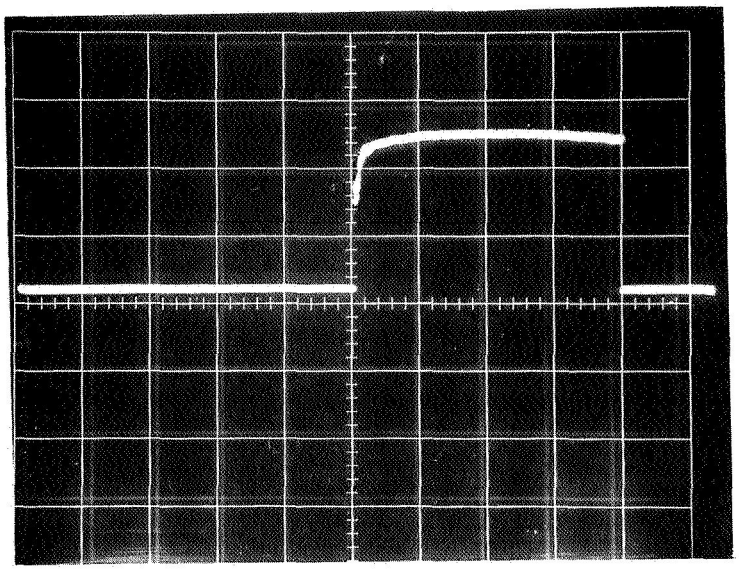

0 200 ms

-8V

Figure 71. Right chamber gate
Right chamber pressure = 9.0×10^{-7} torr
Left chamber pressure = 5.0×10^{-8} torr

+8V

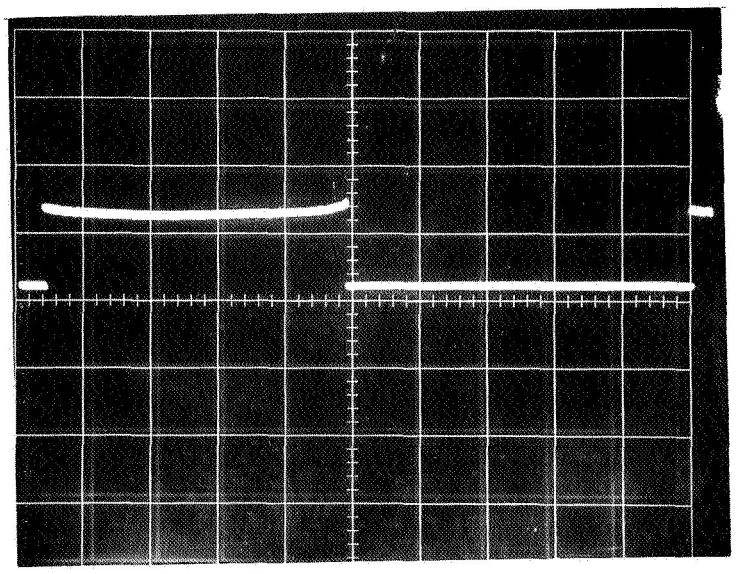

0 200 ms

-8V

Figure 72. Left chamber gate.
Right chamber pressure = 9.0×10^{-7} torr
Left chamber pressure = 5.0×10^{-8} torr

+4V

0

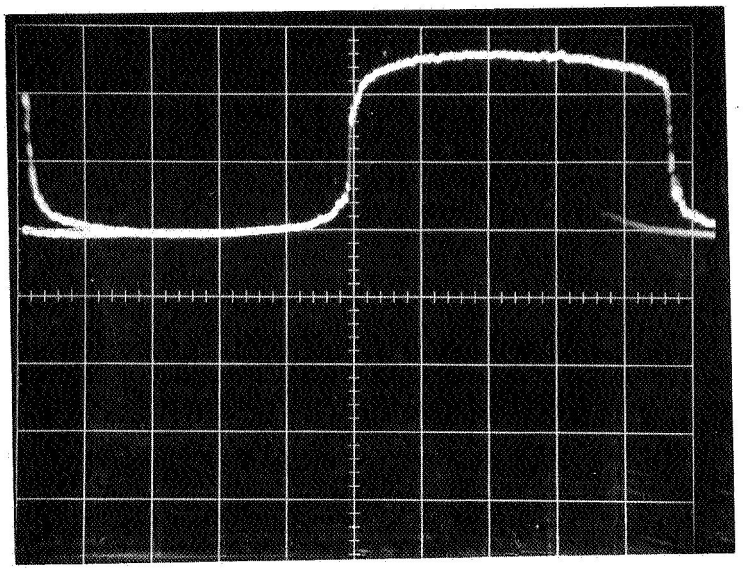

200 ms

-4V

Figure 73. Electrometer output.
Right chamber pressure = 9.2×10^{-7} torr
Left chamber pressure = 4.0×10^{-8} torr

+4V

0

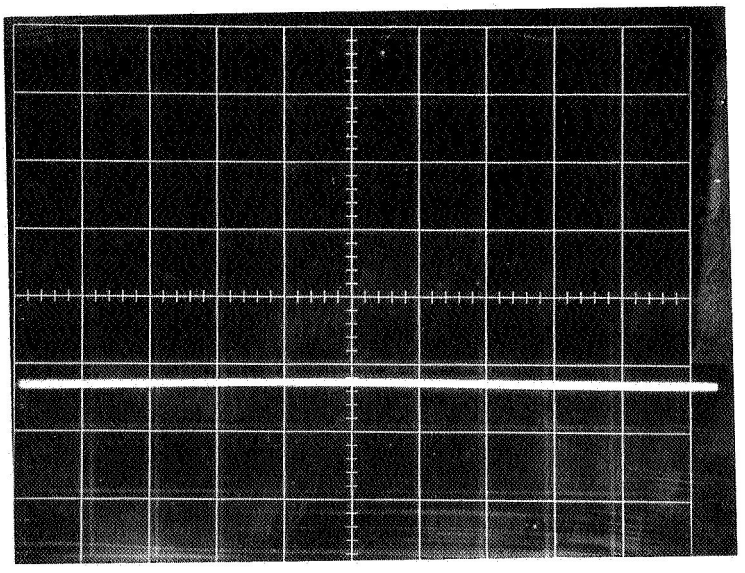

200 ms

-4V

Figure 74. Differential amplifier output.
Right chamber pressure = 9.2×10^{-7} torr
Left chamber pressure = 4.0×10^{-8} torr

6. CONCLUSIONS AND RECOMMENDATIONS

A. Overall System

The basic program objective of building engineering models of a yaw attitude sensor system was realized. It was demonstrated that a single cold cathode ionization type gauge could be used together with a mechanical cycling valve to develop a signal that was related to the difference between two pressures. In an actual flight-type system, the two different pressures would be developed as a result of misalignments in yaw (a similar system would work for misalignments in pitch). The output signal of the ionization gauge was processed by some newly developed electronics and transformed into a dc output voltage proportional to a yaw misalignment angle. The inherent noise in the output signal seemed low enough to permit system resolutions of a few tenths of a degree in yaw. With the aid of a special vacuum test system, it was shown that at least for low frequencies of a few cycles per second, the response time of the system was not limited by the gauge or electronics but only by the small diameter tubulations used to connect the gauge and valve to the pressures being measured.

The remaining sections of this chapter present conclusions and recommendations pertaining to the various phases of the work that were performed. In general, it can be said that system feasibility was demonstrated but that there was insufficient time to test all of the various elements of the system in detail.

B. Pressure Sensor

The GCA model R5 cold cathode ionization gauge appeared to lend itself well as the pressure sensor of this system. The electronics required to operate the gauge consisted simply of a regulated high voltage power supply. Cold cathode gauges are self-regulating and do not require specialized control circuits (such as those circuits required to keep the emission current of a hot filament gauge constant). Among the advantages of a cold cathode ionization gauge of this type are low power consumption, a long lifetime at low pressures (no filament that can sag or burn out) and protection against damage caused by unexpectedly high pressures (the current through the gauge is limited by the power supply). The response time of the R5 gauge did not limit the system response. It was found that the noise inherent in the gauge signal was mostly filtered out by the electronics. The gauge magnet is perhaps its greatest liability since it adds considerable weight to the system and requires extensive shielding.

C. Mechanical Cycling Valves

The feasibility of building several quite different mechanical cycling valves was demonstrated. The construction of the two valves that was carried to completion pointed up the practical problems associated with valve construction. It was found that the operation of gold-plated ball bearings in a vacuum environment was unreliable. The general design of the continuously rotating valve was found to be straightforward, but experience with the use of a single phase, shaded two-pole type of driving mechanism led to the conclusion that a two-phase, four-pole type of drive would be more positive and reliable. The problem of valve position synchronization for the rotary valve could apparently be solved with the use of magnetic reed switches, but the effect of temperature variations on the magnets and reed switches was not investigated. The rotary valve proved to be extremely valuable for its use in determining the response time of the pressure sensor and related electronics since the frequency of this valve could be adjusted over a wide range. Evidence was obtained of the generation of gas in the rotary valve, presumably by the rubbing action at the bearings. It was found that the valve operation could be analyzed by inspecting the output signal of the cold cathode ionization gauge that was connected to the valve.

The flexure-pivot oscillating valve is expected to be a highly reliable practical valve. The design of this valve would probably be modified for any future application. The use of counter-rotating rotors did result in a zero net torque device, but the single-ended suspension of each rotor made it necessary to operate the valve in a vertical position. The advantage of initially designing and machining the two rotors so that they have the same moment of inertia became evident during the tests. The proper design of a flexure-pivot type valve can best be accomplished when the operating frequency is known in advance.

The flexure-pivot type valve is a tuned mechanical oscillator, and, as such, it can be used as the frequency determining element of the drive circuit. When used in such a "self-excited" arrangement, the synchronization of valve position with the output signal of the pressure sensor is quite positive.

The results obtained with the electromagnetic drive for the flexure-pivot valve were gratifying. The results showed that a very simple four-pole external electromagnet could be used in combination with an internal two-pole rotor of pure nickel or other magnetic material to achieve the desired oscillatory motion. The electronic drive circuit for this electromagnet was quite simple in that a single polarity source of power was alternately connected to energize each pole pair of the electromagnet. Two electromagnets were required for the double rotor valve. Where a small net torque can be tolerated, a single rotor valve driven by a single electromagnet can be used.

The reliability of the flexure-pivot bearings has been verified by independent lifetime testing. When used at approximately 40 percent or less of their rated angular travel, these bearings have an unlimited lifetime. The absence of any required lubrication and the ability to operate in high vacuum over a wide range of temperatures make these bearings especially suitable for use in a yaw attitude sensor cycling valve.

D. Electronics

The testing that was performed showed that a logarithmic electrometer with a limited bandpass is quite suitable for use in a yaw attitude sensor system. Such electrometers have the necessary wide dynamic range. They also serve to reduce any high frequency noise present in the gauge output signal. The method of coupling the gauge output into the electrometer can be improved since it was found that transient pulses were sent through the electrometer when the gauge high voltage was turned on.

The synchronous detector worked properly, but there was some coupling of the cycling valve synchronizing pulses into the system output. In addition, there was unnecessary noise present in some of the gating circuits. The difficulties were those associated with overall operation of the system in which there was undesirable interaction between various independent electronic units. There was insufficient time available in the program to delineate and solve these problems, but there is no doubt that all of the difficulties can be removed with additional development work.

In addition to removing the known difficulties, more work should be done to study the detailed operation of the electronics over the full range of the system. For example, it is expected that a more careful matching of certain electronic components will yield more accurate operation over a wider temperature range.

E. Packaging

The rectangular frame method of packaging all of the components, as used in this program, is convenient, but is wasteful of space and adds unnecessary weight. It is recommended that a new method of packaging be developed in which all components are grouped around the cycling valve. Such a method will probably require individual magnetic shielding for sensitive portions of the electronics. The magnetic shielding experiments showed how the strong residual field of the gauge magnet could be reduced to 40 or 50 milligauss at a distance of 12 inches with the use of three layers of shielding material. Additional reductions in the residual magnetic field can be obtained with the use of additional shielding.

F. Test System

The vacuum test system worked very well and fulfilled its function of testing the complete yaw attitude sensor system. When used together with the rotary valve, the test system made it possible to determine the frequency response of the pressure sensor, with or without additional electronics, and the inherent noise of the system at null. The wide range of pressures attainable with the test system, from 10^{-10} to 10^{-4} torr, make it possible to test the yaw attitude sensor over its complete range. The all-dry nature of the vacuum pumps used permitted the mechanical cycling valves to be tested under realistic space vacuum conditions.

In the future, the vacuum test system could be modified to provide automatically programmed leak valves that would change the pressures in the two test chambers to simulate dynamic movement of a space vehicle.

Finally, it should be noted that further development work is indicated to solve some existing problems and to improve the overall accuracy and reliability of the system. Some desirable changes and modifications are listed below:

(1) Increase the diameter of the valve tubulations and shorten them, if possible, to improve the system response time.

(2) Modify the flexure-pivot valve so that its operation is independent of orientation.

(3) Use the natural period of the flexure-pivot valve rotor to determine the driving frequency.

(4) Shield the electronics to remove interactions between independent units.

Additional testing of the system is required under various environmental conditions. The system sensitivity, resolution and accuracy over its entire operating range must be determined.

The research and development work described in this report showed conclusively that differential pressures in the high vacuum region can be detected and measured with a single pressure sensor. The basic concept and techniques disclosed may have other applications.

REFERENCES

1. Newton, G. P., Pelz, D. T., Miller, G. E., Lt. (j.g.), USN, and Horowitz, R., Transactions of the Tenth National Vacuum Symposium of the American Vacuum Society, The Macmillan Co., New York, 208 (1963).

2. Meadows, E. B. and Townsend, J. W., Jr., "IGY Rocket Measurements of Arctic Composition Above 100 Km," Proceedings of the First International Space Science Symposium, ed. by Hilde Kollman Bijl, Amsterdam: North Holland Publishing Co., (1960).

3. Seddon, J. C. and Jackson, J. E., "Ionosphere Electron Densities and Differential Absorption," IGY Rocket Report Series Number 1, National Academy of Sciences, National Research Council, Washington 25, D. C., 149 (1958).

4. Newell, H. E., Jr., High Altitude Rocket Research, Academic Press, Inc., New York, 143 (1953).

5. Jacchia, L. G., "Static Diffusion Models of the Upper Atmosphere with Empirical Temperature Profiles," SAO Special Report No. 170, Smithsonian Institution Astrophysical Observatory, Cambridge, Mass., (1964).

6. Kreisman, W. S., "Development of Cold Cathode Ionization Gauges for Space Vehicles," GCA Technical Report No. 64-17-N, GCA Corporation, Bedford, Mass., 35 (1964).

7. Spencer, N. W., Boggess, R. L., LaGow, H. E. and Horowitz, R., ARS Journal, 29, 290 (1959).

8. GCA Corporation, VVSA Study Program, final report on Contract P. O. No. DX543651, prepared for Honeywell, Inc., Minneapolis, Minn., (1966).

9. Ratcliffe, J. A., Physics of the Upper Atmosphere, Academic Press, New York, 17-22 (1960).

10. Evans, H. E. and Flatley, T. W., "Bearings for Vacuum Operation," Technical Note D-1339, Goddard Space Flight Center, NASA, Greenbelt, Maryland, (1962).

11. Evans, H. E. and Flatley, T. W., "High Speed Vacuum Performance of Gold Plated Miniature Ball Bearings with Various Retainer Materials and Configurations," Technical Note D-2101, GSFC, NASA, Greenbelt, Maryland, (1963).

REFERENCES (Continued)

12. Flatley, T. W., "High Speed Vacuum Performance of Miniature Ball Bearings Lubricated with Combinations of Barium, Gold and Silver Films," Technical Note D-2304, Goddard Space Flight Center, NASA, Greenbelt, Maryland, (1964).

13. Parcel, R. W., Clauss, F. J., O'Hara, G. F., and Young, W. C., Transactions of the Tenth National Vacuum Symposium of the American Vacuum Society, The Macmillan Company, New York, 3 (1963).